DISSERTATION

Titel der Dissertation

Structural changes of minor group human rhinoviruses during uncoating

angestrebter akademischer Grad

Doktor/in der Naturwissenschaften (Dr. rer.nat.)

Verfasserin / Verfasser:	DI(FH) Angela Maria Pickl-Herk
Matrikel-Nummer:	0649100
Dissertationsgebiet (lt. Studienblatt):	Molekulare Biologie
Betreuerin / Betreuer:	Univ.-Prof. Dipl.-Ing. Dr. Dieter Blaas

Wien, am 22. April 2011

Acknowledgements

At the beginning, I want to thank my supervisor Dieter Blaas for four exciting but also challenging years and for supporting me in living up to these challenges.

I would like to say thank you to all my lab colleagues, Abdul, Christoph, Irene, Jürgen, Katharina, Mohit, Nena, Shushan, Tünde, and Xavier, and especially to the "Adduct"-team, Gerry and Victor, for becoming awesome friends during this time.

I am very grateful to everyone, who taught me new techniques or gave me advice, on how to improve my work. In particular, I would like to mention the Rossmann lab at Purdue University in Indiana, Michael, Susan, and Thomas, and the lab of José R. Castón at the Centro Nacional Biotecnología/CSIC in Madrid, José and Dani for great help with the data processing. For all their support and enthusiasm, also on weekends, I would like to say a special thank you to the IMP/IMBA EM facility, Günter, Marlene and Nici. I want to acknowledge my PhD Committee, Kristina and Thomas, as well as the Marlovits lab for sharing their good and bad experiences with the microscopes with me.

All this would not have been possible without the continuous support and understanding of all my friends. I am grateful to all of them, especially to Lisa and Julia, for participating in every little drama of my life, and to Gabriele and Gerald, for great Tuesday evenings.

I owe my deepest gratitude to my family Gerti, Hubert, Beatrix and Matthias for being there for me every moment of my life, tough or joyful, and to il mio AmoRe Matteo for being "the wind underneath my wings".

Table of Contents

Table of Contents

Table of Contents

Abbreviations

CE	Capillary electrophoresis
Ch	Cholesterol
CTF	Contrast transfer function
DGS-NTA	1,2-dioleoyl-*sn*-glycero-3-[(N-(5-amino-1-arboxypentyl)iminodiacetic acid)succinyl]
EGF	Epidermal growth factor
EM	Electron microscopy
FSC	Fourier shell correlation
HRP	Horseradish peroxidase
HRV	Human rhinovirus
ICAM-1	Intercellular adhesion molecule-1
IRES	Internal ribosomal entry site
LDLR	Low-density lipoprotein receptor
LPA	Lysobisphosphatidic acid
LRP	Low-density lipoprotein receptor-related protein
LUV	Large unilamellar vesicles
MBP	Maltose-binding protein
NBD-PC	1-oleoyl-2-[12-[(7-nitro-2-1,3-benzoxadiazol-4-yl)amino] lauroyl]-sn glycero-3-Phosphocholine
NTA	Nitrilotriacetic acid
ORF	Open reading frame

PC	Phosphatidylcholine
PE	Phosphatidylethanolamine
PV	Poliovirus
PVR	Poliovirus receptor
RMSD	Root mean square deviation
SM	Sphingomyelin
TEM	Transmission electron microscopy
UTR	Un-translated region
VLDLR	Very-low-density lipoprotein receptor
VP0	Viral protein 0
VP1	Viral protein 1
VP1-NT	N-terminus of viral protein 1
VP2	Viral protein 2
VP3	Viral protein 3
VP4	Viral protein 4
VPg	Genome-linked viral protein

1 Abstract

Minor group human rhinoviruses (HRVs), causative agents of the common cold, are internalized by receptor-mediated endocytosis. The low endosomal pH (<pH 5.8) triggers the uncoating process. The innermost capsid protein VP4 is released and the amphipathic N-terminus of VP1 is externalized, generating hydrophobic A-particles that interact with the endosomal membrane. Trans-membrane RNA release into the cytoplasm results in empty capsids or B-particles, retained in intact endosomes.

In the current study, the 3D structures of A- and B-particles of HRV2 were solved from cryo-EM data to resolutions below 10 Å. By mutual comparison and docking of the published X-ray coordinates of native HRV2, the main structural changes during rhino-viral uncoating were investigated.

A-particles expanded by 4.7 % compared to native virus and pores opened at the 2- and 5-fold axes. Concomitantly, VP4 was expelled and the VP1 N-terminus was externalized via the pseudo-3-fold axis. The genome became more ordered and an inner RNA shell could be resolved, contacting the capsid at the 2- and pseudo-3-fold axes.

Acid-triggered B-particles differed from A-particles only in the released RNA genome and the VP1 N-terminus that became too disordered to be resolved. By comparison to the published EM map of heat-induced B-particles, equivalence of heating and acidification as triggers for rhino-viral uncoating was demonstrated.

For studying uncoating in the context of membranes, liposomes were decorated with a recombinant receptor fragment of VLDLR and HRV2 was specifically attached.

Viral conversion was triggered by acidification and halted at different stages by EM preparation techniques. New intermediate particles with partially externalized RNA were visualized and empty capsids remained membrane-associated. The kinetics of uncoating was faster than in solution, suggesting a catalytic effect of the membrane or of the pH gradient across it on RNA release.

The current data depict the main conformational changes minor group rhinoviruses undergo during uncoating. They additionally emphasize the importance of investigating rhino-viral RNA release in the context of membranes.

2 Zusammenfassung

Humane Rhinoviren (HRVs) der „minor" Rezeptorgruppe, Erreger der gewöhnlichen Erkältung, werden durch Rezeptor vermittelte Endozytose in die Zelle aufgenommen. Der niedrige pH-Wert in Endosomen (<pH 5.8) induziert den Uncoating-Prozess. Das interne Kapsidprotein VP4 und der amphipathische N-Terminus von VP1 werden externalisiert, wodurch das hydrophobe A-Partikel generiert wird, das an die endosomale Membran bindet. Der darauffolgende trans-Membran RNA-Transfer resultiert in leere Kapside oder B-Partikel, die in den intakten Endosomen zurückbleiben.

In der vorliegenden Studie wurde die Struktur von A- und B-Partikeln von HRV2 von cryo-EM Daten bis zu unter 10 Å Auflösung rekonstruiert. Durch Vergleiche miteinander und Docking der Röntgenstruktur von nativem Virus wurden die Strukturänderungen während des rhino-viralen Uncoating-Prozesses untersucht.

A-Partikel expandierten im Vergleich zu nativem Virus um 4.7 % und Poren öffneten sich an den 2- und 5-fachen Symmetrieachsen. Gleichzeitig wurde VP4 freigesetzt und der VP1 N-Terminus an der pseudo-3-fachen Achse externalisiert. Das Genom wies einen höheren Ordnungsgrad auf und eine interne RNA-Hülle wurde rekonstruiert, die das Kapsid an den 2- und pseudo-3-fachen Achsen berührte.

Säure induzierte B-Partikel unterschieden sich von A-Partikeln in der RNA-Freisetzung und im VP1 N-Terminus, der durch seine hohe, konformative Flexibilität nicht rekonstruiert werden konnte. Vergleiche mit der publizierten Struktur von Hitze

induzierten B-Partikeln bewiesen die Äquivalenz von erhöhten Temperaturen und Säure als Auslöser des Uncoating-Prozesses.

Um Uncoating im Zusammenhang mit Membranen zu untersuchen, wurden Liposome mit einem rekombinanten Rezeptorfragment vom VLDLR dekoriert und HRV2 wurde spezifisch daran gebunden. Virale Strukturänderungen wurden durch Ansäuerung induziert und durch EM-Präparationstechniken angehalten. Dadurch konnten neue Zwischenstadien des Uncoating mit partiell freigesetzter RNA und membrangebundene, leere Kapside visualisiert werden. Die Kinetik des RNA-Transfers war schneller als in Lösung, was auf eine mögliche, katalytische Aktivität der Membrane oder des pH-Gradienten über diese auf die RNA-Freisetzung hinweist.

Die vorliegenden Daten beschreiben die Strukturänderungen von HRVs der „minor" Rezeptorgruppe während des Uncoating-Prozesses. Sie untermauern außerdem die Wichtigkeit, rhino-viralen RNA-Transfer im Zusammenhang mit Membranen zu untersuchen.

3 Introduction

3.1 Pathology

Human Rhinoviruses (HRVs) are the main causative agents of the common cold, an infection of the respiratory tract that is characterized by nasal obstruction, rhinorrhoea, and general malaise (Heikkinen T and Jaervinen A, 2003). Rhino-viral colds are associated with exacerbations of asthma (Message SD *et al.*, 2008) and chronic obstructive pulmonary disease (Mallia P *et al.*, 2006) and can be accompanied by secondary bacterial infections, leading to acute otitis media (Savolainen-Kopra C *et al.*, 2009) or pneumonia (Juven T *et al.*, 2000; Jennings LC *et al.*, 2008). HRVs are responsible for millions of lost working and school hours and the associated financial loss. More importantly, they also pose a threat to children, elderly, and immuno-compromised patients (Johnston SL, 2005).

HRVs are transmitted via respiratory secretions in particle aerosols or on contaminated hands and environmental surfaces (Winther B *et al.*, 2007l). Once they reach the nasopharyngeal mucosa, they infect epithelial cells, using specific receptors. Within 8 h to 10 h, infectious viral particles can be detected in nasal secretions and viral shed peaks around 48 h post inoculation (Winther B *et al.*, 1986; Harris JM 2nd and Gwaltney JM Jr, 1996). The infection is self-limiting and usually restricted to the upper respiratory tract. However, viral RNA has also been detected in the lower airways (Papadopoulos NG *et al.*, 2000; Mosser AG *et al.*, 2005). As found in nasal biopsies, *in vivo*, HRVs do not cause significant histo-pathological changes (Winther B *et al.*, 1984),

it has thus been suggested that the clinical symptoms may be caused by the immune-response of the host. In particular, the levels of interleukin-6 and -8 in nasal mucus were shown to correlate with the severity of symptoms (Turner RB *et al.*, 1998; Papadopoulos NG *et al.*, 2000).

Currently, HRV infections are treated symptomatically using analgesics, antitussives or decongestants, because so far, no specific anti-rhino-viral drugs are approved for clinical use (Rollinger JM and Schmidtke M, 2009). Strategies for their development focus on conserved rhino-viral features such as capsid proteins, proteinases or components of RNA synthesis. This is essential, to target the over 100 known serotypes (Palmenberg AC *et al.*, 2009) and to limit the emergence of escape mutants. Due to the high variability of HRVs, successful vaccination has long been considered impossible. Recently, cross- reactivity of antibodies against viral protein 1 (VP1) and 4 (VP4) have been shown (Katpally U *et al.*, 2009), so that combinations of recombinant capsid proteins might be suitable antigens for vaccination.

Considering the wide medical distribution and the lack of efficient prevention or treatment, further investigation of HRVs is of great importance. Deeper knowledge on the molecular details of their infection pathway may allow identification of conserved drug targets. In addition, findings on HRVs could be extrapolated to other, more pathogenic viruses of the *Picornaviridae*, such as Poliovirus, Hepatitis A Virus and Food- and Mouth Disease Virus.

3.2 Picornaviridae

Human Rhinoviruses belong to the family *Picornaviridae* of the order *Picornavirales.* It is a family of small (i.e. "**pico**" in Latin), non-enveloped, icosahedral viruses with a single-stranded, positive sense **RNA** genome. *Picornaviridae* include many important pathogens for humans and livestock, such as Poliovirus, Coxsackievirus, Hepatitis A Virus, and Food- and Mouth Disease Virus. They are subdivided into the 12 genera *Aphtovirus, Avihepatovirus, Cardiovirus, Enterovirus, Erbovirus, Hepatovirus, Kobuvirus, Parechovirus, Sapelovirus, Senecavirus, Teschovirus*, and *Tremovirus.* Human Rhinoviruses are assigned to the genus *Enterovirus* that consists of seven different Enterovirus species plus the three Human Rhinovirus species A, B, and C (http://www.ictvonline.org/virusTaxonomy.asp, 18.04.2011).

99 serotypes of HRVs, obtained from clinical specimens, were classified according to sequence similarity into the species HRV-A and HRV-B, with 74 and 25 strains, respectively (Ledford RM *et al.*, 2004; Laine P *et al.*, 2005). Alternatively, these rhinoviruses can be grouped on the basis of receptor specificity. 87 serotypes, the major group viruses, use Intercellular Adhesion Molecule-1 (ICAM-1) for attachment to host cells (Greve JM *et al.*, 1989), whereas 12, the minor group viruses, bind members of the Low-Density Lipoprotein Receptor (LDLR) superfamily (Hofer F *et al.*, 1994; Vlasak M *et al.*, 2005). The major group contains both, HRV-A and –B strains, but the minor group consists only of HRV-A serotypes. A third method of rhino-viral classification is their sensitivity to a panel of capsid binding anti-virals, a group of hydrophobic but otherwise chemically divergent compounds. Some HRVs are inhibited by drugs with a long

aliphatic chain, whereas others are neutralized by shorter compounds, classifying them into drug reactive group A and B, respectively (Andries K *et al.*, 1990; Mckinlay *et al.*, 1992). There is a strong correlation between these two groups and the amino acid sequence of the drugs' binding site, a hydrophobic pocket on the viral surface, probably reflecting its geometry. The correlation holds also for the entire rhino-viral genome, so that most antiviral group A viruses belong to the HRV-B species and vice versa (Andries K *et al.*, 1990; Palmenberg AC et al., 2009).

In 2007, new HRV strains were discovered that cause influenza-like illnesses with severe respiratory distress (Lau SK *et al.*, 2007). Sequence analysis revealed that they differ clearly from the previously known 99 serotypes (Palmenberg AC *et al.*, 2009) and they were thus classified into the new species HRV-C. Just recently, HRV-C viruses could be propagated in cell culture, following transfection with viral RNA. First data on reactivity to capsid binders allocated HRV-C15 to drug reactive group B. The host cell receptor is not known yet, but data by Bochkov Y *et al.* (2011) indicated that HRV-C would fall into a separate receptor group.

Figure 1 gives an overview on rhino-viral classification.

Figure 1 Genome tree for all known HRV serotypes. Human Rhinoviruses are phylogenetically grouped into the three species HRV-A, B, and C. Alternatively, HRVs are classified based on receptor specificity into a major (M) and minor (m) group, binding ICAM-1 and members of the LDLR superfamily, respectively. The receptor of HRV-C viruses has yet to be identified. Reactivity to hydrophobic capsid binders assigns HRVs to drug reactive groups A and B (here 1 and 2), being more susceptible to long and short compounds, respectively. Recently, HRV-C15 was allocated to drug reactive group B. The minor group HRV2, belonging to HRV- A species and drug reactive group 2, is studied in the current thesis (arrow). Figure from Palmenberg AC *et al.* (2009).

The current thesis focuses on minor group rhinoviruses, especially on HRV2, its best studied member. It belongs to the HRV-A species and the drug reactive group B.

3.3 Virion structure

The X-ray structure of native HRV2 has been solved to 2.6 Å resolution (Verdaguer N *et al.,* 2000). Human rhinoviruses consist of a 30 nm large, non-enveloped, icosahedral protein capsid that harbors a 7.2 kb long, single-stranded, and positive sense RNA genome. The capsid is composed of 60 copies of each of the four capsid proteins viral protein 1 (VP1), VP2, VP3, and VP4. The first three make up the outer surface of the virus, whereas VP4, as well as the N-termini of VP1 and VP2 are found, partially disordered, in the interior of the capsid (Rossmann MG, 2002). The internal RNA genome lacks symmetry. In the X-ray structure, only weak density in proximity to Tryptophan 2038 of VP2 has been attributed to viral RNA.

Although different in sequence, the surface proteins VP1 to VP3 have similar sizes (32.9 kDa, 29.0 kDa, and 26.1 kDa, respectively) and folds. Eight anti-parallel β-sheets, nine in VP2, form a wedge-shaped β-barrel. At its narrow end, loops connect the anti-parallel β-sheets B and C, H and I, E and D, F and G. These point towards the 5- fold axis in VP1, towards the pseudo-6-fold axis in VP2 and VP3. VP1 to VP3 together form one of the 60 protomers of the viral capsid, resulting in a T=1 (pseudo T=3) surface lattice (Rossmann MG, 2002) (Figure 2).
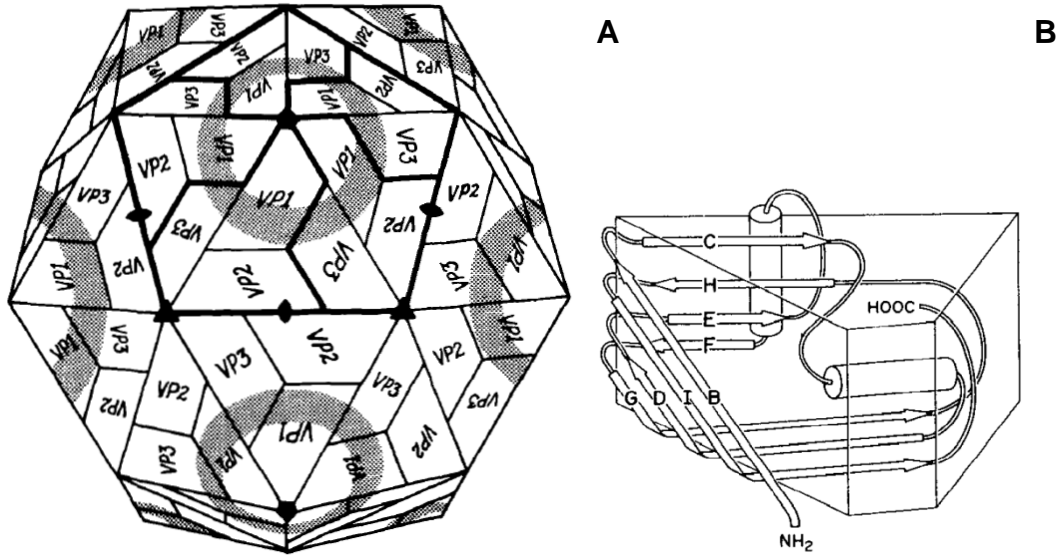
Figure 2 Schematic representation of the picornaviral capsid and the fold of surface proteins. The non-enveloped capsid of picornaviruses is composed of 60 copies of the viral proteins 1 to 4. VP1 to VP3 form a T=1 (pseudo T=3) icosahedron with VP4 located on the capsid interior. Around the 5-fold axis, a depression (outlined in grey) is the binding site for the major group receptor ICAM- 1 and a class of hydrophobic antivirals (A, from Rossmann MG, 1989). The surface proteins VP1 to VP3 fold in a wedge-shaped β-barrel, with antigenic loops connecting their eight anti- parallel β- sheets. The loops of VP1 assemble at the star-shaped dome at the 5-fold axis, forming the attachment site of minor group receptors (B, from Hogle JM *et al.*,1985).

The different serotypes arise from varying amino acid sequences of the surface loops (Rossmann MG *et al.,* 1985; Chapman MS and Rossmann MG, 1993). Especially the loops of VP1 harbor strong antigenic epitopes. In native virions, they assemble at the 5-fold axis, forming a star-shaped dome that is the receptor binding site for minor group viruses (Verdaguer N *et al.*, 2004).

An about 15 Å deep canyon around the 5-fold axis is formed by insertions into the β-barrel structure of all surface proteins but mainly of VP1. In native virions, the pocket factor, a lipophilic molecule, most likely a myristate, is bound to a hydrophobic depression in the canyon floor. The hydrophobic capsid binders, used for rhino-viral classification into drug reactive groups, replace this pocket factor (Rossmann MG, 1989; Zhang Y *et al.*, 2004). They stabilize the capsid and thereby inhibit structural changes

required for uncoating (Gruenberger M *et al.*, 1991; Phelps DK *et al.*, 1998; Okun VM *et al.*, 2002).

3.4 Genome structure

Within the protein capsid, HRVs harbor a single-stranded, positive-sense RNA genome of 7.2 kb length. Functionally, it can be subdivided into different parts.

At its 5' end, the genomic protein VPg is covalently bound to the nucleic acid. It serves as primer for the viral RNA polymerase during positive and negative stand synthesis (Wimmer E, 1982). This is followed by a 5' untranslated region (UTR), containing an internal ribosomal entry site (IRES). Rhino-viral RNA lacks the m7G cap of cellular mRNA, required for recognition by and binding to ribosomes. Instead, the IRES, a characteristically folded RNA secondary structure, promotes binding of ribosomes and thus initiation of translation (Jackson RJ and Kaminski A, 1995; Kaminski A *et al.*, 2010). It gives viral protein expression a selective advantage over cellular polypeptide synthesis, when viral effector proteins shut down cap-dependent translation during the course of infection (Haghighat A *et al.*, 1996; Svitkin YV *et al.*, 1999).

Rhino-viral RNA contains one single open reading frame (ORF), encoding one polyprotein. It can be divided into the three main parts P1 to P3. The P1 region contains the sequence for the structural proteins VP1 to VP4, whereas P2 and P3 encode non-structural proteins. The proteases 2A and 3C autocatalytically cleave the viral polyprotein upon translation (Palmenberg AC *et al.*, 1979; Toyoda H *et al.*, 1986). They are also responsible for shutting off the host cell machinery. The proteins 2B and 2C are

involved in determining the host range of the virus (Yin FH and Lomax NB, 1983; Lomax NB and Yin FH, 1989). Proteins 2C, 3A, VPg, and the RNA polymerase 3D are required for RNA replication.

The 3' non-coding region terminates in a poly-A tail. Rhino-viral RNA thus largely resembles mRNA and can directly serve as template for protein synthesis and replication.

Figure 3 gives an overview of the rhino-viral genome.
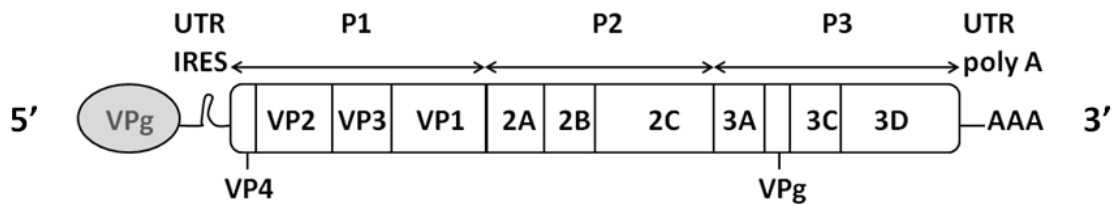
Figure 3 Schematic representation of the rhino-viral genome. At its 5' end, rhino-viral RNA is linked to the genomic protein VPg (grey), followed by a 5' untranslated region (UTR). It contains an internal ribosomal entry site (IRES) for the initiation of translation. The open reading frame encodes one single polyprotein with the structural and non- structural proteins in regions P1 and P2/P3, respectively. The 3' UTR terminates in a poly-A tail.

3.5 Receptor binding

For identification of and attachment to target cells, minor group rhinoviruses use the Low-Density Lipoprotein Receptor (LDLR), the Very-Low-Density Lipoprotein Receptor (VLDLR) or LDLR-Related Protein (LRP) (Hofer F *et al.*, 1994; Vlasak M *et al.*, 2005; Marlovits TC *et al.*, 1998).

Members of the LDLR superfamily bind a variety of different ligands (Herz J and Strickland DK, 2001; Blacklow SC, 2007). Structurally, they consist of different numbers of ligand binding modules, the 40 to 50 residue-long complement repeats. One individual repeat has generally low affinity towards natural ligands but several modules

bind concertedly with high avidity (Andersen OM *et al.*, 2000; Wruss J *et al.*, 2007). C-terminally of the complement repeats, lipoprotein receptors contain an epidermal growth factor (EGF)-precursor domain with a six-bladed β-propeller. At the acidic pH within endosomes, the propeller forms an intra-molecular bond with the ligand binding modules, thereby displacing attached ligands (Rudenko G *et al.*, 2002; Konecsni T *et al.*, 2009). In LDLR and VLDLR there is a heavily O-glycosilated domain before the trans-membrane domain. The cytoplasmic tail of the receptors contains a clathrin-localization sequence, required for clathrin-mediated endocytosis (Brown MS *et al.*, 1997) (Figure 4).
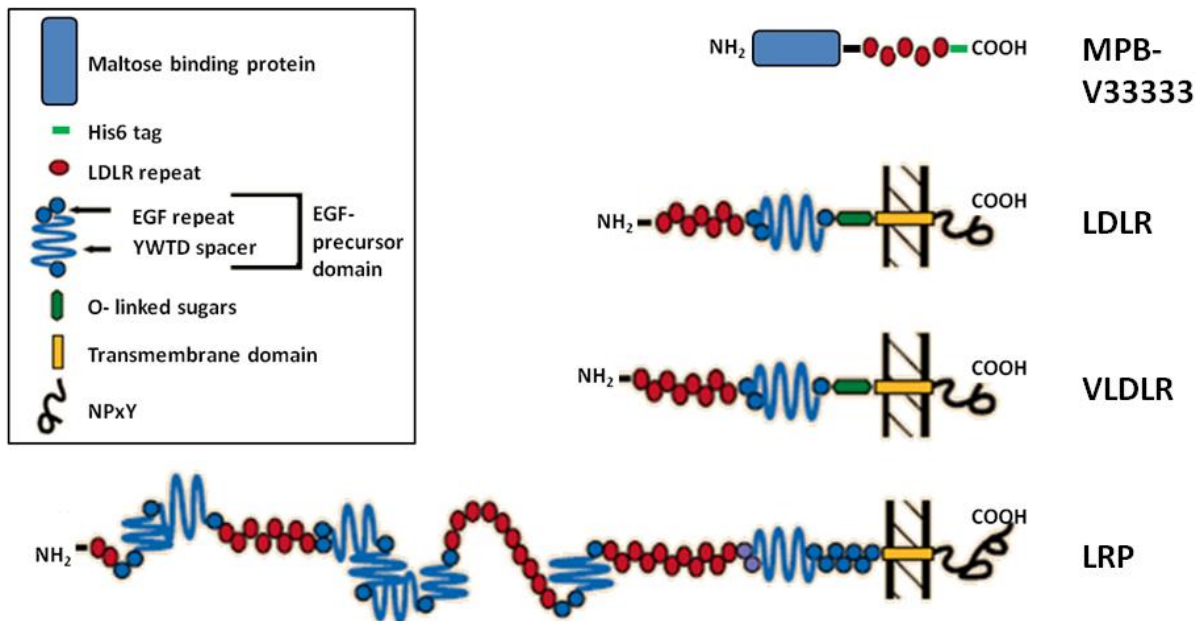
Figure 4 Scheme of low-density lipoprotein receptors, binding minor group rhinoviruses, and of a recombinant VLDLR mini-receptor, used in the current thesis. Low-Density Lipoprotein Receptor (LDLR), Very-Low-Density Lipoprotein receptor (VLDLR), and LDLR-Related Protein (LRP), the receptors of minor group rhinoviruses, contain three important domains for rhino-viral infection. At the N-terminus or throughout LRP, various numbers of complement type repeats (red) constitute the ligand binding domain. The β-propeller (YWTD) within the epidermal growth factor (EGF) precursor domain (blue) interacts with the complement repeats at acidic pH of endosomes, so that bound virus is dissociated. Finally, the cytoplasmic tail contains a clathrin-localization sequence (NPxY), required for clathrin-mediated endocytosis. Soluble VLDLR mini-receptors, used for studying virus-receptor interactions *in vitro*, consist of different binding modules, fused to maltose-binding protein (MBP) for solubility, and of a His6 tag for purification. V33333, a concatemer of the high affinity binding module 3, was used in the current thesis. Adapted from Brown MS *et al.* (1997).

23

Binding of VLDLR to the minor group virus HRV2 is best studied. Of the eight binding modules, complement repeats V2 and V3 attach to the virus, with the latter having the highest affinity (Neumann E *et al.*, 2003; Verdaguer N *et al.*, 2004). X-ray structures of concatemers V23 or V33333, bound to HRV2, showed receptor binding on the star-shaped dome at the 5-fold axis. One complement repeat is attached per viral protomer, interacting with the surface loops BC, DE and HI of two adjacent VP1s. (Verdaguer N *et al.*, 2004; Querol-Audi J *et al.*, 2009) (Figure 5).
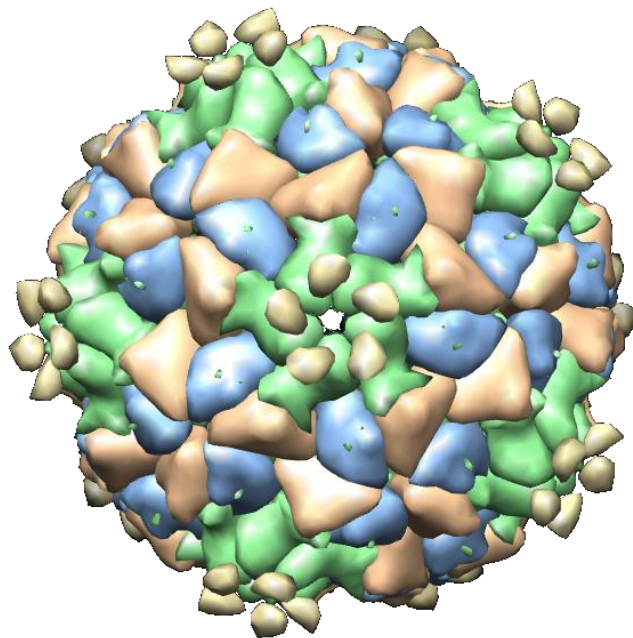
Figure 5 X-ray structure of V33333 bound to HRV2, view on 5-fold axis. The binding modules of the VLDLR mini-receptor attach to HRV2 in a ring-like structure around the star-shaped dome of the viral 5- fold axis. One complement repeat (yellow) interacts with two adjacent VP1 proteins (green). VP2 (rose) and VP3 (blue) are not involved in receptor binding (Querol-Audi J *et al.*, 2009).

The mini-receptor V33333 attaches to all five VP1s at a viral vertex, forming a ring-like structure. Occupancy of 100 %, with 12 receptor molecules per virion, was observed (Querol-Audi J *et al.*, 2009, Konecsni T *et al.,* 2004). Of all investigated

VLDLR-derived mini-receptors, V33333 has the highest binding avidity towards HRV2, without causing significant aggregation (Verdaguer N *et al.*, 2004; Moser R *et al.*, 2005; Wruss J *et al.*, 2007). In the current thesis, it was thus chosen for binding HRV2 to liposomal membranes.

3.6 Infection pathway

Upon binding to lipoprotein receptors on the cell surface, minor group rhinoviruses are taken up by clathrin-mediated endocytosis (Snyers L *et al.*, 2003). If this pathway is blocked, internalization can also occur via clathrin-independent routes (Bayer N *et al.*, 2001; Huber M *et al.*, 2001). In both cases, virus is trafficked to early endosomes. At their mildly acidic pH (pH 6.5 to pH 6.0) (Mellman I *et al.*, 1986; Mukherjee S *et al.*,1997), the ligand binding domain of the receptor folds back and interacts with the β-propeller, thereby displacing the bound cargo (Brabec M *et al.*, 2003; Konecsni T *et al.*, 2009). The lipoprotein receptors are recycled to the cell surface, whereas released virus is further trafficked to endosomal carrier vesicles and late endosomes. Values of pH below pH 5.8 trigger conformational changes of the viral capsid, generating hydrophobic A-particles. It is believed that externalized, amphipathic viral residues insert into the endosomal membrane, forming a trans-membrane pore, through which the viral RNA is released into the cytoplasm. Empty capsids remain within intact endosomes and are further trafficked to lysosomes for degradation (Prchla E *et al.,* 1994; Schober D *et al.*, 1998). Although so far never visualized, *in vitro* and *in vivo* data strongly support this pore-hypothesis (Prchla E *et al.*, 1995; Weiss VU *et al.*, 2010). Ten kDa FITC Dextran, co-internalized with HRV2, was released into the

cytoplasm as result of viral infection, whereas 70 kDa FITC-Dextran remained within the endosomal compartment (Brabec M *et al.*, 2005). This indicates that size selective pores formed in the endosomal membrane during HRV2 infection. In addition, HRV2 was shown to transfer its genome into liposomal nanocontainers, filled with a reverse transcription mixture, without inducing leakage of the components (Bilek G *et al.*, submitted).

In the cytoplasm, the positive-sense, single-stranded RNA genome serves as template for protein synthesis and replication. The Internal Ribosomal Entry Site (IRES) in the 5' UTR recruits ribosomes, translating a polyprotein composed of structural and non-structural proteins. It is autocatalytically cleaved by the proteases 2Apro and 3Cpro. The genomic protein VPg serves as primer for transcription of negative-sense RNA by the virally encoded RNA-dependent RNA polymerase, followed by plus-strand synthesis. The accumulating capsid proteins VP0, VP1 and VP3 assemble into pentamers and package the VPg-RNA into non-infectious provirions. Upon maturation, VP0 is cleaved into VP2 and VP4 and the infectious rhinovirus is released from the cell.

The current thesis focuses on the uncoating process of minor group rhinoviruses, especially on the structure of subviral particles.

3.7 Subviral particles

Native HRVs, released from host cells, are metastable. They traffic their viral RNA between target cells. Exposure to pH values below pH 5.8, as found in endosomal carrier vesicles and late endosomes, triggers conformational changes of the capsid and

the formation of subviral particles. The inner capsid protein VP4 is expelled and the amphipathic N-terminus of VP1, internal in native virions, is externalized. The resulting hydrophobic A-particle interacts with the endosomal membrane and subsequently releases its RNA genome into the cytoplasm, leaving behind the empty capsid or B-particle.

Lonberg-Holm K and Noble-Harvey J (1973) first isolated subviral particles A and B from extracts of infected cells 15 min and 60 min post infection, respectively. Both exhibit changed antigenicity, when compared to native virus, and fail to bind to the cellular receptor (Lonberg-Holm K and Yin FH, 1973; Noble J and Lonberg-Holm K, 1973; Neubauer C *et al.*, 1987). In addition, they can be distinguished by difference in sedimentation behavior in density gradients or varying electrophoretic mobilities (Lonberg-Holm K and Noble-Harvey J, 1973; Okun VM *et al.*, 2002; Weiss VU, 2009).

Both particle species can also be generated *in vitro*. They show comparable antigenicity, sedimentation and polypeptide composition as their equivalents, found in infected cells (Korant BD *et al.*, 1972; Lonberg-Holm K and Noble-Harvey J, 1973). Findings on particles, generated *in vitro*, may thus be applied to *in vivo*.

3.7.1 A-particle

A-particles are stable intermediates of the uncoating process. They are found in infected cells 15 min post infection but can also be generated *in vitro* by exposure to acidic pH or incubation at elevated temperatures (Korant BD *et al.*, 1972; Lonberg-Holm K and Yin FH, 1973; Lonberg- Holm K and Noble- Harvey J, 1973; Weiss, VU, 2009). They have expelled the inner capsid protein VP4 and externalized the N-terminus of VP1, but still harbor their RNA genome. In density gradients, they sediment

about 10 % more slowly than native virions i.e. at 135 S instead of 150 S. Being hydrophobic, A-particles attach to membranes and *ex vivo* isolates were found to be associated with cellular membranes (Lonberg-Holm K and Korant BD, 1972; Lonberg-Holm K *et al.*, 1976).

3.7.2 B-particle

A so far unknown trigger converts A- into B-particles. They are empty protein capsids and the final stage of the uncoating process. In addition to loss of VP4 and externalization of the VP1 N-terminus, they have also released their RNA genome, sedimenting thus at 80 S. *In vitro*, they can be formed by exposure to elevated temperatures.

The cryo-EM structure of heat- induced B-particles, generated by incubation of native HRV2 at 55 °C for 30 min, was solved to 15 Å resolution. It allows more detailed insights into the conformational changes the capsid undergoes during uncoating. Compared to native virions, the capsid of B-particles expands by about 4 %. Structural rearrangements at the 2-fold axis cause a thinning of the capsid and formation of protuberances at its inner surface. The star-shaped dome at the 5-fold axis rotates by 7 degrees, opening a 10 Å wide channel. This pore has been suggested as exit site of the viral genome (Hewat EA *et al.*, 2002) (Figure 6).

Native HRV2 | B- particle
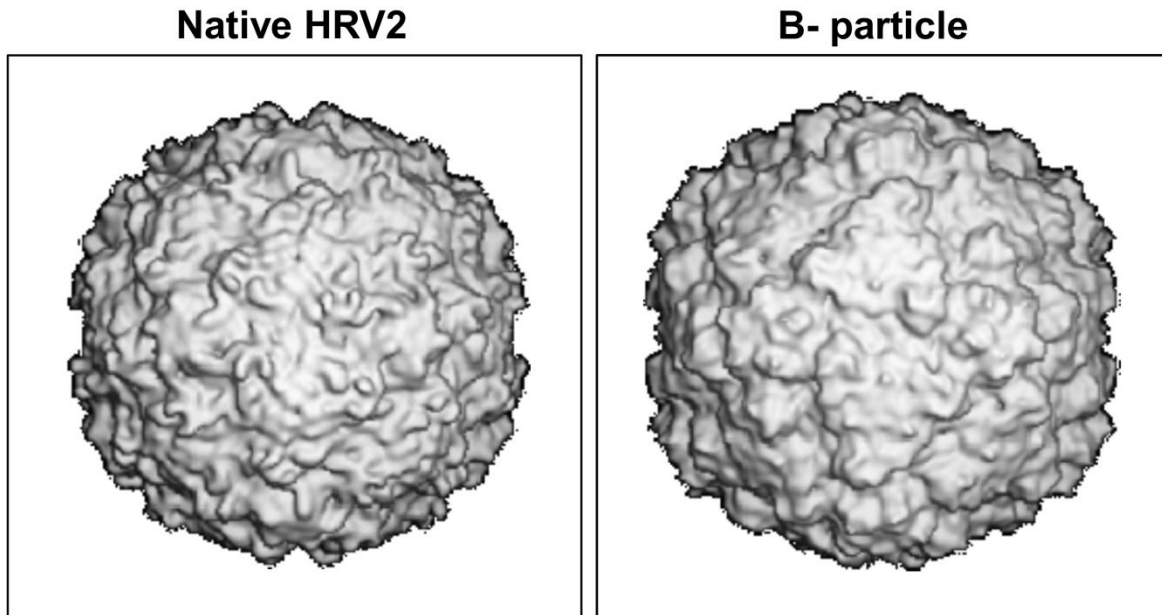
Figure 6 B-particles are 4 % larger than native HRV2 and have a 10 Å large pore at the 5-fold axis. The X-ray structure of native HRV2, filtered to 12 Å resolution, is shown in comparison to the EM map of heated-induced B-particles at 15 Å. Upon uncoating, HRV2 expands by 4 %. The star-shaped 5-fold axis rotates clockwise, opening a channel. Figure from Hewat EA *et al.* (2002).

4 Objectives

Structural data is available for the start and endpoint of rhino-viral uncoating, but little is known about intermediates, such as A-particles. It was the goal of the first part of this thesis, to determine a medium resolution structure of A-particles.

As *in vivo* uncoating occurs in close proximity to the endosomal membrane, the second part of this thesis examines viral conversion in the context of membranes. By investigating uncoating intermediates from a structural point of view, we expect deeper insights into early events of rhino-viral infection.

5 Materials and Methods

5.1 Materials

5.1.1 Chemicals

All chemicals were purchased from Sigma Aldrich (Steinheim, DE), if not indicated otherwise. Lipids were obtained from Avanti Polar Lipids (Alabastar, US).

5.1.2 Antibodies

Antibody conjugates were bought from Jackson ImmunoResearch Laboratories (West Grove, US).

5.1.3 Cells

HeLa Ohio cells were obtained from the European Collection of Cell Culture.

5.1.4 Virus

Human rhinovirus serotype 2 (HRV2) was originally obtained from the American Type Culture Collection (ATCC). Its identity was routinely confirmed with guinea pig anti-HRV2 antibodies from ATCC.

5.2 Methods

5.2.1 Cell propagation

HeLa Ohio cells were grown in Minimal Essential Medium (MEM) supplemented with 1 % L-glutamine (GIBCO, Paisley, GB), 10 % heat-deactivated fetal calf serum,

and 1 % penicillin/streptomycin (GIBCO, Paisley, GB) at 37 °C and 5 % CO2. For splitting, cells were washed with PBS and detached with trypsin-EDTA (PAA, Pasching, AT). Trypsin was deactivated with growth medium. Cells were pelleted in a Heraeus Megafuge 1.0 (Kendro, Langenselbold, DE) at 1200 rpm for 5 min, resuspended in growth medium and split accordingly for further cultivation.

5.2.2 Virus growth and purification

HeLa Ohio cells were grown to confluence in 18 162 cm2 tissue culture flasks, detached as described above and transferred to 6 L MEM supplemented with 7 % horse serum (GIBCO, Paisley, GB), 1 % L-glutamine (GIBCO, Paisley, GB) and 1 % penicillin/streptomycin (GIBCO, Paisley, GB) (Suspension Medium). Suspension cultures were grown in spinner flasks at 37 °C and 25 rpm rotation for 4 days. Cells were pelleted in a in a J6-HC Beckman centrifuge (Beckman Coulter, Brea, US), using a JLA rotor at 2000 rpm and room temperature (RT) for 15 min. They were resuspended in MEM supplemented with 2 % horse serum (GIBCO, Paisley, GB), 3 mM MgCl2, 1 % L-glutamine (GIBCO, Paisley, GB), and 1 % penicillin/streptomycin (GIBCO, Paisley, GB) (Infection Medium). Cells were infected with HRV2 at a multiplicity of infection (MOI) of 1 and incubated for 16.5 h in a Heraeus Thermo electron corp. incubator at 34 °C and 25 rpm rotation. Cells were pelleted in a J6-HC Beckman centrifuge using a TY.JS4.2 rotor at 4200 rpm and 4 °C for 15 min. The pellet was resuspended in 60 mL 10 mM Tris- HCl pH 7.4, 10 mM EDTA (Virus Buffer B) and subjected to three cycles of freezing at -80 °C and thawing. It was dounced 40 times in a tight fitting vessel. After 3 min sonication, 60 mL 20 mM Tris- HCl pH 7.5, 2 mM MgCl2 (Virus Buffer A) were added and cell debris was pelleted in a RC5C Sorvall Centrifuge (Thermo Fisher

Scientific, Waltham, US), using an SS34 rotor at 20000 rpm and 4 ºC for 30 min. Virus in the supernatant was pelleted in an XL-70 Beckman Ultracentrifuge (Beckman Coulter, Brea, US), using a Ti45 rotor at 30000 rpm and 4 ºC for 2 h. The pellet was resuspended in 2 mL virus buffer A and digested with 50 µL 5 mg/ml DNase 1 (Roche, Wien, AT), 5 mg/ml RNase A (Roche, Wien, AT) for 10 min at RT. 500 µL trypsin-EDTA were added and it was incubated at 37 ºC for 5 min. The solution was adjusted to 10 % N-lauryl sarcosine and left over night (ON) at 4 ºC. After removal of insoluble material by pelleting in a 5415 D Eppendorf table top centrifuge (Eppendorf, Hamburg, DE) at 14000 rpm, the supernatant was applied to a 30 mL 7.5 % - 45 % sucrose gradient in virus buffer A and centrifuged in an XL-70 Beckman Ultracentrifuge, using an SW28 rotor at 25000 rpm and 4 ºC for 3.5 h. Virus bands were visible upon illumination from above and were extracted with needle and syringe. The virus was pelleted in an XL-70 Beckman Ultracentrifuge, using an SW28 rotor at 25000 rpm and 4 ºC ON. Purified virus was resuspended in 200 µL 50 mM Na borate pH 7.4. Borate buffer was chosen for quality analysis in capillary electrophoresis.

5.2.3 Generation of subviral A-particles

Purified HRV2 in 50 mM Na borate pH 7.4 was brought to pH 5.0 with 1.4 volumes 50 mM Na acetate pH 5.0 for 15 min at RT, reneutralized with 1.2 volumes 100 mM Na borate pH 8.3 and incubated for 1 h at RT. If indicated, the protocol by Korant BD *et al.* (1972) was used. Virus was mixed with an equal volume of 1 M Tris-HCl pH 5.0, incubated at RT for 20 min, chilled on ice and re-neutralized with one volume 0.5 M Tris base.

5.2.4 Immunization of rabbits

To generate antibodies against the VP1 N-terminus (VP1-NT), a rabbit was immunized with 1 mg VP1-6K peptide. It consists of the 24 N-terminal amino acids of VP1 plus 6 C-terminal Lysines for solubility (NPVENYIDEV LNEVLVVPNI NSSN KKKKKK). After 20 days and 42 days, the rabbit obtained boosts of 1 mg peptide each. It was sacrificed 75 days after the first injection.

5.2.5 Activity ELISA of anti-VP1-NT serum

The peptide VP1-6K was bound to a micro- titer plate at 5 µg/well in 50 mM Tris pH 8.0. It was blocked with 1 % BSA/50 mM Tris pH 8.0. Pre-immune and immunized rabbit serum were applied in a 1:3 dilution series from 1:100 to 1:81000 in 50 mM Tris pH 8.0. Binding of antibodies was detected with goat anti-rabbit HRP conjugates at a 1:10k dilution in 1 % BSA/50 mM Tris pH 8.0. As background controls, rabbit serum at 1:300 dilution was added to BSA- coated wells or it was replaced by BSA on peptide coated wells. It was incubated in 100 µL/well substrate solution of 100 mM Na acetate pH 6.0, 30 µg/mL TMB, 1:3000 H_2O_2 in until a visible signal developed. The reaction was quenched with 50 µL/well of 1 M H_2SO_4. The absorbance at 450 nm was measured with a Multiskan RC plate reader (Labsystems, Quickborn, DE).

5.2.6 Antibody purification

A 1 mL HiTrap rProtein A column (GE Healthcare, Waukesha, US) was equilibrated with 10 column volumes 100 mM Tris pH 8.0. Rabbit serum, adjusted to 100 mM Tris pH 8.0, was applied in 1 mL aliquots and the column was washed with five column volumes of 100 mM Tris pH 8.0. Bound antibodies were eluted with 100 mM

glycine pH 3.0 into 1/10th volume 1 M Tris pH 8.0. Protein containing fractions were checked for purity on a 15 % reducing SDS gel.

5.2.7 Generation of Fab fragments

Purified IgGs were dialysed against 100 mM NaAcetate pH 5.5 ON and concentrated to roughly 5 mg/ml using centriprep concentrators with a molecular weight cut-off of 30 kDa (Amicon, Beverly US). Cysteine and EDTA were added to final concentrations of 50 mM and 1 mM, respectively. Ten µg papain (Roche, Wien, AT) were added per mg antibody and the mixture was incubated at 37ºC for 75 min. The digestion was quenched in 75 mM iodoacetamide at RT for 30 min. The papain reaction mix was dialysed against 50 mM Tris pH 8.0 ON.

5.2.8 Purification of Fab fragments

A 1 mL HiTrap rProtein A column was equilibrated with 50 mM Tris pH 8.0. The papain digestion mix in 50 mM Tris pH 8.0 was applied in 5 mL aliquots. The column was washed with five column volumes 50 mM Tris pH 8.0. The Fab containing flow through was collected and concentrated using centriprep concentrators with a molecular weight cut-off of 30 kDa. Bound Fc fragments and undigested antibodies were eluted with 100 mM glycine pH 3.0 into 1/10th volumne 1 M Tris pH 8.0. The purity of isolated Fab fragments was checked on 15 % reducing and non-reducing SDS gels.

5.2.9 Detection of Fab binding to viral proteins by Western Blot

Ten µg HRV2 and 10 µg HRV14 as control were run on a 15 % reducing SDS gel. An Immobiolon transfer membrane (Millipore, Billerica, US) was pre-activated with methanol and proteins were blotted in 25 mM Tris-HCl pH 8.0, 30 % methanol, 194 mM

glycine (Blotting Buffer) for 1.5 h, using a Transfer SD Semi-Dry Transfer Cell (Biorad, Hercules, US). The membrane was blocked with 5 % dry milk powder in PBS for 1 h at RT (Maresi, Vienna, AT). Fab fragments were added at 11 µg/mL and incubated for 1.5 h at RT. Immune-complexes were detected with goat anti-rabbit HRP conjugates at 1:10000 dilution for 1 h. The membrane was soaked in a substrate solution of 1:1 SuperSignal West Pico Stable Peroxide solution : SuperSignal West Pico Luminol/Enhancer Solution (ThermoFisher, Waltham, US). CL-X Posure X-ray films (ThermoFisher, Waltham, US) were exposed to the membrane and developed in a CURIX 60 developing machine (AGFA, Mortsel, BE). As control, a separate gel was stained with coomassie brilliant blue after SDS gel electrophoresis.

5.2.10 Purification of A-particle:Fab complexes

Seventy-three µg freshly made A-particles were incubated with 10 mg Fab fragments for 30 min at RT. This corresponds to a molar ratio of Fab:VP1 of 370:1. Samples were applied to an 11 mL 7.5 % - 45 % sucrose density gradient in Virus Buffer A and centrifuged in an XL-70 Beckman Ultracentrifuge, using an SW Ti45 rotor at 35000 rpm and 4 ºC for 2 h. Fractions (0.5 mL) were collected from the top of the gradient and complexes were identified by anti-rabbit and anti-HRV2 dot blot.

An Immobilon transfer membrane was activated with methanol and rinsed with Blotting Buffer. Five µL of each fraction were applied, as positive control 0.4 µg HRV2 or 1.6 µg Fab were used. The membrane was air dried and blocked with 5 % dry milk powder in PBS. For detection of virus, the monoclonal antibody 8F5 (Skern T *et al.*, 1987), diluted 1:1000 in 5 % milk/PBS, was bound for 1 h at RT, followed by a goat anti-mouse HRP conjugate, diluted at 1:10000 dilution in 5 % milk/PBS for 1 h at RT. Fab

fragments were directly detected with a goat anti-mouse HRP conjugate at 1:10000 dilution in 5 % milk/PBS. The membrane was soaked in a substrate solution of 1:1 SuperSignal West Pico Stable Peroxide solution : SuperSignal West Pico Luminol/Enhancer Solution (ThermoFisher, Waltham, US). CL-X Posure X-ray films (ThermoFisher, Waltham, US) were exposed to the membrane and developed in a CURIX 60 developing machine (AGFA, Mortsel, BE).

Complex-containing fractions were pooled, adjusted to 10 mL with Virus Buffer A and pelleted ON in an XL-70 Beckman Ultracentrifuge, using an SW Ti45 rotor at 35000 rpm and 4 ⁰C. The pellet was resuspended in 15 µL 50 mM Na borate pH 8.3.

5.2.11 Preparation of recombinant receptor V33333

E.coli TB1 were transformed with the maltose-binding protein (MBP)-V33333-His6 fusion protein in the expression vector pMalc2b (Moser R *et al.*, 2005). The recombinant receptor was expressed according to Ronacher B *et al.* (2000) with modifications. Briefly, bacteria were grown in 1 L LB medium at 37 ⁰C to a density of A600 of 0.7. Protein expression was induced with 0.3 mM IPTG at 30 ⁰C ON. Cells were pelleted in a Sorvall RC5C centrifuge, using a GS-3 rotor at 5000 rpm and 4 ⁰C for 20 min. The pellet was resuspended in 30 mL 25 mN Tris- HCl pH 7.5, 150 mM NaCl, 2 mM CaCl2 (TBSC) and sonicated 6 times for 10 s on ice, using a Bandelin Sonoplus HD200 sonicator (Bandelin, Berlin, DE). Cell debris was pelleted in a Sorvall RC5C centrifuge, using an SS34 rotor at 19000 rpm and 4 ⁰C for 20 min. The supernatant was incubated with 5 mL Ni-NTA slurry (Qiagen, Venlo, NL) for 2 h at RT. Ni-NTA beads were separated by centrifugation in a Heraeus Megafuge 1.0 at 4000 rpm and 4 ⁰C for 10 min. They were washed three times with 30 mL 10 mM imidazole/TBSC for 20 min

each. Receptor was eluted in 4 mL aliquots with 0.2 M imidazole/TBSC. The eluted fractions were dialysed at 4 ºC against 1 mM cystamin, 10 mM cysteamin in TBSC with buffer changes 3 times per day until imidazole was diluted below 10 µM.

5.2.12 Liposome Preparation

Table 1 Lipids and their molar ratios used for preparation of large, uni-lamellar vesicles

Lipid	Abbreviation	Ratio [mol]
Cholesterol	Ch	1.5
1-palmitoyl-2-oleoyl-sn-glycero-3-phosphocholine	POPC	1
L-α-phosphatidylethanolamine	PE	1
Sphingomyelin	SM	1
1,2,-dioleoyl-sn-glycero-3-[(N-(5-amino-1-carboxypentyl) iminodiacetic acid) succinyl] (nickel salt)	DGS-NTA	0.5
1-oleoyl-2-[12-[(7-nitro-2-1,3-benzoxadiazol-4-yl)amino] lauroyl]-sn-glycero-3-phosphocholine	NBD-PC	0.05

Lipids, dissolved in chloroform, were mixed at molar ratios shown in Table 1 to a total amount of 10.1 µmol lipid. The mixture was rotated in a point bottom flask under a continuous stream of nitrogen gas, using a Büchi Rotavapor (Büchi Labortechnik GmbH, Essen, DE) at 55 rpm for 3 h. The dried lipid film was hydrated in 1.3 mL 50 mM Tris pH 8.0 at 45 rpm for 2 h, with three short intervals of vortexing during the last 30 min. The suspension of multi-lamellar vesicles was stored over night at 4 ºC. Liposomes were homogenized to large, uni-lamellar vesicles (LUVs) by sequential extrusion through 400 nm and 200 nm polycarbonate membranes (Whatman, Kent, GB), using a mini extruder (Avanti Polar Lipids, Alabaster, US).

5.2.13 Preparation of membrane-attached viral particles

Large uni-lamellar vesicles, containing NTA-lipids, were decorated with His6-tagged V33333 mini-receptor for 30 min at RT. Purified HRV2 was bound for 30 min at RT. Molar ratios were as indicated in the results section.

5.2.14 Flotation of liposome-containing samples

Samples were adjusted to 200 µL 50 % sucrose in 50 mM Tris pH 8.0. They were sequentially overlaid with 0.9 mL 25 % sucrose/ 50 mM Tris pH 8.0 and 0.9 mL plain buffer. Samples were subjected to ultracentrifugation in an Optima Benchtop Ultracentrifuge (Beckman Coulter, Brea, US), using a TLS55 swing-out rotor at 45000 rpm and 4 °C for 4 h. 167 µL aliquots were taken from the top of the gradient. Liposome-containing fractions were identified by fluorescence measurements, using a Wallac 1420 Victor V plate reader (Perkin Elmer, Waltham, US) at 485 nm and 535 nm excitation and emission wavelength, respectively. The virus concentration of individual fractions was determined by end point dilution assays (TCID50) (Blake K and O'Connell S, 1993). The fraction with highest fluorescence was used for further experiments.

5.2.15 Preparation of membrane-attached uncoating intermediates

V33333-decorated LUVs were separated from free receptor by flotation. Virus was attached to receptor-decorated liposomes for 30 min at RT at the molar ratios indicated. Five µL of the complex were brought to pH 5.4 with 2.6 µL 1 M Na acetate pH 5.4, as previously determined on a larger scale. After different acidification times, samples were directly applied to carbon-coated copper grids and prepared for negative stain transmission electron microscopy (TEM).

5.2.16 Capillary electrophoresis (CE)

CE measurements were performed on a 3D CE instrument (Agilent, Waldbronn, Germany), using a fused silica capillary of 50 µm inner diameter, 375 µm outer diameter, 60.0 cm total and 51.5 cm effective length (Polymicro, Phoenic, US). Electrophoresis was performed at 2.5 kV (positive polarity mode) with 100 mM Na borate buffer pH 8.3, 10 mM Thesit as background electrolyte (BGE). Viral particles or immune-complexes were diluted with 100 mM Na borate buffer pH 8.3 to the concentrations indicated. Samples were injected with 50 mbar for 9 s and detected via UV adsorption at 205 nm and 260 nm.

5.2.17 Negative stain Transmission Electron Microscopy (TEM)

Carbon-coated copper grids (Agar Scientific, purchased via Groepl, Tulln, Austria) were glow-discharged at 20 mA for 30 min or for 1 min, in case of liposome-containing specimens, in the Bal-Tec SCD Sutter Coater (Scotia, US). Four µL sample was adsorbed for 1 min, washed and stained with 2 % Na phosphor-tungstate pH 7.2 for 1 min. Specimens were imaged in a n 80 kV FEI Morgagni 268 transmission electron microscope (Hillsboro, US) and images were taken, using an 11 Mpixel Morada CCD camera.

5.2.18 Cryo-TEM

Viral samples were frozen as described in Resch GP *et al.* (2011). Briefly, Quantifoil 400 nm copper grids with a 1.2/1.3 holey carbon film (Jena, DE) were glow discharged at 20 mA for 5 min in a Bal-Tec SCD Sputter Coater (Scotia, USA) or for 1 min in an glow discharging device according to Aebi U and Pollard TD (1987). Using the Leica EM Grid Plunger (Vienna, Austria), 4 µL sample were applied per grid in a

humidified chamber at 80 % humidity and 25 °C. Samples were adsorbed for 30 s, blotted for 0.8 s with Whatman filter paper 1 (Kent, GB) and plunge frozen in liquid ethane, cooled with liquid nitrogen to -174 °C.

Cryo-samples were imaged in a FEI Tecnai F30 Polara cryo-TEM (Hillsboro, Oregon, US) at 300 kV, with C2 and objective aperture adjusted to 70 μm and 100 μm, respectively. The nominal magnification was set to 50000 fold. The electron dosage was limited to 20 electrons per Å2. Images were taken between -0.8 μm and -3.5 μm defocus with a GIF 2002 2k CCD camera, using the automatic image acquisition software Leginon (Carragher B *et al.*, 2000).

Samples of membrane-bound HRV2 were frozen on C-flat holey carbon grids (Protochips, Raleigh, North Carolina, USA) and cryo-imaged in a Philips CM200 TEM by Heather A. Holdaway at Purdue University, US.

5.2.19 Icosahedral Reconstruction

For all micrographs, the parameters for correcting the contrast transfer function (CTF) were calculated, using the software ctffind3 within the xmipp package (Mindell JA and Grigorieff N, 2003; Sorzano CO *et al.*, 2004). In case of bad correlations of theoretical and actual Thon rings, the CTF-parameters were additionally determined by hand in bsoft (Heymann JB and Belnap DM, 2007) or robem (Yan X *et al.*, 2007). Images were manually selected for regular Thon rings, extending beyond 10 Å resolution. All further processing steps were done in xmipp (Sorzano CO *et al.*, 2004). Micrographs were phase-flipped. Particles were automatically picked, visually inspected and manually selected for 3D reconstruction. As starting model, the X-ray structure of native HRV2 was scaled to the radial average of the particles and filtered to 30 Å.

Particles were assigned to different defocus groups for alignment by icosahedral projection matching. This was sequentially done with images binned by a factor of 2 and unbinned data. For the final reconstruction, 90 % of the particles were used, based on the correlation coefficient of their alignment. 3D maps were corrected for amplitude decay using the program embfactor (Fernandez JJ *et al.*, 2008).

5.2.20 Determination of the actual magnification

The X-ray structure of native HRV2 was scaled to different sizes. It was compared to the reconstructed EM map of native HRV2, using a program by Daniel Luque Buzo. Based on their cross-correlation, the actual size of the reconstruction was determined with respect to the X-ray structure of native HRV2.

5.2.21 Fitting of X-ray coordinates into EM maps

The X-ray coordinates of the viral capsid proteins were written into individual coordinate files, preserving their relative orientations. Using the software UROX 2.0 (Siebert X and Navaza J, 2009), they were fitted into the amplitude-corrected electron density map, allowing separate movements of the proteins with respect to each other.

6 Results

6.1 Cryo-EM structure of A-particles

The X-ray structure of native HRV2 was solved to 2.6 Å (Verdaguer N *et al.*, 2000) and a cryo-EM map of B-particles was reconstructed to 15 Å (Hewat EA *et al.*, 2002). Structural data is thus available on particles, corresponding to the start and end point of the uncoating process. However, little is known about the conformational changes involved and the structure of intermediates.

A-particles, stable intermediates of the uncoating process, were already described by Lonberg-Holm K and Korant BD in 1972, but for rhinoviruses, they have so far not been addressed from a structural point of view. It was the aim of the first part of this thesis to obtain a medium resolution structure of A-particles and, by comparison to native HRV2, to gain further insights into the structural changes, minor group HRVs undergo during uncoating.

Upon binding to their cellular receptor, minor group HRVs are endocytosed and transported to endosomes. The low pH environment within these vesicles triggers an irreversible conformational change, leading to the formation of hydrophobic A-particles (Korant BD *et al.*, 1972). They have expelled their inner capsid protein VP4 but still contain their RNA genome.

These sub-viral particles can be generated *in vitro* by acidification to pH 5.0. They resemble viral particles isolated from HeLa cells 15 min post infection (Lonberg-Holm K and Noble- Harvey J, 1973). Alternatively, A-particles can also be generated by

43

incubation at 56 ºC (Okun VM *et al.*, 2002; Weiss VU, 2009). In the current thesis, the physiological trigger for viral conversion, acidic pH, was chosen to generate A-particles.

6.1.1 A-particles are generated by acidification with buffers of high or low ionic strength

The original protocol by Korant BD *et al.* (1972) suggests 1 M Na acetate pH 5.0 for acidification of 20 min and 0.5 M Tris base for re-neutralization. Such high ionic strength buffers give considerable background in cryo-electron microscopy (EM), the method of choice for structure determination of intermediates, contaminated with other particle species and of unknown long-term stability. Especially in cryo-EM, it is recommended to manipulate the sample as little as possible to avoid damage or deformations. This would introduce structural in-homogeneity, limiting the resolution that can be achieved (Zhou ZH, 2008). For that reason an alternative method for generating A-particles was set up, using low ionic strength buffers. Virus was acidified with 50 mM Na acetate pH 5.0 for 15 min and re-neutralized with 100 mM Na borate pH 8.3.

Both protocols yielded sub-viral particles that had indistinguishable appearances in negative stain transmission electron microscopy (TEM). The contrast material penetrated into the core of A-particles, revealing internal structures, but the genome prevented complete filling of their interior. This partial stain penetration clearly distinguished A-particles from empty capsids, having completely filled cores, and from native virus, that was impermeable to the negative stain and had thus homogeneous density (Figure 7).

Native HRV2	A-particles Korant BD *et al.* (1972)	A-particles Low ionic strength
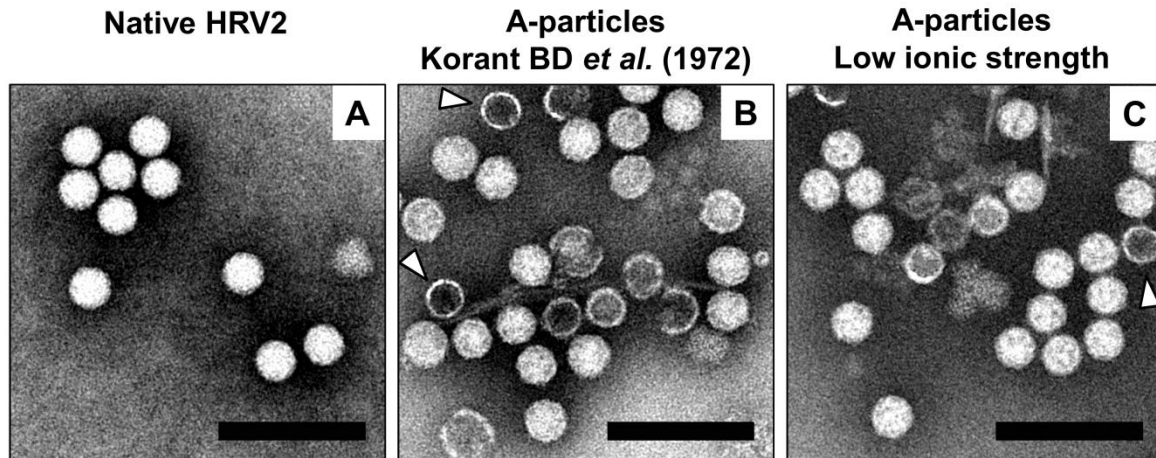
Figure 7 High and low ionic strength acidification: Visually identical A-particles in negative stain TEM. A-particles were generated from purified HRV2 (A) according to Korant BD *et al.* (1972) (B) or by acidification with 50 mM Na acetate pH 5.0 for 15 min and re-neutralization with 100 mM Na borate pH 8.3 (C). Samples were diluted to 0.4 mg/ml, adsorbed to glow-discharged carbon-coated copper grids and stained with 2% phosphotungstate pH 7.2. Images were taken in an 80 kV Morgagni TEM, using an 11 Mpixel CCD camera. Native virus has homogeneous electron density (A), whereas A-particles of both preparations are partially penetrated by the negative stain, revealing internal structures. Both samples additionally contain empty capsids with dark, completely filled cores (arrow heads) and broken particles (B, C). Size bar=100 nm.

Heat-induced A-particles, described by Weiss VU (2009) had identical appearance in negative stain TEM. In contrast, Okun VM *et al.* (2002) observed empty and broken capsids. Characterization of these particles was outside the scope of their work so that the identity of their proposed A-particles was not confirmed.

In parallel, A-particles, generated by different procedures, were analyzed in capillary electrophoresis (CE), a well-established method for separating native virus and sub-viral particles (Okun VM *et al.*, 1999; Kremser L *et al.*, 2006; Kremser L *et al.*, 2009). Acidification with high and low ionic strengths buffers yielded A-particles with identical electrophoretic mobility of $16.6*10-9$ m2/Vs $\pm$ $0.4*10-9$ m2/Vs and $17.4*10-9$ m2/Vs $\pm$ $1.2*10-9$ m2/Vs, respectively. These results were in agreement with CE data from heat-induced A-particles, migrating at $17.8*10-9$ m2/Vs (Weiss VU, 2009) (Figure 8, left panel). Based on their electrophoretic mobility, they could be clearly distinguished

45

from native HRV2 and temperature-triggered B-particles, migrating at 6.6*10-9 m2/Vs ± 0.5*10-9 m2/Vs and 8.5*10-9 m2/Vs (Weiss VU, 2009), respectively (Figure 8, right panel).

As already seen in negative stain TEM, both preparations of acid-triggered A-particles also contained a small fraction of empty capsids. Unlike native virus and A-particles, they lacked UV adsorption at 260 nm, indicating that they had lost their RNA genome. Unlike empty capsids so far described, they were generated by acidification, the physiological trigger, and not by incubation at elevated temperatures. However, with 8*10-9 m2/Vs ± 0.3*10-9 m2/Vs, acid-triggered empty capsids had a similar electrophoretic mobility as head-induced B-particles.
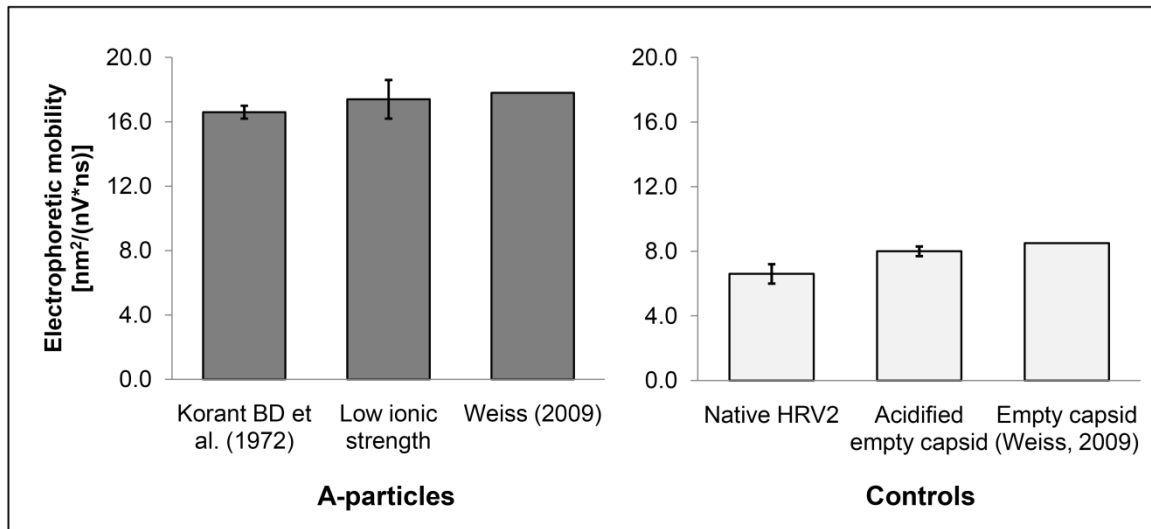
Figure 8 Acidification with high and low ionic strength buffers: A- particle with identical electrophoretic mobility. A-particles were generated from purified HRV2, according to Korant BD *et al.* (1972) or by acidification with 50 mM Na acetate pH 5.0 for 15 min and re-neutralization with 100 mM Na borate pH 8.3. Subviral particles and native virus as control were diluted to 1.1 mg/ml and adjusted to 1:4000 DMSO as marker for the electro-osmotic flow. They were analyzed in capillary electrophoresis, using 100 mM Na borate pH 8.3, 10 mM Thesit as background electrolyte. A-particles prepared by acidification with high and low ionic strength buffers had an electrophoretic mobility of 16.6*10-9 m2/Vs ± 0.4*10-9 m2/Vs (n=5) and 17.4*10-9 m2/Vs ± 1.2*10-9 m2/Vs (n=5), respectively. This corresponds well to the data of heated A-particles, migrating at 17.8 *10-9 m2/Vs, shown for comparison (Weiss VU, 2009). A-particles thus clearly differed from native virus migrating at 6.6*10-9 m2/Vs ± 0.6*10-9 m2/Vs (n=5), from acid-triggered empty capsids with 8*10-9 m2/Vs ± 0.3*10-9 m2/Vs (n=5) and from heated-induced empty capsid with 8.5*10-9 m2/Vs (Weiss VU, 2009) electro-phoretic mobility.

Acidification of purified HRV2 with low ionic strength buffers induced the formation of subviral particles that, in TEM and CE, were found identical to A-particles, generated according to Korant BD *et al.* (1972) or Weiss VU (2009). They were thus directly plunge frozen in liquid ethane and imaged in cryo-electron microscopy. As control, cryo-data were collected from native HRV2.

6.1.2 The cryo-EM structure of native HRV2 validates the chosen reconstruction strategy

As control for cryo-imaging and data processing, cryo-data were collected from native HRV2. Micrographs with regular Thon rings and data extending beyond 10 Å resolution were selected for further processing. Particles were automatically picked, followed by manual sorting. The parameters for the correction of the contrast transfer function (CTF) were automatically determined and manually revised. As starting map for projection matching, the X-ray coordinates of native HRV2 were scaled to the radial average of boxed particles and filtered to 30 Å resolution. Icosahedral refinement was employed until no further improvement in resolution could be achieved. The final reconstruction was corrected for amplitude decay.

The structure of native HRV2 was reconstructed from 7946 particles. It converged at 8.2 Å resolution, according to its Fourier Shell Correlation (FSC) of 0.5.

In surface view, the reconstructed density showed all rhino-viral features, such as the star-shaped mesa at the 5-fold axis and the surrounding canyon. The triangular plateau at the 3-fold axis with its protrusions and the depression at the 2-fold axis were also well visible. The comparison with the X-ray structure, filtered at 8.2 Å, revealed small differences at the 5-fold axis.

As X-ray structure not the experimentally determined electron density map was used. Instead, the X-ray structure was derived from the pdb coordinates, describing an ideal situation. This data contained full amplitude information; more details and thus slight differences were expected for the X-ray map.

In the X-ray structure of native HRV2, the viral genome was not resolved, due to its structural in-homogeneity. Only low density was visible for ordered RNA in close proximity to Tryptophan 2038 of VP2 (Verdaguer N *et al.*, 2000). The EM map had a significantly lower resolution, so that conformational differences of residues, smaller than 8.2 Å, fell under its detection limit. Consequently, also less-ordered regions, such as parts of the viral genome, could be visible in the EM map. Additional density at the inner surface of the capsid, seen in the EM reconstruction, was thus attributed to encapsidated RNA (Figure 9).
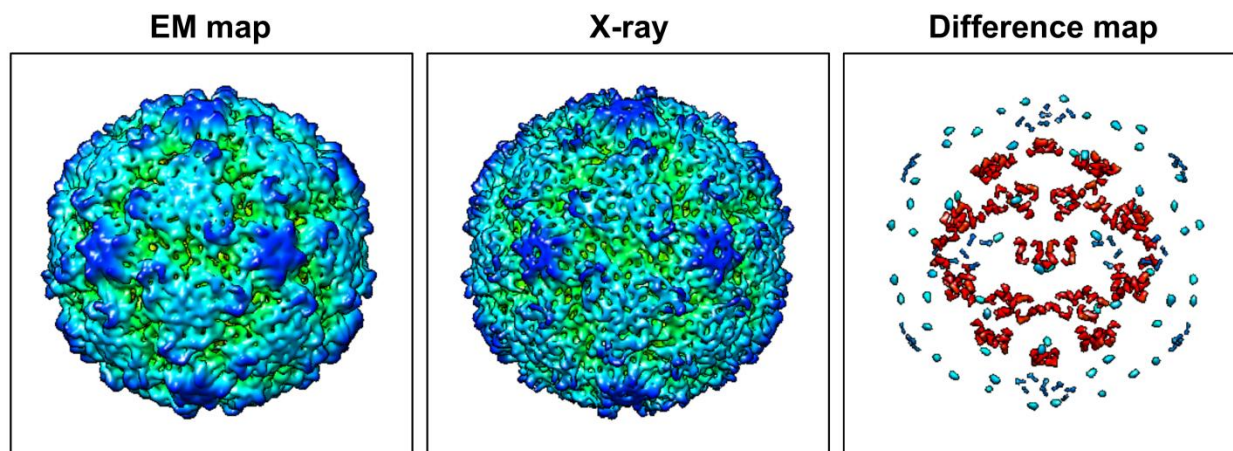
Figure 9 The reconstructed EM map of native HRV2 is comparable to its published X-ray structure but additionally reveals RNA density. 7946 particles of native HRV2 were aligned by icosahedral projection matching. The reconstruction converged at 8.2 Å resolution (left panel). The X-ray structure of native HRV2 (Verdaguer N *et al.*, 2000) was filtered to the same resolution (central panel). The difference map reveals slight differences at the 5-fold axis. Additional density in the EM map, on the inner surface of the capsid, was attributed to RNA (right panel). Graphs were made in chimera and radially colored (Pettersen EF *et al.*, 2004). The EM structure and difference map were presented at 2.5 σ i.e standard deviation of the electron density. The X-ray map was contoured to enclose the same volume as the EM map. In the difference map, densities smaller than 8.23 Å3 were not displayed, as they lay under the resolution limit of the reconstruction.

The X-ray coordinates of the capsid proteins VP1 to VP3 were saved in individual coordinate files. They were fitted into the electron density map of native HRV2 with the software UROX 2.0 (Siebert X and Navaza J, 2009), allowing their independent arrangement with respect to each other. The position of VP4 was kept relative to VP2. Because of its small size, its independent fitting did not converge. The new orientations of the capsid proteins differed from the published coordinates by a root-mean-square-deviation (RMSD) of about 1 Å, which was too small to be resolved at the resolution of the EM map (Figure 10).
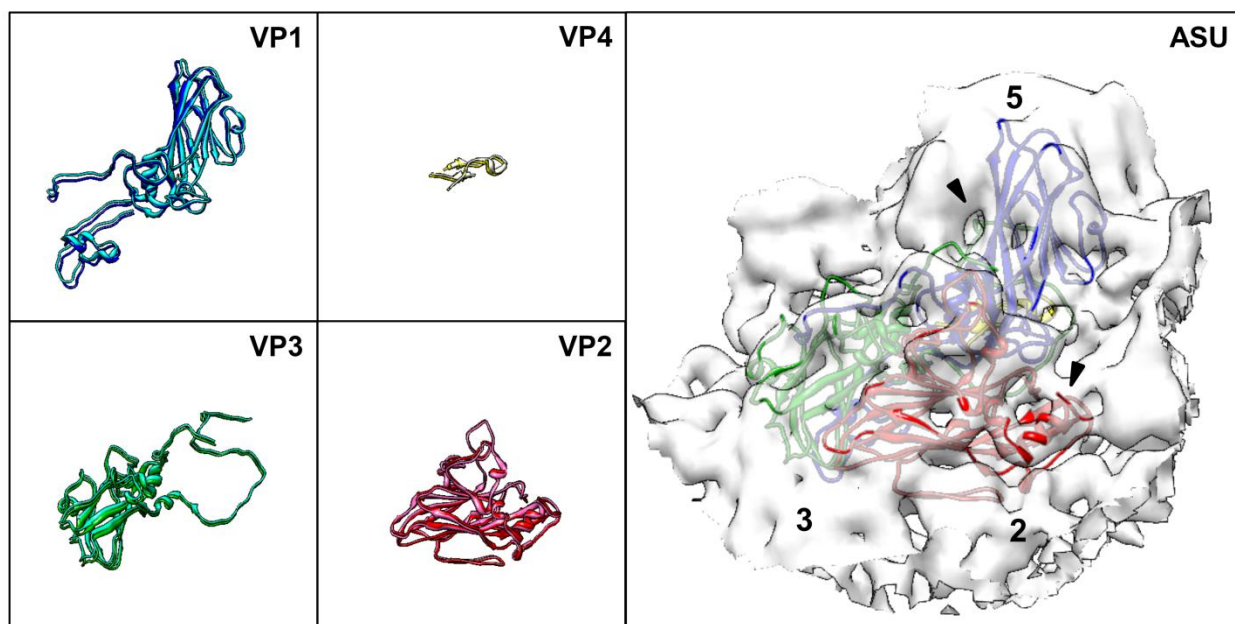
Figure 10 Fitting the X-ray coordinates of VP1 to VP4 into the EM map confirms the original orientations. The coordinates of the capsid proteins VP1 to VP3 were saved as separate coordinate files while VP4 was linked to VP2. The proteins were fitted into the EM density map using the software UROX 2.0 (Siebert X and Navaza J, 2009). The original and fitted coordinates are displayed in light and dark colors, respectively. At the present resolution of 8.2 Å, re-orientations of the capsid proteins by about 1 Å were insignificant (left panel). The fitted coordinates are displayed together with the EM structure, showing well resolved α-helices and β-sheets. This is especially visible for the VP2 α-helix close to the 2-fold axis, and VP1 β-sheets, forming the 5-fold axis (arrow heads). The viral asymmetric unit (ASU) is shown; symmetry axes are indicated by numbers (right panel). Figures were made in chimera.

The successful reconstruction of native HRV2 from cryo-EM data to 8.2 Å resolution validates the chosen cryo-imaging and processing approach.

6.1.3 Structure of HRV2 A-particles at 8.9 Å resolution

Cryo-images of A-particles were processed identically to the data of native HRV2. Projection matching of 15170 particles converged at 8.9 Å resolution, considering a FSC of 0.5.

Comparing the three-dimensional reconstructions of native and A-particles, an overall expansion of the virus by about 4 % to 31.4 nm diameter could be detected upon acidification (Figure 11 and 12). Concomitantly, a pore opened at the depression of the 2-fold axis. The conformational changes involved were most apparent at the inner surface of the capsid, where protuberances at the 2-fold rearranged. In addition, the star-shaped dome at the 5-fold axis rotated clockwise by 11 degrees, creating a channel at its center (Figure 11).
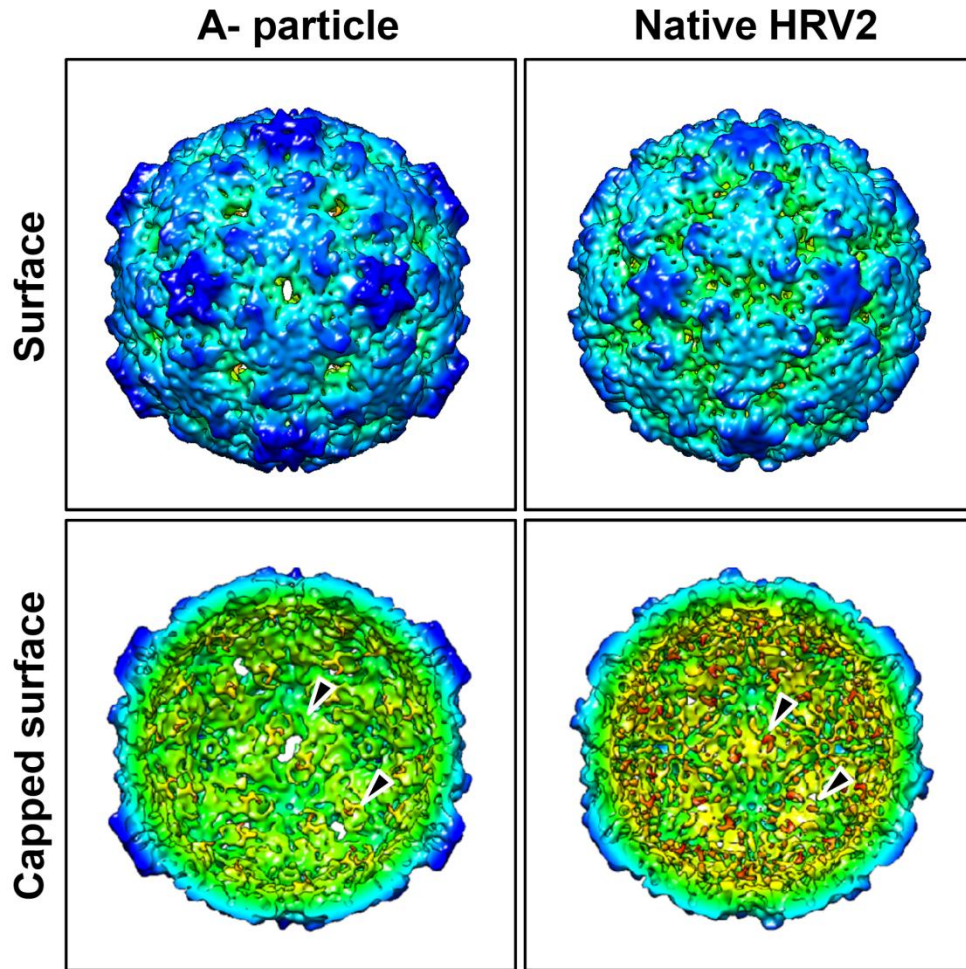
Figure 11 A-particles are 4 % larger than native virus and have pores in their capsid. 15170 A-particles were aligned by icosahedral projection matching and reconstructed to 8.9 Å resolution. For comparison the EM map of native HRV2 was filtered to the same resolution. Upon acidification, viral particles expanded by 4 %. Pores formed at the 2-fold (arrow heads) and 5-fold axes. Figures were made in chimera. Maps were contoured to 2.5 σ and radially colored.

The rotational average of the structure of A-particles revealed an additional peak of density underneath the 3.6 nm thick protein capsid. Empty capsids lacked this signal; it was thus attributed to a shell of viral RNA. Different Class averages of particles also showed this layer of genomic density, excluding that it was an artifact of icosahedral averaging (Figure 12).
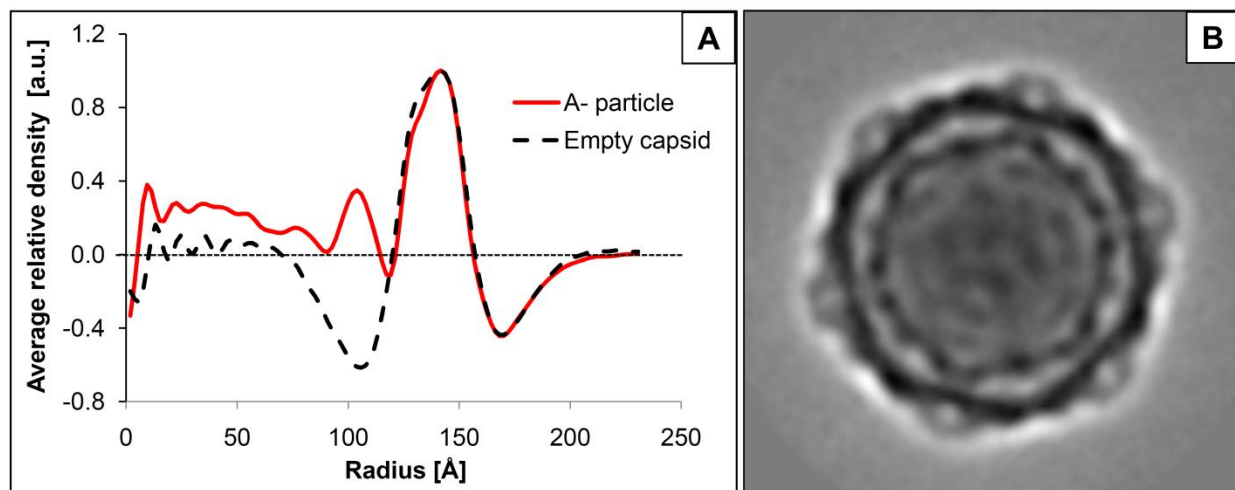
Figure 12 A-particles contain a layer of ordered RNA at the inner surface of the capsid. The 3D reconstruction of A-particles and empty capsids were rotationally averaged, using the software spider (Shaikh TR *et al.*, 2008). For B-particles, the empty protein capsid yields a single peak at a radius of 120 Å to 157 Å. The genomic RNA, only present in A-particles, gives an additional density peak at a radius of 87 Å to 157 Å, in close proximity to the protein shell (A). 3114 images of individual A-particles were aligned and averaged, using maximum-likelihood multi-reference refinement (Scheres SH *et al.*, 2005). The class average of the raw data also shows this layer of ordered RNA density (B).

At contour levels of the 3D map lower than 1.5 σ, the RNA shell became apparent at the inner surface of the protein capsid. In native virions, density for the viral genome was restricted to the 2-fold axis, where limited RNA-protein contacts were already reported in the X-ray structure (Verdaguer N *et al.*, 2000). During conversion from native to A-particle, also the genome expanded and got more ordered. It created a layer of density at the inner surface of the capsid, resolvable at 8.9 Å resolution. At the 2-fold axis the already existing RNA contact with VP2 became more prominent and RNA was visible directly beneath the opening in the capsid. Additional RNA interactions with viral proteins localized to the pseudo-3-fold axis (Figure 13).
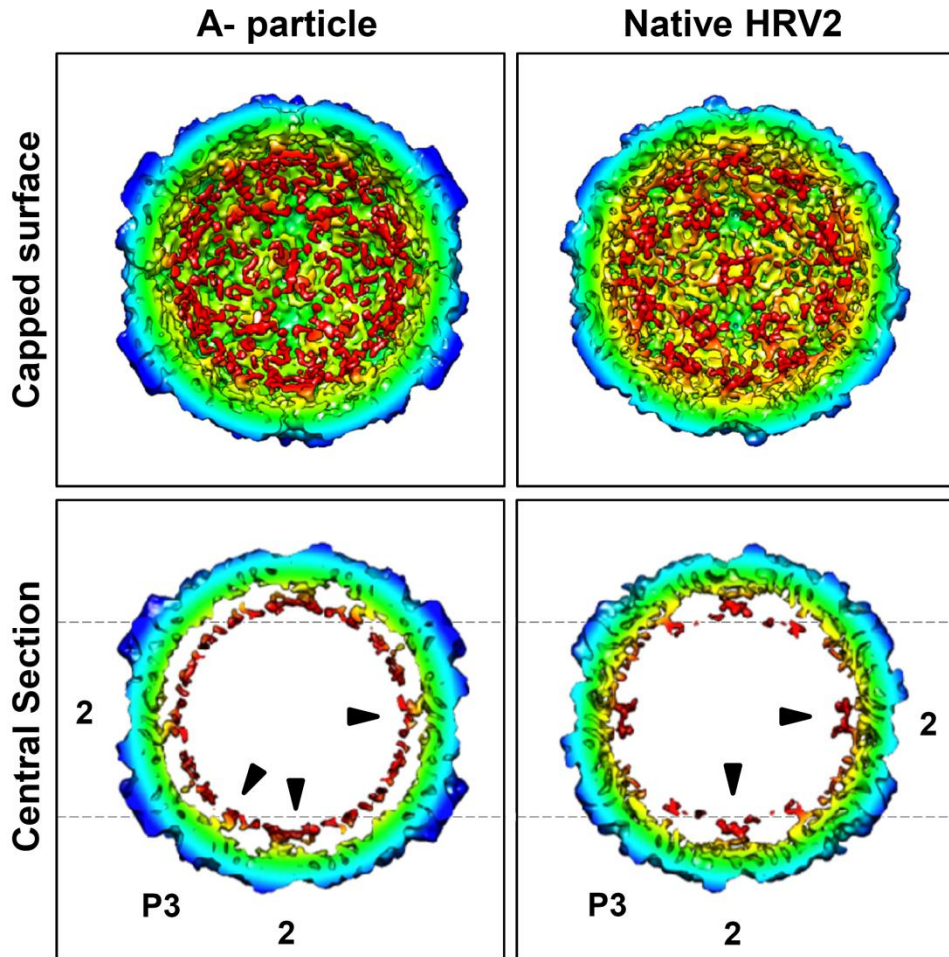
Figure 13 In A-particles, the viral genome contacts the capsid at the 2- and pseudo-3-fold axes. At 1.5 σ contour level, density attributed to RNA, is visible. In native HRV2, few parts of the genome are resolved, contacting the protein capsid at the 2-fold axis. In A-particles, the genome is more ordered and forms a shell in closer proximity to the capsid. RNA-protein interactions localize to the 2- and pseudo-3-fold axes. Figures were made in chimera. Maps are contoured to 1.5 σ and radially colored. Reference lines are shown for better visualization of the RNA expansion.

6.1.4 Fitting the X-ray coordinates of native HRV2 into A-particles reveals the largest changes at the N-terminal residues of VPs

The X-ray coordinates of VP1 to VP3 from native HRV2 were fitted into the EM map of A-particles as described above. Since subviral particles expelled the inner capsid protein VP4, it was excluded from the analysis.

Compared to its position in native HRV2, VP1 in A-particles moved radially outwards by about 7 Å. The β-sheets, that form the 5-fold axis, shifted clockwise, opening a channel at the center of the star-shaped dome.

Based on data from the related poliovirus (Fricks CE and Hogle JM, 1990), Hewat EA *et al.* (2002) suggested that during conversion from native rhinovirus to A-particles, the N-terminus of VP1 got externalized. Accordingly, in the EM structure of A-particles, no density on the inside of the capsid could be attributed to the 60 N-terminal residues of VP1. Instead, new density appeared on the surface of the particle at the pseudo-3-fold axis, at the junction of VP1 to VP3. After docking the X-ray coordinates of VP1 to VP3 into the EM map of A-particles, this new density was not occupied by any of the protein residues. In addition, it was in proximity to the last resolved N-terminal amino acid of VP1. It may thus represent its externalized N-terminus (Figure 14).

Supporting these data, there was a spherical region of low density i.e. a solvent-filled bubble at the pseudo-3-fold axis of native HRV2. Upon conversion to A-particles, this area is filled with density, most likely the exiting VP1 N-terminus (Figure 34).

In the cryo-EM structure of heat-induced B-particles, Hewat EA *et al.* (2002) also described missing density for the 59 N-terminal residues of VP1on the inside of the capsid. They also observed the appearance of density in the formerly solvent-filled bubble at the pseudo-3-fold axis. It was thus proposed as exit site for the VP1 N-terminus. However, they did not describe the appearance of additional density on the surface of B-particles.
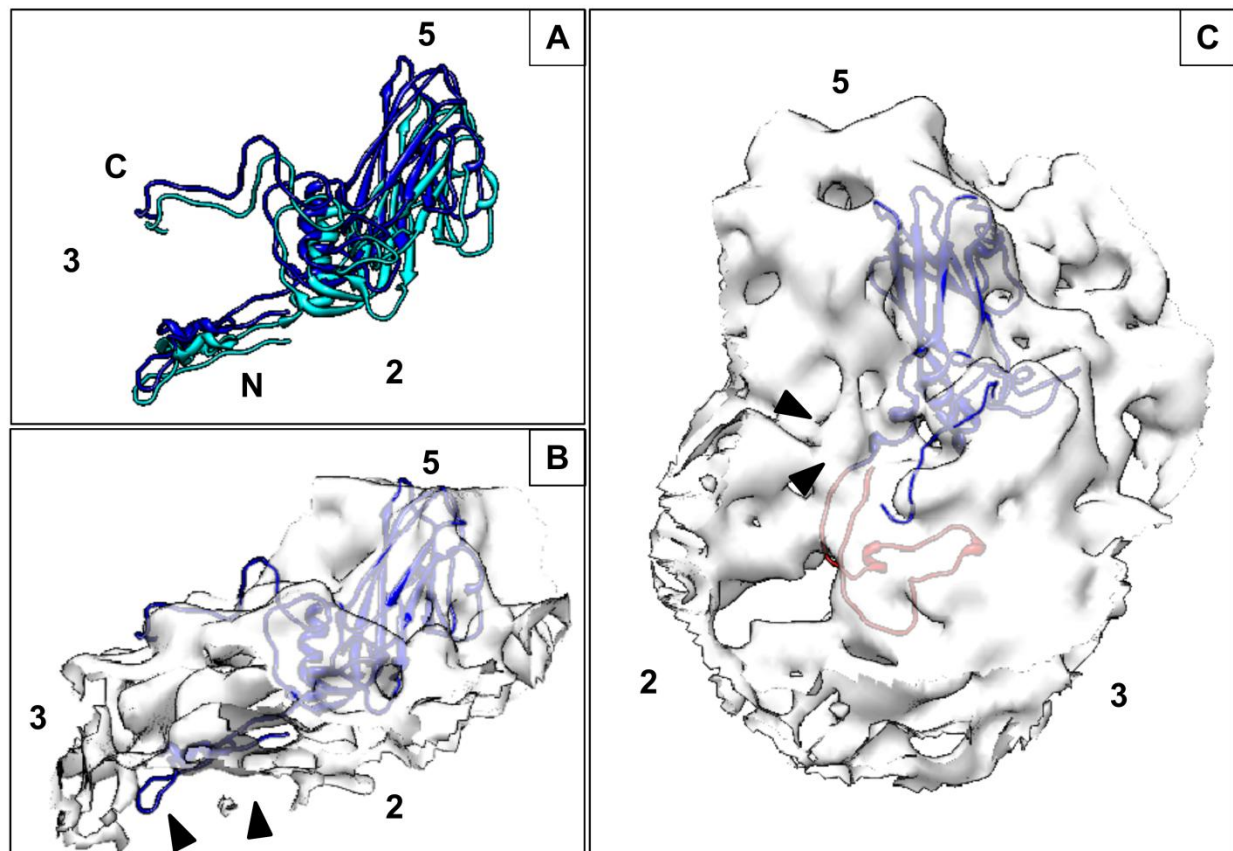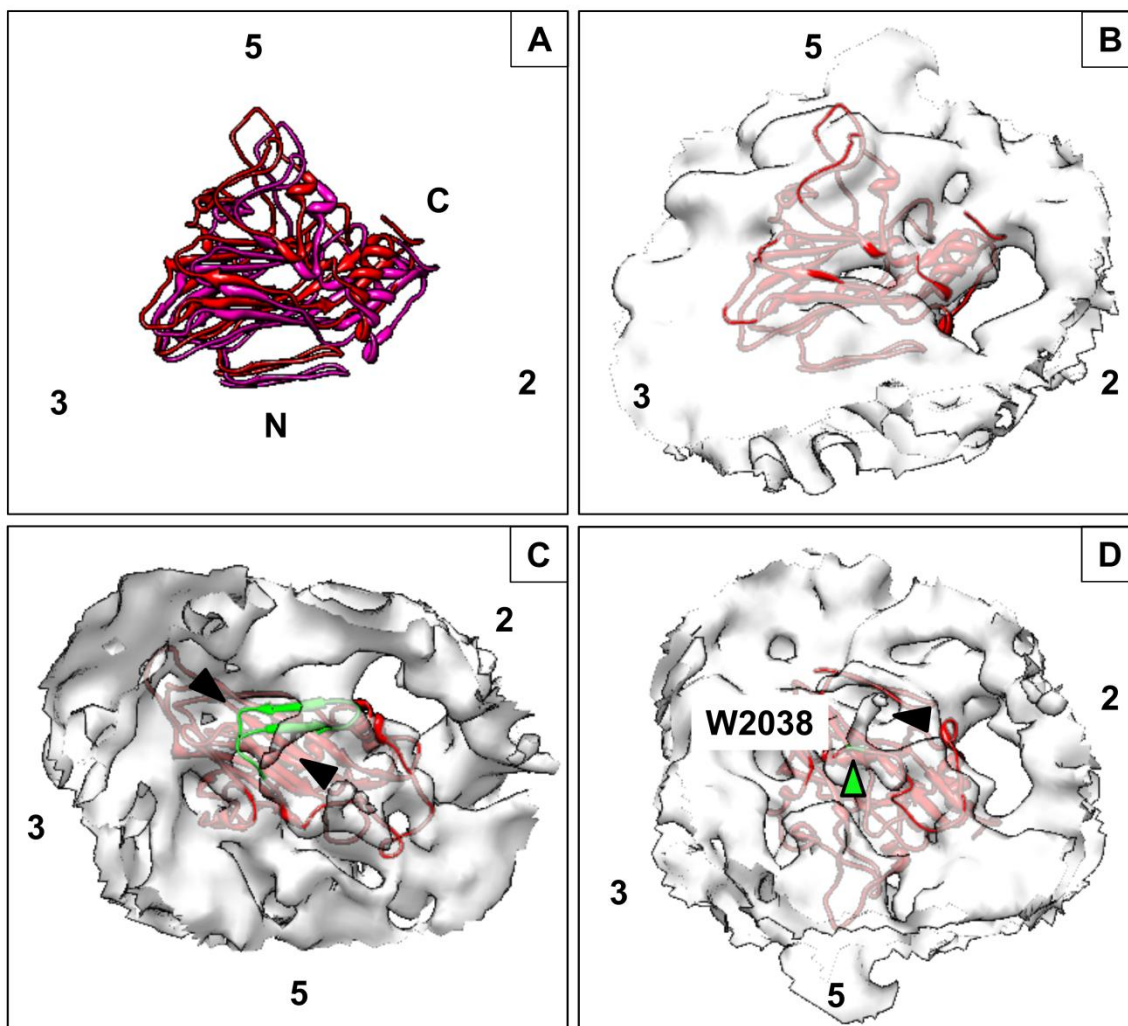
Figure 14 Fitting the coordinates of native HRV2 into A-particles reveals movement of VP1 by 7 Å and externalization of the VP1 N-terminus. The coordinates of the capsid proteins VP1 to VP3 were saved as separate coordinate files and fitted into the EM map of A-particles, using the software UROX 2.0. VP4 was excluded, as it was expelled from A-particles. The original and fitted coordinates of VP1 are displayed in light and dark blue, respectively. In A-particles, VP1 moved radially by 7 Å (A). On the interior of the capsid, no density is found for the 60 N-terminal residues of VP1 (arrow heads) (B). At the surface of the particle, new density appeared (arrow heads), probably the externalized VP1 N-terminus. To emphasize the proximity of this new density and the first resolved amino acid of VP1, the 60 N-terminal residues, not seen as density on the interior of the capsid, are colored in red (C). Figures were made in chimera. The EM map is contoured to 2.5 σ. Symmetry axes and VP1 termini are indicated by numbers and letters, respectively.

Upon conversion to A-particles, VP2 shifted outwards by about 5 Å, probably as part of capsid expansion. Concomitantly, a pore opened at the 2-fold axis between two symmetry related VP2s. On the interior surface of the capsid, about 30 N-terminal residues of VP2 rotated towards the center of the particle.

The cryo-EM structure of native HRV2 showed that Tryptophan 2038 of VP2 was in contact with the viral genome. In A-particles this interaction was maintained. In

addition, significantly more RNA density was observed close to the 2-fold axis, indicating a higher degree of order within the genome. At 1.5 σ contour level, the RNA shell was clearly visible, extending beneath the pore at the 2-fold axis. It is thus very suggestive, that the viral genome is externalized through this opening in the capsid (Figure 15).

Figure 15 In A-particles, the fitted coordinates of native VP2 shifted by 5 Å, opening a pore at the 2-fold axis. The N-terminus rotated inwards and is in proximity to the viral genome. The coordinates of VP2 were fitted into the EM map of A-particles as described in Figure 14. The original and fitted coordinates of VP2 are displayed in red and pink, respectively. The VP2 coordinates, fitted into the EM map of A-particles, shifted outwards of the capsid by 5 Å (A), opening a pore at the 2-fold axis (B). Density attributed to the VP2 N-terminus (arrow heads) indicates a movement of the 30 N-terminal residues (green) towards the center of the particle (C). Tryptophan 2038 (green arrow head) is in close contact to density attributed to the viral genome (arrow head) (D). Figures were made in chimera. The EM map is contoured to 2.5 σ. Symmetry axes and protein termini are labeled.

As part of capsid expansion during the formation of A-particles, VP3 moved radially towards the outside of the capsid by about 5 Å. The biggest change occurred at the N-terminus, where the first 20 residues shifted outwards by 10 Å. This is in accordance with data from heat-induced B-particles (Hewat EA *et al.,* 2002) (Figure 16).
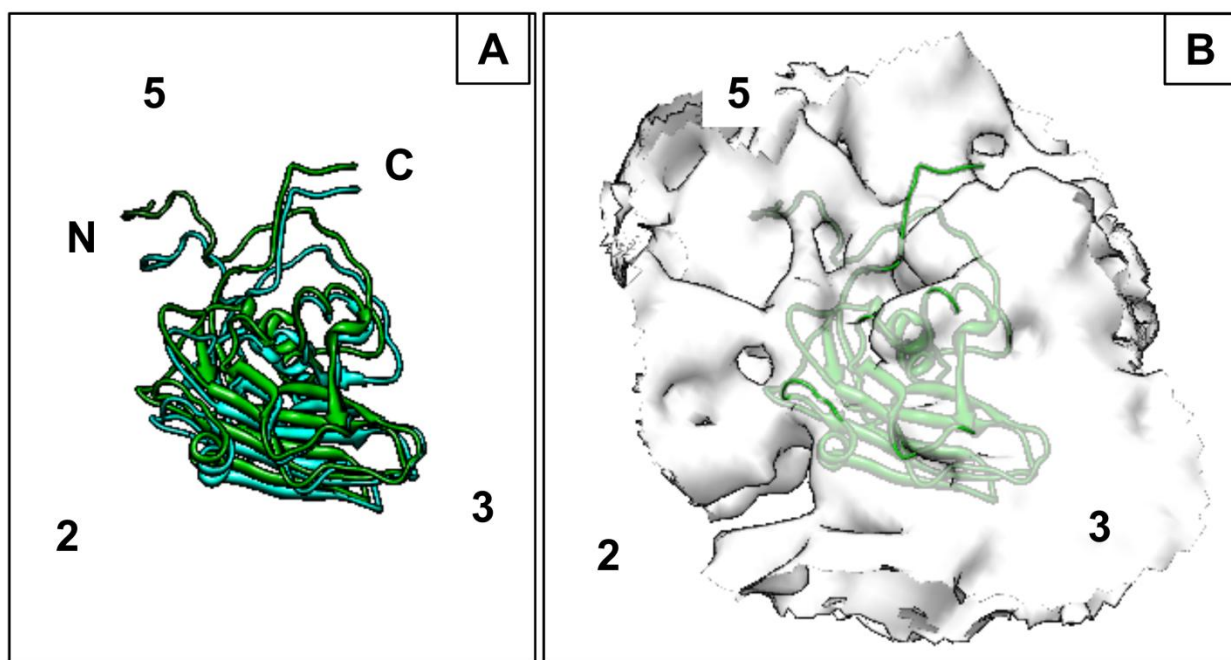
Figure 16 Upon fitting into the EM density of A-particles, native VP3 and its N-terminus shift radially by 5 Å and 10 Å, respectively. The coordinates of VP3 were fitted into the EM map of A-particles as described in Figure 14. The original and fitted coordinates of VP3 are displayed in dark and bright green, respectively. In A-particles, VP3 is displaced radially by 5 Å towards the outside of the capsid. At the 5-fold axis its 20 N-terminal residues were shifted outwards by 10 Å. Figures were made in chimera. The EM map is contoured to 2.5 σ. Symmetry axes and protein termini are labeled.

In general, all three capsid proteins shifted towards the outside of the capsid, upon conversion from native to A-particles. The β-sheets within one VP largely maintained their relative orientations. The biggest conformational changes were observed for the N-terminal loops.

6.1.5 Structure of acid-triggered B-particles at 9.8 Å resolution

Most published data of HRV B-particles stems from samples, generated by incubation at elevated temperatures. This includes the published structure of HRV2 B-particles, reconstructed from cryo-EM images to 15 Å resolution (Hewat EA *et al.*, 2002). However, it was never proven that elevated temperatures and acidification, as triggers for uncoating, lead to structurally identical particles.

CE and TEM data showed that acid-triggered preparations of A-particles contained a small fraction of empty capsids. Although being generated by the natural trigger, these particles have so far not been investigated from a structural point of view. For comparison to the structures of native and A-particles, they were picked and processed as described above. The icosahedral reconstruction of 2976 particles converged at 9.8 Å resolution, according to a FSC of 0.5.

At the parameters of the published structure i.e. 15 Å resolution and 1 σ contour level, heat- and acid-triggered capsids were identical in surface view and central sections (Figure 17). No difference map was calculated, due to the different sampling sizes of the two EM structures.
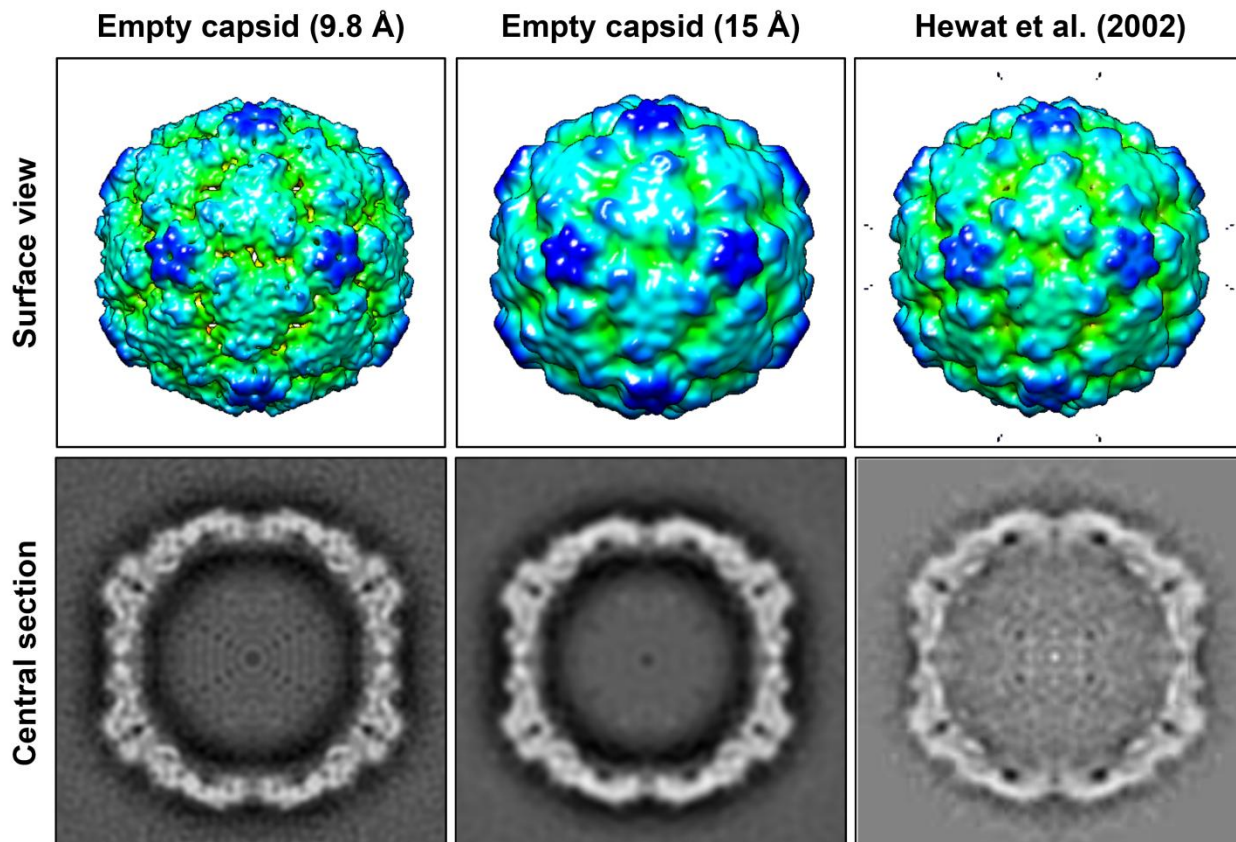
Figure 17 EM maps of heat- and acid-triggered empty capsids are identical up to 15 Å resolution.
The cryo-EM structure of acid-induced capsids was filtered to 15 Å resolution and compared to heat-triggered B-particles (Hewat EA *et al.*, 2002). No significant differences can be detected in surface view or central sections. Figures were made in chimera. EM maps are contoured to 1 σ and radially colored. Central sections were displayed with the software bshow from the bsoft package (Heymann JB and Belnap DM, 2007).

Verdaguer N *et al.* (in preparation) recently solved the X-ray structure of heat-triggered B-particles. They generously provided their data for comparisons to cryo-EM structures in this thesis.

The coordinates of VP1 to VP3 of heat-induced B-particles were saved in separate files. They were fitted into the EM map of acid-triggered capsids with the software UROX 2.0, allowing independent movement of the proteins with respect to each other.

Compared to their original positions, VP1 to VP3 were displaced by about 1 Å in the EM-map of acid-triggered capsids. As the reconstruction had a resolution of 9.8 Å, these shifts were insignificant (Figure 18).
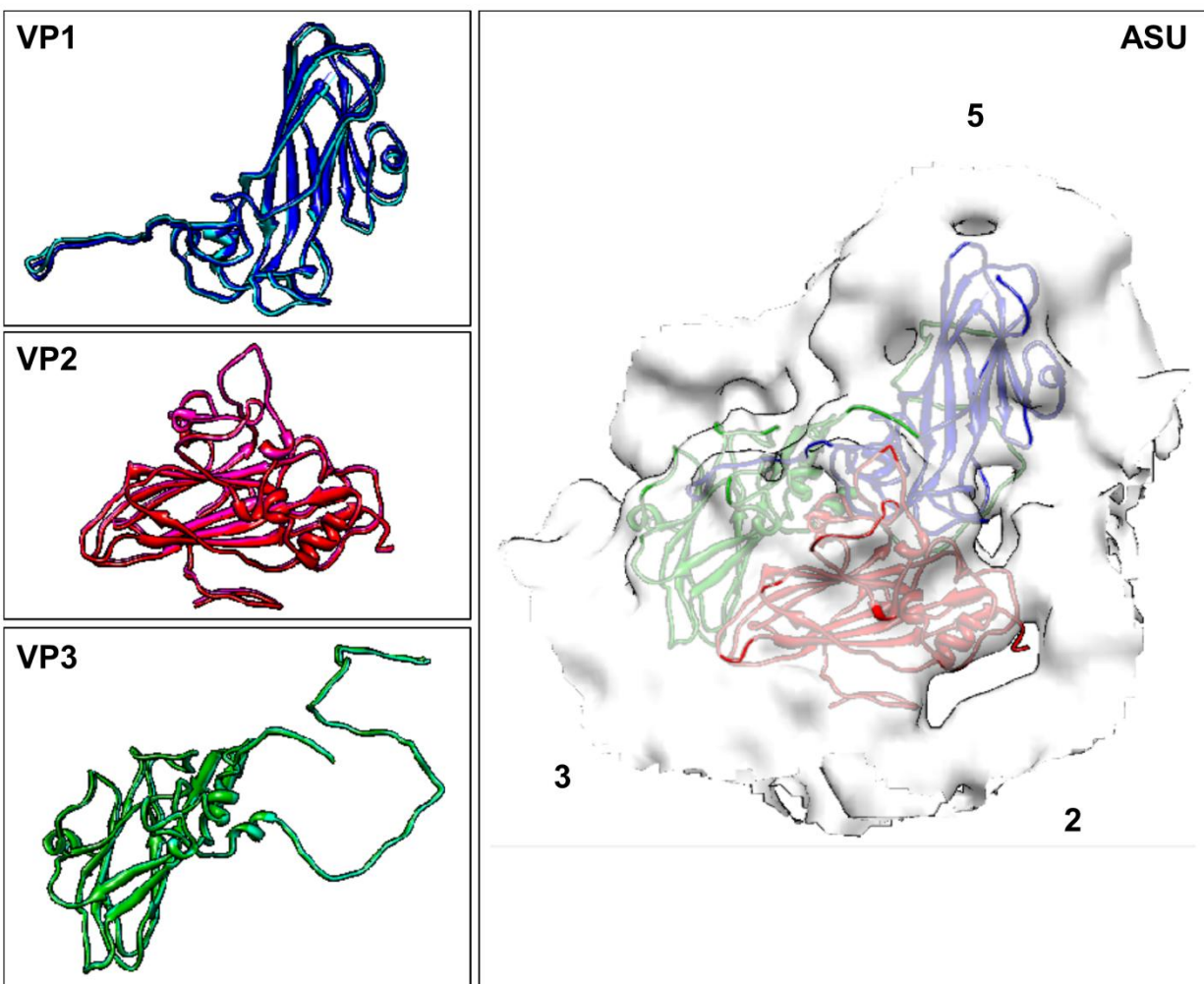
Figure 18 Fitting the X-ray coordinates of VP1 to VP4 from heat-induced B-particles into the EM map of acid-triggered capsids confirms the original orientations. The coordinates of the capsid proteins VP1 to VP3 from heat-induced B-particles were saved as separate coordinate files. The proteins were fitted into the EM density map of acid-triggered capsids, using the software UROX 2.0 (Siebert X and Navaza J, 2009). The original and fitted coordinates are displayed in light and dark colors, respectively. At the present resolution of 9.8 Å, re-orientations of the capsid proteins by about 1 Å are insignificant (left panel). The fitted coordinates are displayed together with the EM structure, showing a good fit of the viral asymmetric unit (ASU) (right panel). Symmetry axes are indicated by numbers. Figures were made in chimera.

The current data demonstrate for the first time the equivalence of heating and acidification as triggers for rhino-viral uncoating. Empty capsids generated by both methods are identical up to 9.8 Å resolution.

6.1.6 A- and B-particles differ in the presence of the genome and the location of the VP1 N-terminus

The cryo-EM structure of A-particles was filtered at 9.8 Å resolution and compared to that of B-particles. By calculating the difference map of A- minus B-particles, additional density was found in A-particles.

The release of the viral genome lead to the formation of empty capsids. As expected, the RNA shell, seen in A-particles, was lost in B-particles. Surprisingly, the difference map revealed that density at the pseudo-3-fold axis, attributed to the externalized VP1 N-terminus in A-particles, also disappeared in B-particles (Figure 19).
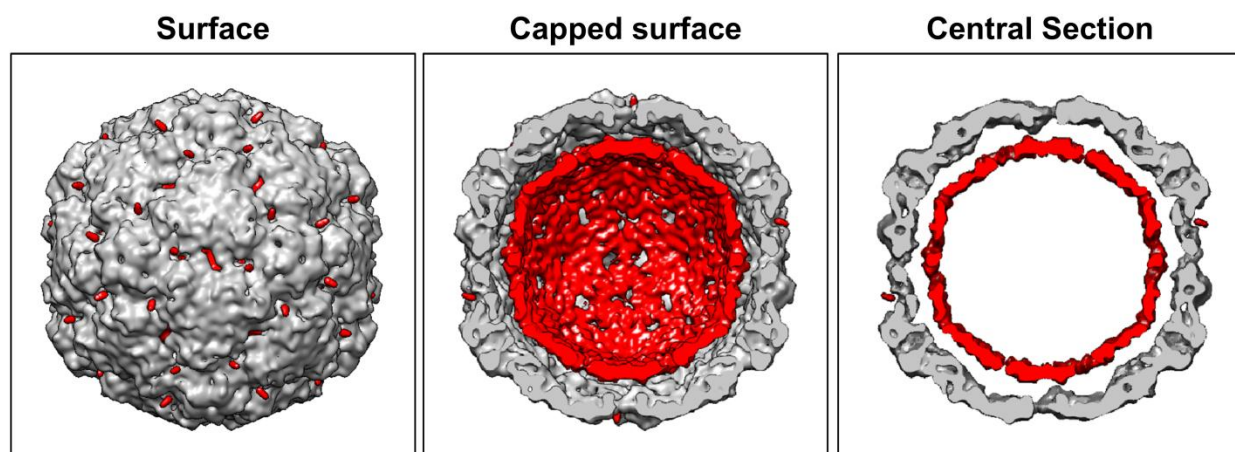
Figure 19 During conversion from A- to B-particles, the viral genome is released and density, attributed to the VP1 N-terminus, disappears from the capsid surface. The EM map of A- particles was filtered to 9.8 Å resolution and the structure of B-particles subtracted from it. The difference map (red) is shown together with the EM map of B-particles (grey). The viral genome, seen as RNA shell in A-particles, gets released upon formation of B-particles. At the pseudo-3-fold axis, density, assigned to the VP1 N-terminus, is lost in empty capsids. Figures were made in chimera. EM maps are displayed at 2.5 σ. In the difference map, densities smaller than 9.83 Å3 are not displayed, as they are insignificant at the present resolution.

In addition, the EM map of A-particles was subtracted from the structure of B-particles, to reveal densities of empty capsids that are not seen in A-particles. Surprisingly, no significant additional density was seen at 2.5 σ contour level. At 9.8 Å resolution, the localization of the VP1 N-terminus could thus not be determined in empty capsids. It might not be resolved due to structural in-homogeneity.

6.1.7 Fitting the X-ray coordinates from empty capsids into the density of A-particles additionally reveals rotation of the VP1 surface loops

The comparison of the EM structures of A- and B-particles was limited to the lower resolution of the map of the empty particles. The X-ray coordinates of heat-induced empty capsids (Verdaguer N *et al.*, in preparation) were thus fitted into the structure of A-particles, as described above.

With respect to their original positions, the coordinates of VP2 and VP3 were displaced by 1 Å, upon fitting into the structure of A-particles. At 8.9 Å resolution, these movements lay under the detection limit.

A considerable shift occurred at the loops of VP1, forming the star-shaped mesa at the 5-fold axis. As shown in section 6.1.11.2, during conversion from A- to B-particles, the star-shaped dome rotated counter-clockwise by 4 degrees.

In the X-ray structure of heat-triggered B-particles, about 60 N-terminal residues of VP1 were not resolved, indicating conformational flexibility. In the EM map of A-particles, density at the pseudo-3-fold axis, attributed to the externalized VP1 N-terminus, was not occupied by any of the fitted VPs from empty capsids. The data thus underline that this density may be the exit site of the VP1 N-terminus (Figure 20).
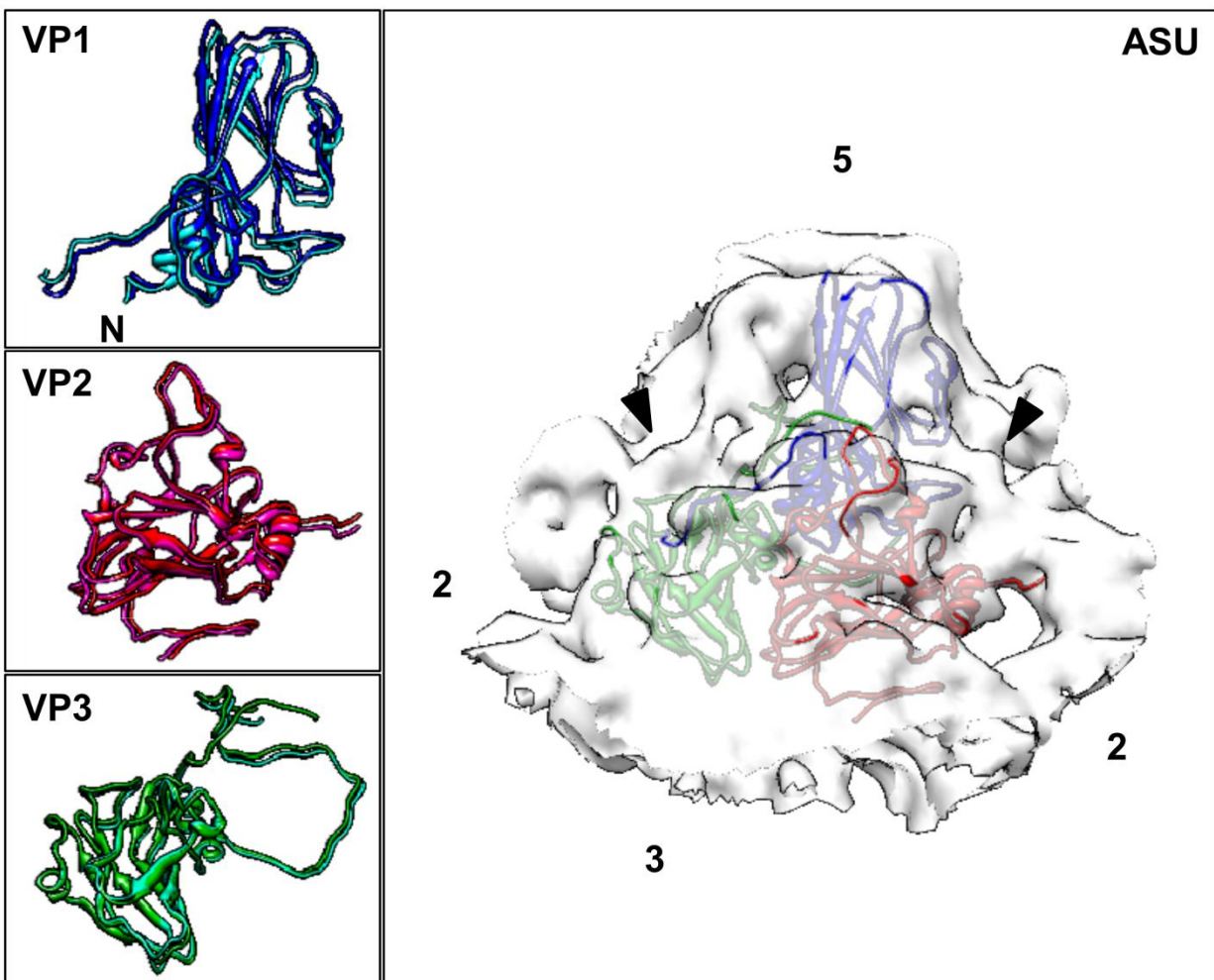
Figure 20 A- and B-particles differ in the conformation of the loops and of the N-terminus of VP1. The X-ray coordinates of VP1 to VP3 from B-particles were saved in individual coordinate files. They were fitted into the EM density of A-particles with the software UROX 2.0, allowing individual movement of VPs with respect to each other. At 8.9 Å resolution, movements of VP2 and VP3 during fitting were insignificant. In VP1 a considerable shift of the surface loops is visible. The X-ray structure does not resolve the 60 N-terminal residues of VP1. In A-particles, density at the pseudo-3-fold axis cannot be assigned to any X-ray coordinates, confirming it as exit site of the externalized VP1 N-terminus (arrow heads). Figures were made in chimera. The EM map is contoured to 2.5 σ. Symmetry axes and the truncated VP1 N-terminus are indicated.

6.1.8 Generation of Fab fragments against the VP1 N-terminus

The cryo-EM structures of HRV2 particles strongly suggested that the VP1 N-terminus (VP1-NT) was externalized via the pseudo-3-fold axis of the capsid. As final

confirmation of these data, we intended to identify the exit site of VP1-NT by binding of specific Fab fragments.

Antibodies against the VP1-NT were raised in a rabbit by immunization with a synthetic peptide. It comprised the 24 N-terminal residues of the protein plus six C-terminal Lysines for increased solubility (NPVENYIDEV LNEVLVVPNI NSSN KKKKKK) (Skern T *et al.*, 1985). In accordance with the membrane-modulating activity of the VP1-NT (Lonberg-Holm K *et al.*, 1976; Fuchs R and Blaas D, 2010), Weiss VU *et al.* (2010) demonstrated that this peptide induced leakage in liposomal membranes at acidic pH.

In immunoprecipitation assays with 35S-labeled HRV2, the anti-VP1-NT serum precipitated 67 % ± 8 % of acidified and re-neutralized virions, while binding only 8 % ± 1 % of native virus. The elevated background levels (binding native HRV2) may be explained by transient exposure of the VP1-NT, due to viral breathing (Lonberg-Holm K *et al.*, 1976; Roivainen M *et al.*, 1993; Li Q *et al.*, 1994) (Figure 21A).

For their use in cryo-EM, Fab fragments were generated from serum antibodies to prevent aggregation of immune-complexes. In Western Blots, anti-VP1-NT Fabs specifically reacted with VP1 of HRV2. They failed to cross-react with other capsid proteins or the major group HRV14 that has a dissimilar VP1-NT sequence (Stanway G *et al.*, 1984) (Figure 21B).
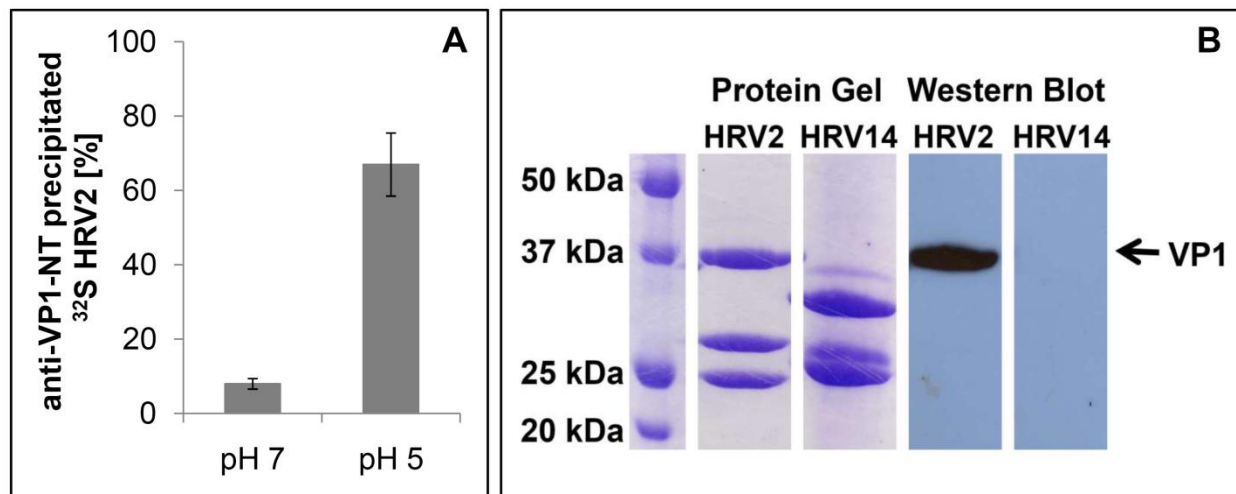
Figure 21 Antibodies and Fabs against the VP1 N-terminus (VP1-NT) specifically bind VP1 of HRV2 and preferentially acidified virions. Subviral particles and denatured virions of 32S-labeled HRV2 were precipitated by 2G2 antibodies bound to *Staphylococcus aureus*. Remaining native virus in the supernatant was exposed to pH 5.0 for 20 min and reneutralized. Acidified virions were precipitated by *Staphylococcus aureus*-conjugated anti-VP1-NT antibodies. As control, native HRV2, kept at pH 7, was immunoprecipitated. Anti-VP1-NT immunoglobulins bound 67 % ± 8 % (n=2) of acidified virus, while recognizing only 8 % ± 1 % (n=2) of HRV2 kept at pH 7. Data by Abdul Ghafoor Khan (A). Ten µg of HRVs were denatured and run on a 15 % reducing SDS gel and transferred to membranes. Blots were exposed to anti- VP1-NT Fab fragments and binding was detected by anti-rabbit HRP-conjugates. Fabs specifically bound VP1 of HRV2. Cross-reaction with the major group virus HRV14 was not detectable. Blots are representatives of three independent experiments (B).

Due to their specificity and preferred recognition of acidified virus, anti-VP1-NT Fab fragments were used for structural studies with A-particles.

6.1.9 A-particles decorated with anti-VP1-NT Fab fragments

Fab fragments from anti-VP1-NT rabbit serum were incubated with A-particles at a molar ratio of 370:1 Fab:VP1. Complexes were separated on a 7.5 % - 45 % sucrose gradient, identified by anti-rabbit and anti-HRV2 dot blots and pelleted by ultracentrifugation. In capillary electrophoresis, Fab binding shifted the peak of A-particles from 17.4*10-9 m2/Vs ± 1.2*10-9 m2/Vs to 11.8*10-9 m2/Vs ± 1.2*10-9 m2/Vs (Figure 22). Fab fragments alone migrated at 4.0*10-9 m2/Vs ± 0.1*10-9 m2/Vs.

Increasing the Fab:VP1 ratio to 593:1 resulted in the same electrophoretic mobility of the complex, suggesting saturation.
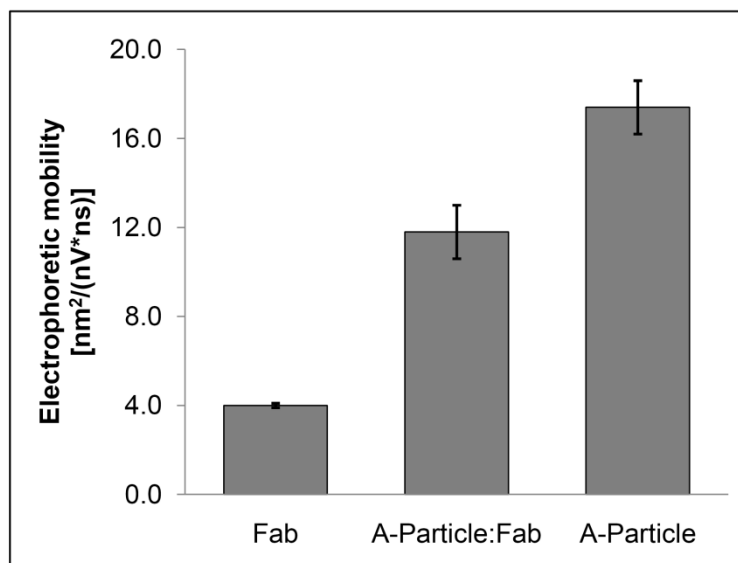
Figure 22 Fab binding shifted the electrophoretic mobility of A- particles.
A-particles were incubated with anti-VP1-NT Fabs at a molar ratio of 370 Fab:VP1. Complexes were purified on sucrose gradients, pelleted by ultracentrifugation and analyzed in capillary electrophoresis. Experimental conditions were as described in Figure 8. A-particle:Fab complexes, migrating at 11.8*10-9 m2/Vs ± 1.2*10-9 m2/Vs (n=6), could be clearly separated from undecorated A-particles and Fabs at 17.4*10-9 m2/Vs ± 1.2*10-9 m2/Vs (n=5) and 4.0*10-9 m2/Vs ± 0.1*10-9 m2/Vs (n=5), respectively. Measurements were performed by Xavier Subirats.

Purified complexes were frozen and imaged in cryo-TEM. Cryo-data was analyzed as described above.

6.1.10 The structure of A-particle:Fab complexes

The structure of A-particles with bound anti-VP1-NT Fabs was solved to 8.7 Å resolution, considering a Fourier Shell Correlation of 0.5. It was filtered to 8.9 Å and compared to the EM map of un-decorated A-particles that have the same resolution.

Despite being visible in cryo-images, no additional density for Fab fragments could be detected in the EM-map of immune-complexes, but surprisingly, the visible

density for the externalized VP1 N-terminus was diminished. The pore at the 2-fold axis appeared smaller for immune-complexes, but these changes were insignificant at 2.5 σ contour level (Figure 23).
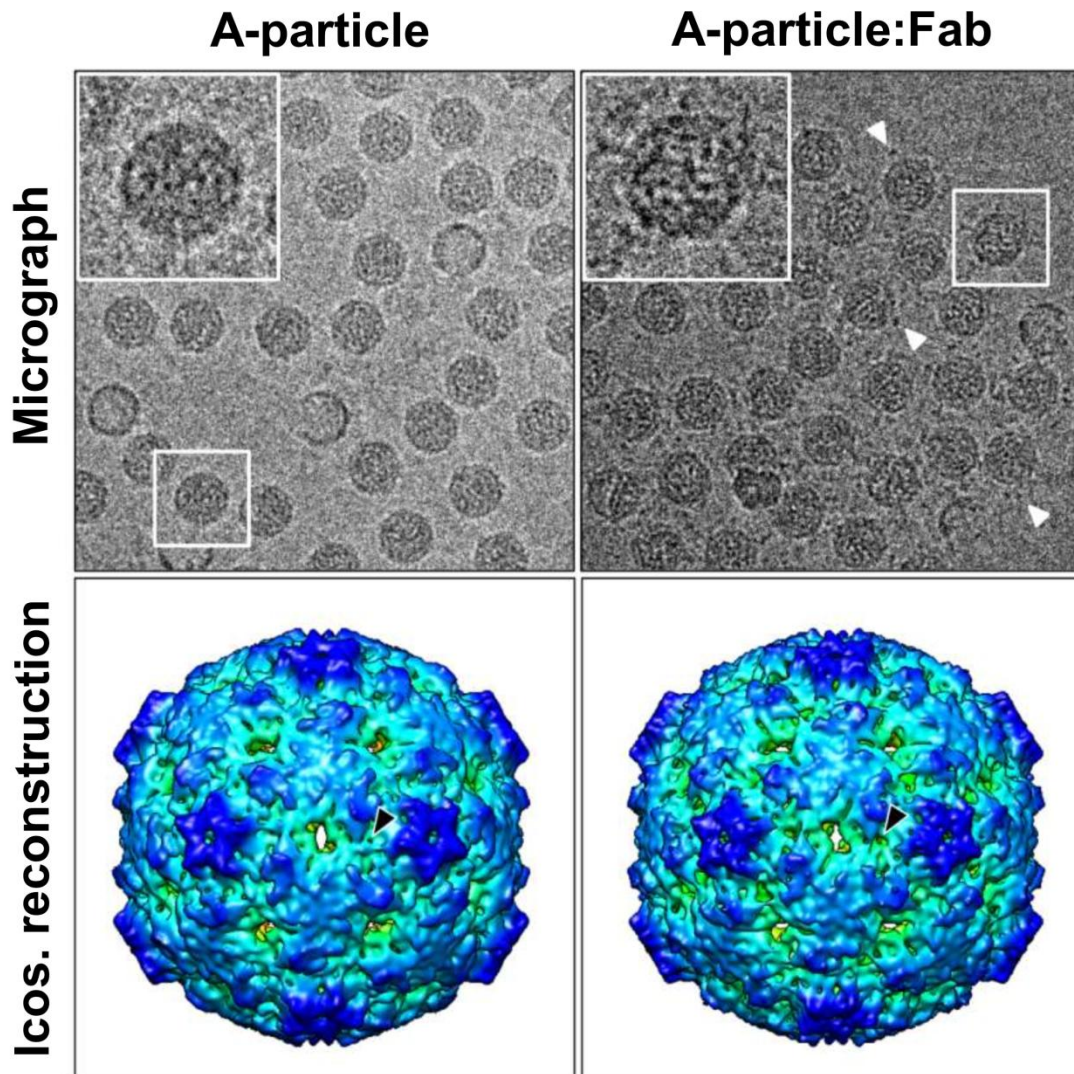
Figure 23 Fab fragments bound to A-particles are visible in cryo-images but not in the icosahedral 3D reconstruction. Frozen, hydrated specimens were imaged in a FEI Polara cryo-TEM at -3.4 μm defocus and 20 e-/Å2 electron dosage. A-particles have a smooth surface; bound Fab fragments are visible as corona-like density around the virus (arrow heads). 15170 and 10500 images were used for the icosahedral reconstruction of A-particles and of A-particles decorated with anti-VP1-NT Fabs. In the 3D map of the immune-complexes, no additional density can be seen for bound Fab fragments, when compared to the structure of un-decorated A-particles. Surprisingly, density for the VP1 N-terminus seems to have diminished (arrow heads). Micrographs were auto-adjusted for contrast in Adobe Photoshop 6.0 (www.adobe.com). Figures were made in chimera. EM maps are contoured at 2.5 σ and radially colored.

In the X-ray structure of native HRV2, the VP1 N-termini are disordered (Verdaguer N *et al.*, 2000). Fab fragments bound to these flexible residues may be visible in low-resolution micrographs. During icosahedral reconstruction, however, their density could be averaged out due to conformational in-homogeneity, so that the Fab signal became indistinguishable from the background noise.

The individual images of A-particles and A-particle:Fab complexes were thus classified using maximum-likelihood multi-reference refinement, to identify structural sub-populations (Scheres SH *et al.*, 2005).

Comparing the class average of A-particles to that of A-particle:Fab complexes, there appeared to be some weak, additional density above the 2-fold axis of the immune-complexes. It was smeared out and did not allow allocation to a particular site on the viral surface (Figure 24).
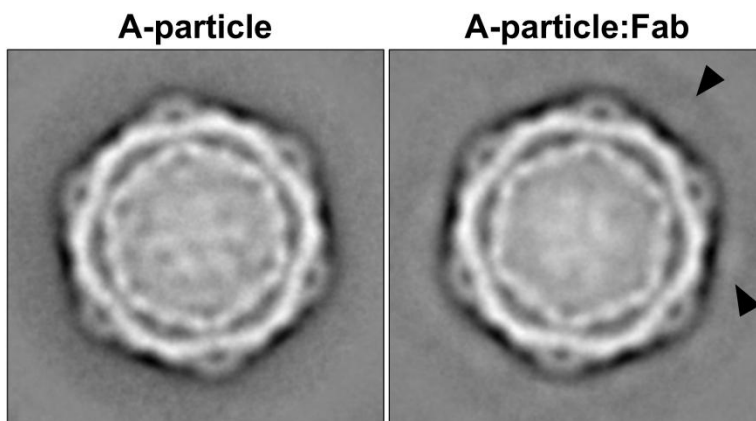
Figure 24 In Class averages of A-particle:Fab complexes, smeared-out density is visible for the bound Fabs. Images of A-particles and A-particle:Fab complexes were aligned and classified using maximum-likelihood multi-reference refinement (Scheres SH *et al.*, 2005). The depicted class averages contain 1782 particles each. For the immune-complex there seems to be additional density smeared out over the 2-fold axis (arrow heads).

Further classification of the data above into several different classes did not yield any improvement but visually comparable class averages. The program also failed to

distinguish between A-particles and A-particle:Fab complexes, when both data sets were pooled. The resulting class averages contained a ratio of about 60:40 and 30:70 A-particles to immune-complexes. It seems that the density of the Fab fragments is too weak so that the capsid is dominant during classification.

The circumference of the capsid was thus selected with a crown mask and particles were rotationally aligned, according to surface density, using figure 24 as reference. For A-particle:Fab complexes, the additional density of the Fab fragments was clearly visible in the resulting class average, but the features of the capsid were smeared out to a homogenous ring. Broadening of the mask to include some pixels of the capsids retained faint 5-folds at the expense of Fab alignment (Figure 25).
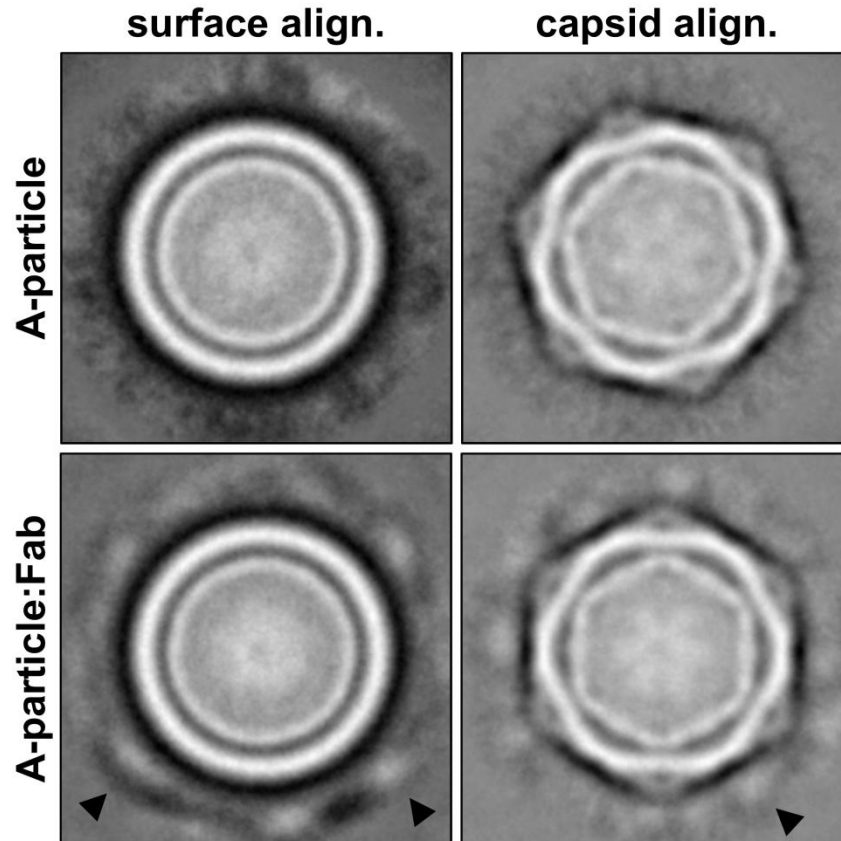
Figure 25 Rotational alignment of A-particle:Fab complexes, based on surface density, better resolves Fab density. The circumference of the images of A-particles and A-particle:Fab complexes was masked and rotationally aligned. Density for Fab fragments at the viral surface is clearly visible for immune complexes, in contrast to A-particles particles alone, confirming Fab binding (arrow heads). However, the capsid structure is smeared out making allocation of the binding site impossible. Including parts of the virus during alignment resolved capsid features but decreased Fab contrast.

In an attempt to resolve some viral characteristics, the entire particles were rotationally re-aligned without restriction, using the class average of aligned Fabs (Figure 25) as reference. Two iterations yielded discernable 5-fold axes; after four iterations the capsid was fully aligned. However, during this process the Fab fragments got progressively averaged out. Restricting rotational rearrangements to 60 º, the angle between two adjacent 5-fold axes, slightly improved the Fab signal but did not reveal a discrete attachment site (Figure 26).
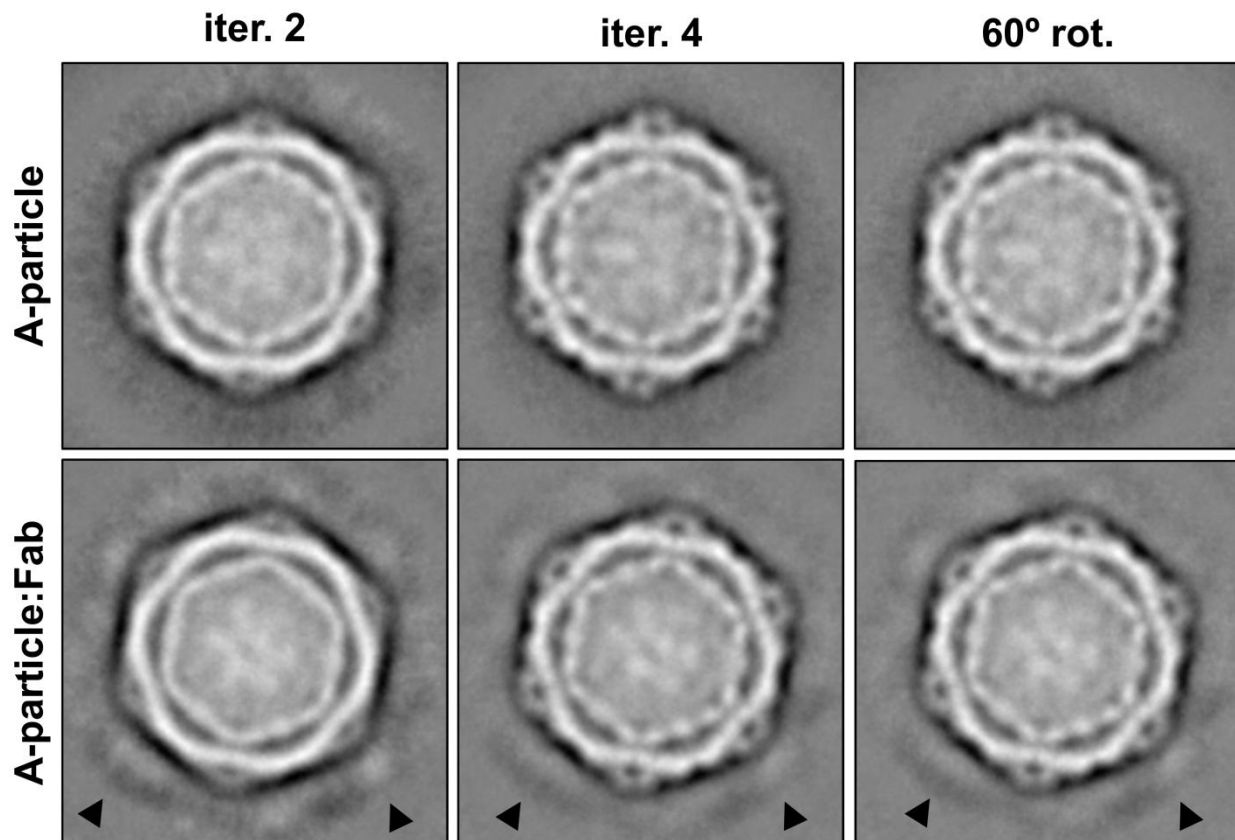
Figure 26 Limited rotational re-alignment of A-particle:Fab complexes resolves capsid features at the expense of Fab contrast. The radial restriction of the alignment was removed and entire particles were rotationally re-aligned for different iterations. After two cycles, capsid features are recognizable in class averages and after four iterations, the virion is resolved. In parallel, however, the Fab fragments get gradually averaged out. Limiting rotations to 60 º does not significantly improve Fab signals; they remain smeared out between the 5-fold axes (arrow heads).

Careful alignment of A-particle:Fab complexes and of A-particles as control confirmed that Fab fragments were attached to the viral capsid. However, their density was smeared out between adjacent 5-fold axes, making allocation of the binding site, even by single particle analysis, impossible.

The rational of these experiments was based on X-ray data of native HRV2, showing that the 15 N-terminal residues of VP1 are disordered (Verdaguer N *et al.*, 2000). For identifying the externalized VP1-NT in A-particles, Fab fragments were thus generated, that target the 24 N-terminal amino acids. However, the recent X-ray

71

structure of empty capsids revealed that in subviral particles, the 60 N-terminal amino acids of VP1 are disordered (Verdaguer N *et al.*, in preparation). Based on that, the location of bound Fab fragments is expected to be highly variable on the surface of A-particles. Considering also the polyclonal nature of the Fab fragments, this may explain why their density is averaged out during icosahedral reconstruction.

For identifying the exit site of the VP1 N-terminus, monoclonal antibodies may be used in the future that target residues closer to the structurally stable protein chain. Alternatively, an indirect approach may be chosen, by digesting externalized protein residues with proteases and by identifying the missing densities in EM structures. This approach was chosen by Bubeck D *et al.* (2005b) to allocate the exit site of VP1-NT in A-particles of poliovirus.

6.1.11 Structural changes during uncoating of minor group HRVs

Already in low contrast cryo-images, different HRV particles could be visually distinguished by their different core densities. Native virions appeared as spheres of homogenous density, while A-particles seemed to be less dense and internally more structured. Acid-triggered B-particles, equivalent to heat-induced empty capsids, differed most strongly from other particle species; they were visible as solvent-filled circles of empty capsids (Figure 27).

Native HRV2   A- particle
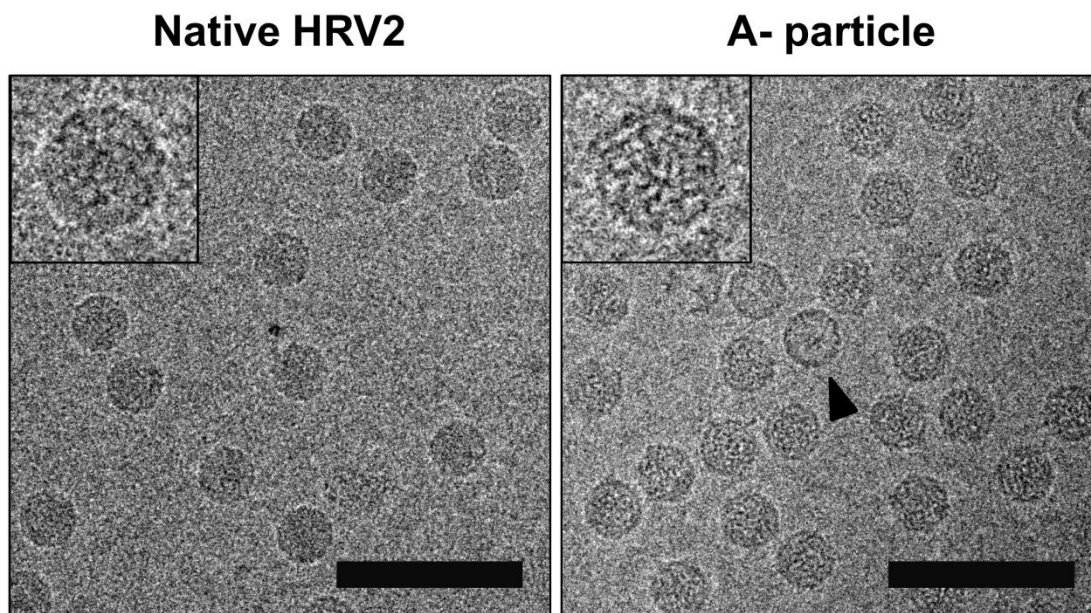
Figure 27 Different HRV2 particles are distinguishable in cryo-images by different core densities. Frozen, hydrated specimens were imaged in a FEI Polara cryo-TEM at -2.2 µm defocus and 20 e-/Å2 electron dosage. Native HRV2 has homogeneous density. A-particles appear to have internal structures. Acid-triggered B-particles, found in the preparation of A-particles, lack core density (arrow head). Images were auto-adjusted for contrast in Adobe Photoshop 6.0 (www.adobe.com). Size bar = 100 nm.

The EM maps of all three particle species, native, A- and B-particles, were reconstructed by the same processing strategy, as described above. The reconstructions resulted in structures of different resolutions. 7946 images yielded an EM map of native HRV2 of 8.2 Å resolution. With considerably less particles i.e. 2976, B-particles were reconstructed to 9.8 Å resolution. Surprisingly, 15170 images, used for determining the structure of A-particles, achieved only a resolution of 8.9 Å. Attempts at improving this EM map by a more stringent particle selection failed, which suggests the presence of subpopulations or conformational flexibility of these particles.

In the future this question might be solved by 2D classification of raw images. Particles could also be grouped according to different density levels of their genome, which could possibly identify intermediates with partially released RNA.

For direct comparison, all three EM maps were filtered at 10 Å resolution. In the surface view, several main differences between native and subviral capsids became apparent. During uncoating HRV2 expanded. Concomitantly, the star-shaped dome at the 5-fold axis rotated and a channel opened at its center. The inner capsid protein VP4, localized at the 5-fold axis, was expelled. An additional pore formed at the 2-fold axis, in close proximity to contact sites of the protein capsid and the genome. In A-particles the RNA got more ordered and formed a shell of density close to the inner surface of the capsid, contacting it at the 2- and pseudo-3-fold axis. In B-particles it was released. At the pseudo-3-fold axis, the VP1 N-terminus was externalized in A-particles; in B-particles, however, it became too disordered to be resolved (Figure 28).
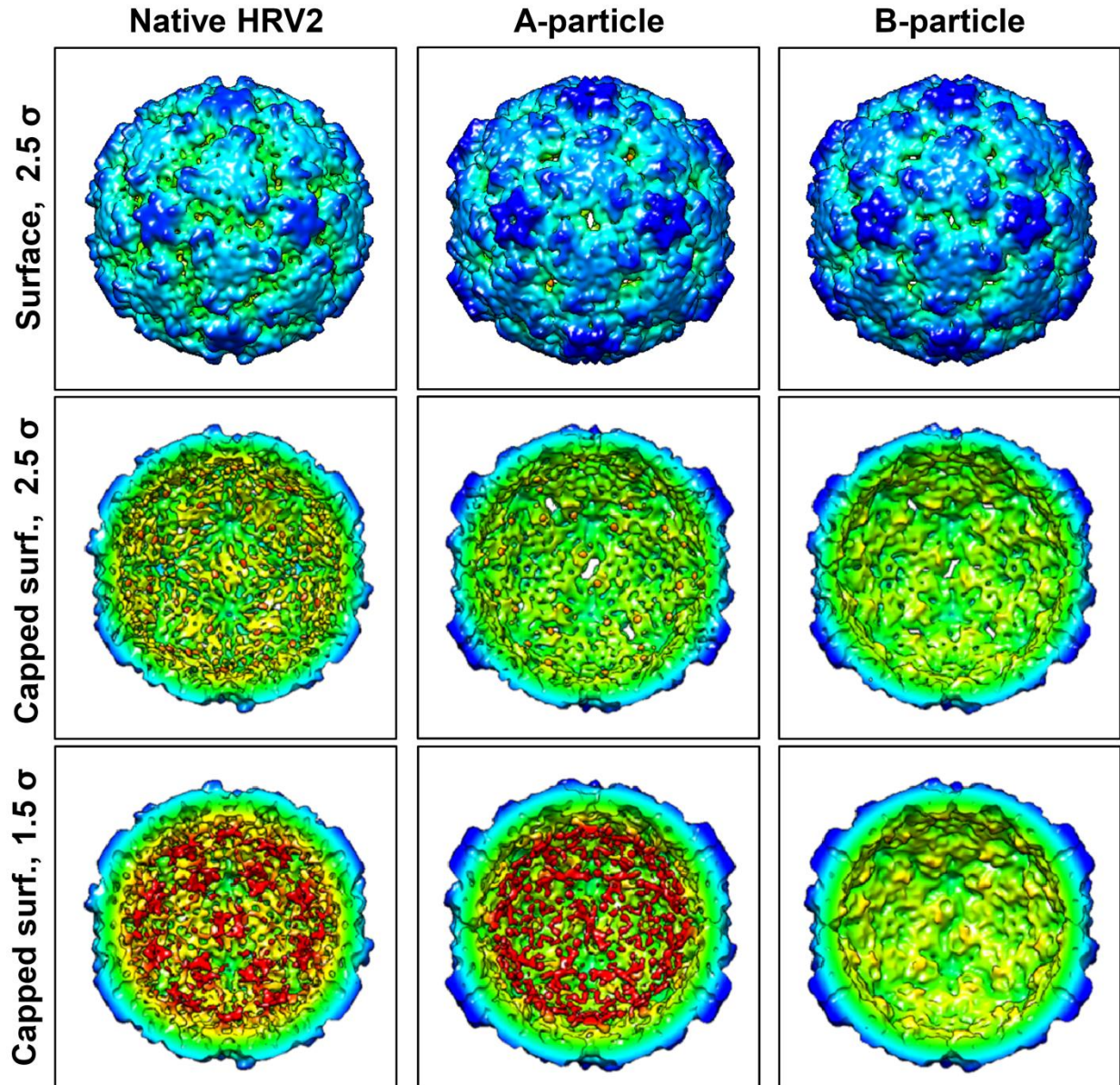
Figure 28 Subviral particles are larger than native virus and pores are formed in their capsid. The particles differ in the externalization of VP4, of the VP1 N-terminus and of the RNA genome. EM maps of native HRV2, A- and B-particles were filtered to 10 Å resolution. Upon uncoating, the capsid of HRV2 expanded and pores opened at the 2- and 5-fold axes. In A-particles the VP1 N-terminus is externalized at the pseudo-3-fold axis, in B-particles, it cannot be localized. At 1.5 σ contour level, ordered parts of the genome are resolved. Upon conversion to A-particles, the RNA becomes more ordered and forms a density shell on the inner surface of the capsid, contacting it at the 2-fold axis. In B-particles, the genome is expelled. These changes will be described in detail in the next figures. Figures were made in chimera. EM density maps are displayed at 2.5 σ and 1.5 σ and radially colored.

The following sections address these changes in detail.

6.1.11.1 Capsid Expansion

During the reconstruction process, the actual magnification of the microscope was determined by scaling the EM map of native HRV2 to the X-ray structure (Verdaguer N *et al.*, 2000). The EM structure of native virus had thus the expected diameter of 30 nm.

Comparing the rotational averages of the maps from native and subviral particles, the dimensions of A- and B-particles were determined. Both subviral particles had the same size of 31.4 nm in diameter, corresponding to a capsid expansion by 4.7 % (Figure 29).
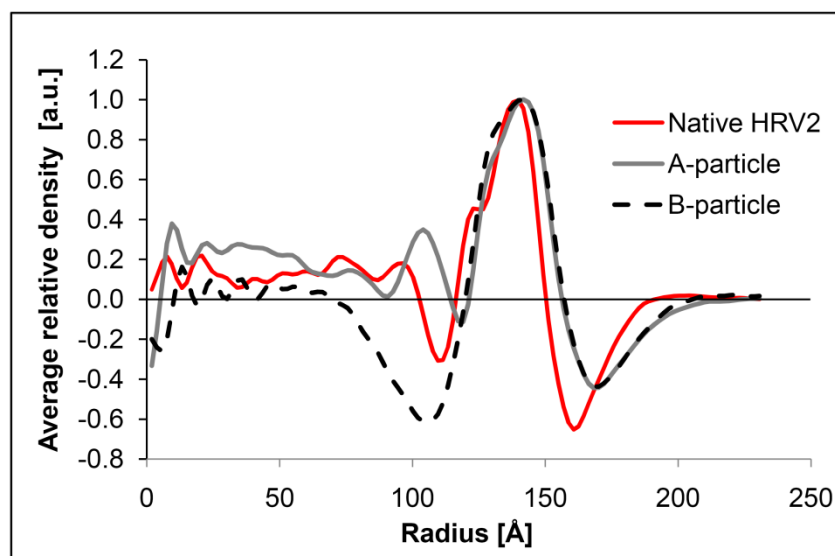
Figure 29 Subviral particles are 4.7 % larger than native HRV2. The rotational averages of the EM maps from native, A- and B-particles were calculated with spider. Density values were scaled to 1. Native HRV2 has radius of 150 Å. A- and B-particles have the same size, with 157 Å radius.

Hewat EA *et al.* (2002) described an overall size increase of 4 % from native to empty capsids, but mentioned a stronger expansion at the 5-fold axis. However, these authors did not specify, how this size increase was determined. Rotational averages consider the entire capsid, including the protruding 5-fold axis. As a consequence, the

overall expansion of the capsid, that was determined here, might be slightly larger than that of the capsid base. It is thus likely that current results and data by Hewat EA *et al.* (2002) reflect the same capsid expansion.

6.1.11.2 Rotation of the 5-fold axis and opening of a pore

During conversion from native HRV2 to A-particles the tips of the star-shaped mesa at the 5-fold axis rotated clockwise by 11 degrees and a pore opened at its center. Surprisingly, upon generation of B-particles, a counter-clockwise movement of 4 degrees occurred, slightly decreasing the diameter of the central channel (Figure 30).
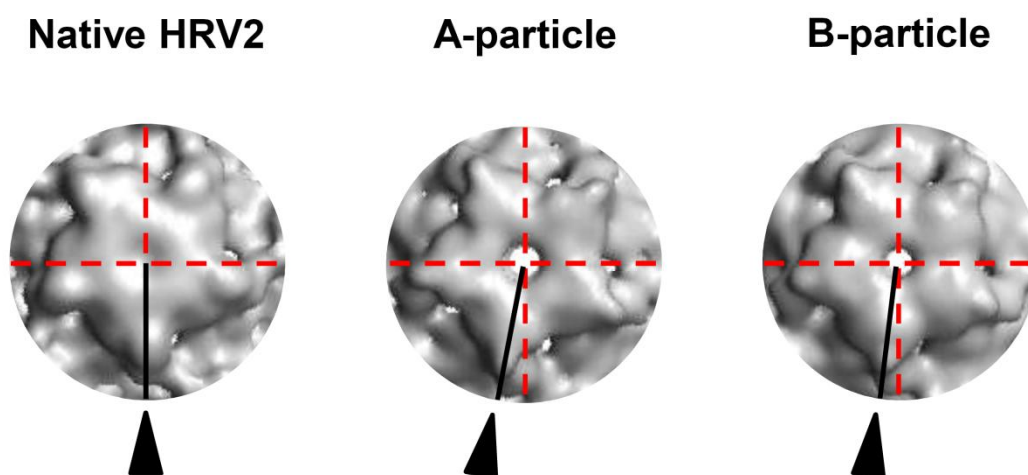
Figure 30 Compared to native HRV2, the tips of the star-shaped dome at the 5-fold axis rotate clockwise by 11 and 7 degrees in A- and B-particles, respectively. The EM maps were filtered to 10 Å resolution. The structure of native virus was displayed simultaneously with the maps of A- or B-particles in chimera. It was rotated in 1 degree steps, until the tips of the star-shaped mesa at the 5-fold axis were aligned with those of subviral particles. In A- and B-particles the star-shaped dome at the 5-fold axis is rotated clockwise by 11 and 7 degrees, respectively, when compared to native HRV2. Figures were made in chimera. EM densities around the 5-fold axis are displayed at 2.5 σ. Reference lines are show for better visualization of the rotation.

The results of empty capsids correspond well to data by Hewat EA *et al.*, (2002), who also observed a clock-wise rotation of the star-shaped dome by 7 degrees, when compared to native HRV2.

6.1.11.3 Loss of VP4

In native HRV2, the inner capsid protein VP4 was localized to the 5-fold axis. Due to its small size, only parts of it were resolved in the cryo-EM map of native virus. In B-particles, this density was lost, indicating release of VP4 during uncoating. This is in accordance with data by Lonberg-Holm K and Korant BD (1972) who described that VP4 was expelled in subviral particles.

From the structure of A-particles, loss of VP4 could not be unequivocally confirmed. Parts of the RNA shell, found in these particles, extended below the 5-fold axis, close to the position of VP4 in native virions. At the current resolution, it could not be distinguished whether all of this density stemmed from RNA or partially from shifted VP4 (Figure 31).
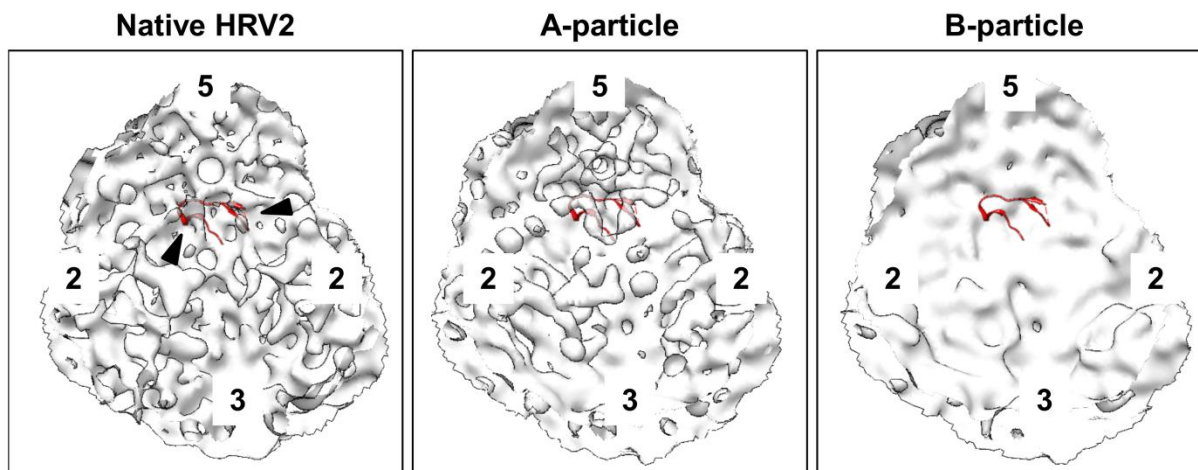
Figure 31 Density attributed to VP4 in native HRV2 is lost in B-particles. EM-density maps, filtered to 10 Å resolution, were simultaneously displayed with the X-ray coordinates of VP4 (red), fitted into the native structure. In native HRV2, density at the 5-fold axis on the inner surface of the capsid can be attributed to VP4 (arrow heads). Due to its small size and the limited resolution, only parts of the protein are resolved. In empty capsids this density is missing, indicating release of VP4. Due to the RNA shell, extending beneath the 5-fold axis, loss of VP4 cannot be confirmed in A-particles. Figures were made in chimera. EM maps are contoured to 1.5 σ, their inner surface is shown. Symmetry axes are labeled.

However, Weiss VU (2009) demonstrated that VP4 was expelled from heat-induced A-particles.

6.1.11.4 Opening of a pore at the 2-fold axis

As part of viral expansion during uncoating, a pore opened in the capsid of A-particles at the 2-fold axis. It was also present in the structure of B-particles but visually appeared to be smaller. This size difference of the pore was insignificant at 2.5 σ contour level. However, the density, narrowing the pore at the 2-fold axis of B-particles, became visible in difference maps at contour levels of 1.7 σ or below. This indicated that it was less conserved than other parts of the capsid.

In the cryo-EM structure of heat-triggered B-particles, Hewat EA *et al.* (2002) described a thinning of the capsid at the 2-fold axis, when compared to native virions, but these authors did not observe the opening of a pore. This discrepancy can be explained by the significantly lower resolution of their EM-map and the low contour level, at which it was displayed.

Docking of the X-ray coordinates from B-particles into the cryo-EM map of A-particles showed that the protein capsids of both subviral particles were identical around the 2-fold axis at 10 Å resolution. In the structure of A-particles, however, additional density was resolved on the inner surface of the capsid, beneath the 2-fold axis. It was thus attributed to ordered regions of the genome. By docking the coordinates of native HRV2, this RNA density was shown to contact Tryptophan 2038 of VP2 (Figure 15). After filtering the map to 10 Å resolution, RNA was visible as discrete dots of density at 2.5 σ contour level (Figure 32).

Tryptophan 2038 of VP2 was already found to be in proximity of ordered RNA, in the X-ray structure of native HR2 and of other rhino- and enteroviruses (Filman DJ *et al.*, 1989; Arnold E and Rossmann MG, 1990; Hadfield AT *et al.*, 1997, Verdaguer N *et*

al., 2000). The cryo-EM map of native virus, contoured to 1.5 σ, also showed this protein-RNA interaction. Additional density, attributed to the viral genome, localized around the 2-fold axis.

At the same contour level, significantly more RNA density was visible in A-particles. It extended over the pore at the 2-fold axis, suggesting this point as site for RNA externalization during the formation of B-particles.
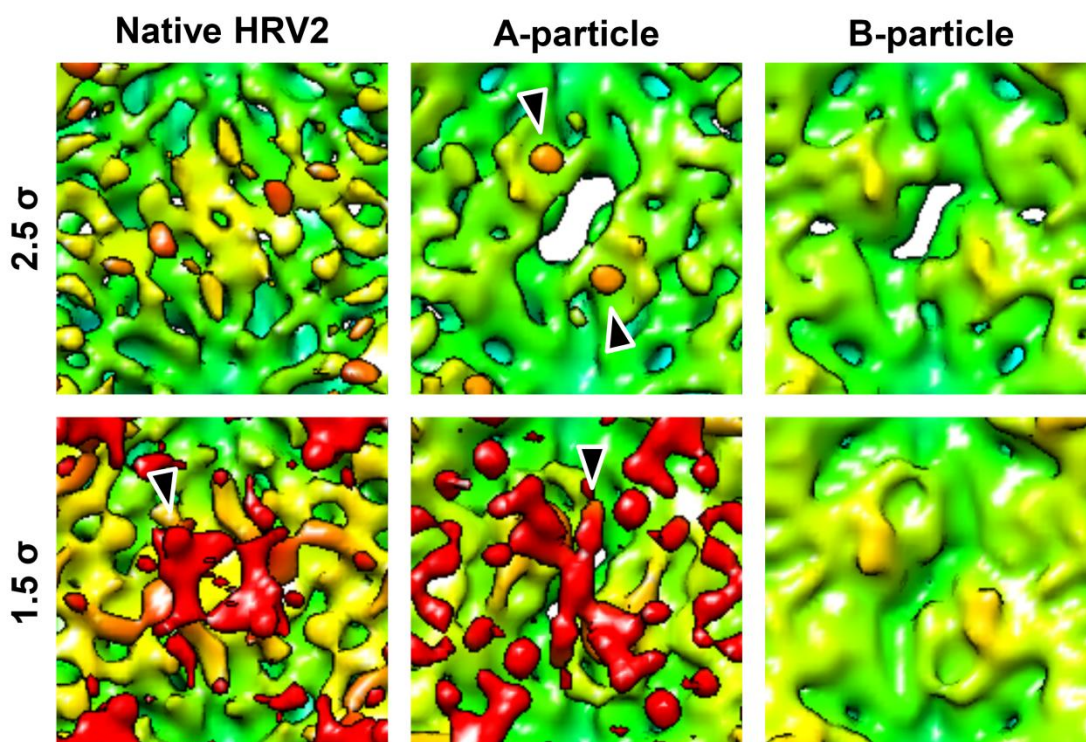
Figure 32 In A-particles, the viral genome extends over the pore at the 2-fold axis. EM maps of native and subviral particles were filtered to 10 Å resolution. Their inner surface is displayed, looking at the 2-fold axis. Compared to native virions, a pore opened at the 2-fold axis in subviral particles. In A-particles, density, attributed to the viral genome, is resolved close to this opening, at 2.5 σ contour level (arrow heads). Contouring the maps to 1.5 σ, more RNA density becomes visible. In native HRV2, it is localized around the 2-fold axis, contacting, among other residues, Tryptophan 2038 of VP2 (arrow heads). In the structure of A-particles, the genome extends over the pore; in B-particles, it is completely lost. Figures were made in chimera. EM maps are radially colored.

6.1.11.5 Externalization of the VP1 N-terminus

In native HRV2, the amphipathic N-terminus of VP1 was found on the interior surface of the capsid, close to the 2- and pseudo-3-fold axes (Figure 14). Upon conversion to A-particles, these residues were externalized at the pseudo-3-fold axis, visible as small dot of density (Figure 33). According to data from docking analysis, on the inner surface of A-particles, density was missing for the 60 N-terminal residues of VP1. Density corresponding to this protein fragment would be considerably larger than the newly appearing dot on the surface of A-particles. However, it is expected that most of the residues may be disordered and thus not resolved. This has already been shown for the externalized N-terminus of VP1 in poliovirus (Bubeck D *et al.*, 2005b).

Surprisingly, the VP1 N-terminus could not be resolved in B-particles. Instead, an additional pore was visible at the pseudo-3-fold axis. This is in accordance with EM and X-ray data on empty capsids by Hewat EA *et al.* (2002) and Verdaguer N *et al.* (in preparation), respectively.

Native HRV2	A-particle	B-particle
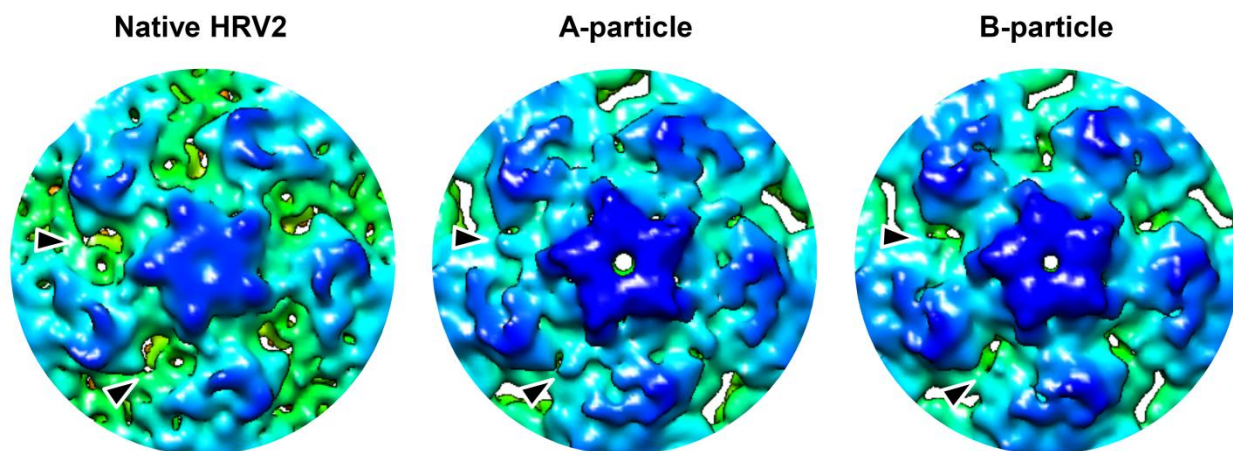
Figure 33 The VP1 N-terminus is externalized at the pseudo-3-fold axis of A-particles, it is not resolved in B-particles. The cryo-EM maps of native and subviral particles were filtered to 10 Å resolution. In native HRV2, the VP1 N-terminus is localized at interior of the capsid, in proximity to the 2- and pseudo-3-fold axes. Upon conversion to A-particles it is externalized at the pseudo-3-fold axis (arrow heads). In empty capsids it is not resolved but a pore becomes visible at the pseudo-3-fold axis (arrow heads). Figures were made in chimera. EM maps around the 5-fold axis are displayed at 2.5 σ and radially colored.

In the central section of the EM map from native HRV2, an area of low density was visible at the pseudo-3-fold axis, corresponding to a solvent-filled bubble. During the transition from native to A-particle, this area was filled with density, probably the externalized VP1 N-terminus. In empty capsids, this bubble remained occupied with density, indicating that the N-terminal residues of VP1 were still in place and passing through the viral shell (Figure 34). This has already been described for heat-triggered B-particles (Hewat EA *et al.*, 2002).

6.1.11.6 *Formation of an RNA shell in A- and genome release in B-particles*

As described above, RNA-protein contacts were resolved close to the 2-fold axis in native HRV2. This ordered fragment of the genome was also visible in the central section of the EM map.

Upon conversion to A-particles, a significantly larger part of the genome became ordered enough to be visible in the EM structure, forming an RNA shell on the interior of

the capsid. The RNA-protein contact at the 2-fold axis was maintained in A-particles. In the central section of this structure, it seemed that an additional interaction site formed at the 5-fold axis. However, no contact could be resolved at 1.5 σ contour level.

The interior density shell completely disappeared, during the formation of B-particles, confirming it as stemming from RNA (Figure 34).
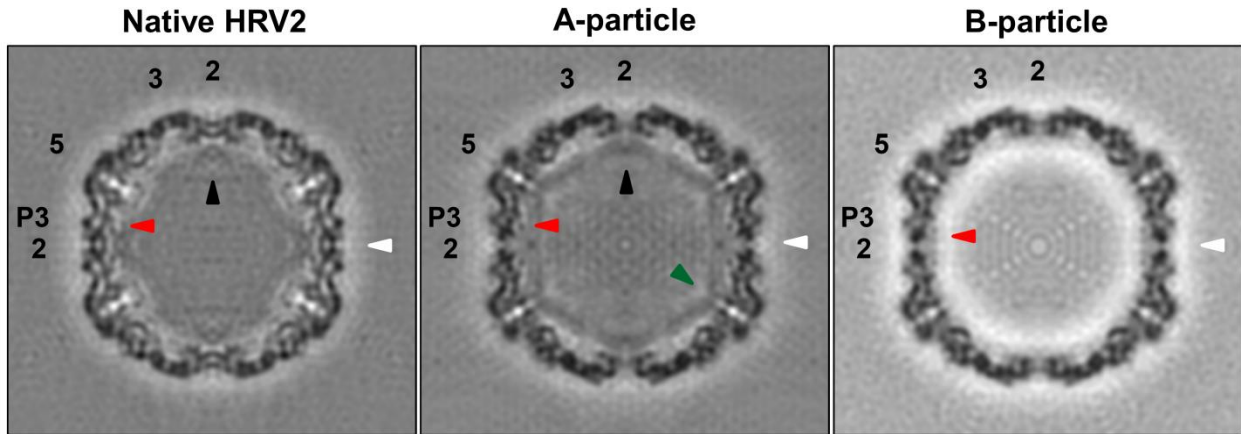
Figure 34 The genome becomes more ordered in A- and is expelled in B-particles. EM-maps of native and subviral particles were filtered to 10 Å. Central sections are displayed. In native HRV2, parts of ordered RNA are resolved beneath the 2-fold axis (black arrow head). In A-particles, the genome becomes more ordered and forms an RNA shell within the capsid. It contacts the capsid at the 2-fold axis (black arrow head) and extends beneath the pore (white arrow heads). The RNA shell is also in close proximity to the protein shell at the 5-fold axis, however, no contact points of RNA and protein densities are seen at 1.5 σ (green arrow head). Density, attributed to RNA, is lost in B-particles. In native virus, a solvent-filled area at the pseudo-3-fold axis is visible. It is occupied by density in subviral particles, possibly by the externalized VP1 N-terminus (red arrow heads). Central sections were displayed with bshow. Symmetry axes are indicated.

6.2 Membrane-attached uncoating intermediates of minor group rhinoviruses

In vivo, uncoating of human rhinoviruses occurs in the context of cellular membranes. Hydrophobic subviral particles are generated in endosomes due to the acidic pH and attach to the endosomal membrane. Although so far not visualized, it is believed that their externalized amphipathic residues form a trans-membrane pore, through which the viral genome is released into the cytoplasm. To fully understand the uncoating process, intermediate particles need thus to be studied also in the context of lipid bi-layers. The goal of the second part of this thesis was to set up a model system for investigating these membrane-attached uncoating intermediates from a structural point of view.

Despite being physiological, isolated endosomes are not well suited for structural studies where concentrated and pure samples are required. The variability, introduced by the associated and endosomal proteins, would introduce a considerable background and the cellular source limits the amounts of the organelle that can be purified (Beaumelle BD and Hopkins CR, 1989). Alternatively, using liposomes as model membranes, Bubeck D *et al.* (2005a) solved the structure of membrane-attached native poliovirus and Bilek G *et al.* (2007) showed attachment of HRV2 to PEGylated liposomes in capillary electrophoresis. Here we chose a similar but more physiological approach, to study membrane-bound uncoating intermediates of the minor group rhinoviruses HRV2.

6.2.1 HRV2 specifically binds to receptor-decorated liposomes of endosome-like composition

Liposomes were prepared with a lipid composition close to that of late endosomes with 30 mol% cholesterol (Ch), 20 mol% phosphatidylcholine (PC), 20 mol% phosphatidylethanolamine (PE) and 20 mol% sphingomyelin (SM). In order to allow efficient binding of His6-tagged recombinant receptors, 10% 1,2-dioleoyl-*sn*-glycero-3-[(N-(5-amino-1-carboxypentyl)iminodiacetic acid)succinyl] (DGS-NTA) lipids were additionally included. NBD-PC, 1-oleoyl-2-[12-[(7-nitro-2-1,3-benzoxadiazol-4-yl)amino] lauroyl]-sn-glycero-3-phosphocholine, served as fluorescent tracer. Lysobisphosphatidic acid (LPA), an endosomal lipid involved in membrane fusion and the generation of multi-vesicular bodies, was excluded from the liposome composition. Successful HRV2 infection from the plasma membrane, that lacks this lipid, proved LPA to be irrelevant for trans-membrane RNA release of rhinoviruses (Kobayashi T *et al.*, 2002; Brabec M *et al.*, 2003; Matsuo H *et al.*, 2004; van Meer G *et al.*, 2008). Similar liposome compositions were previously used to study poliovirus, attached to receptor-decorated liposomes or pH-dependent membrane-fusion of Semliki Forest virus. (White J and Helenius A, 1980; Bubeck D *et al.*, 2005a).

The well studied, high affinity mini-receptor V33333 was bound via its His6-tag to NTA-groups of the liposomes. It is a derivative of VLDLR and consists of concatemers of the high affinity complement repeat 3. (Moser R *et al.*, 2005; Wruss J *et al.*, 2007; Querol-Audi J *et al.*, 2009).

Native HRV2 specifically attached to these receptor-decorated model membranes and co-migrated with liposomes on sucrose density gradients. In the

absence of receptor, virions failed to bind to the vesicles and remained in the bottom fraction of the gradient (Figure 35).
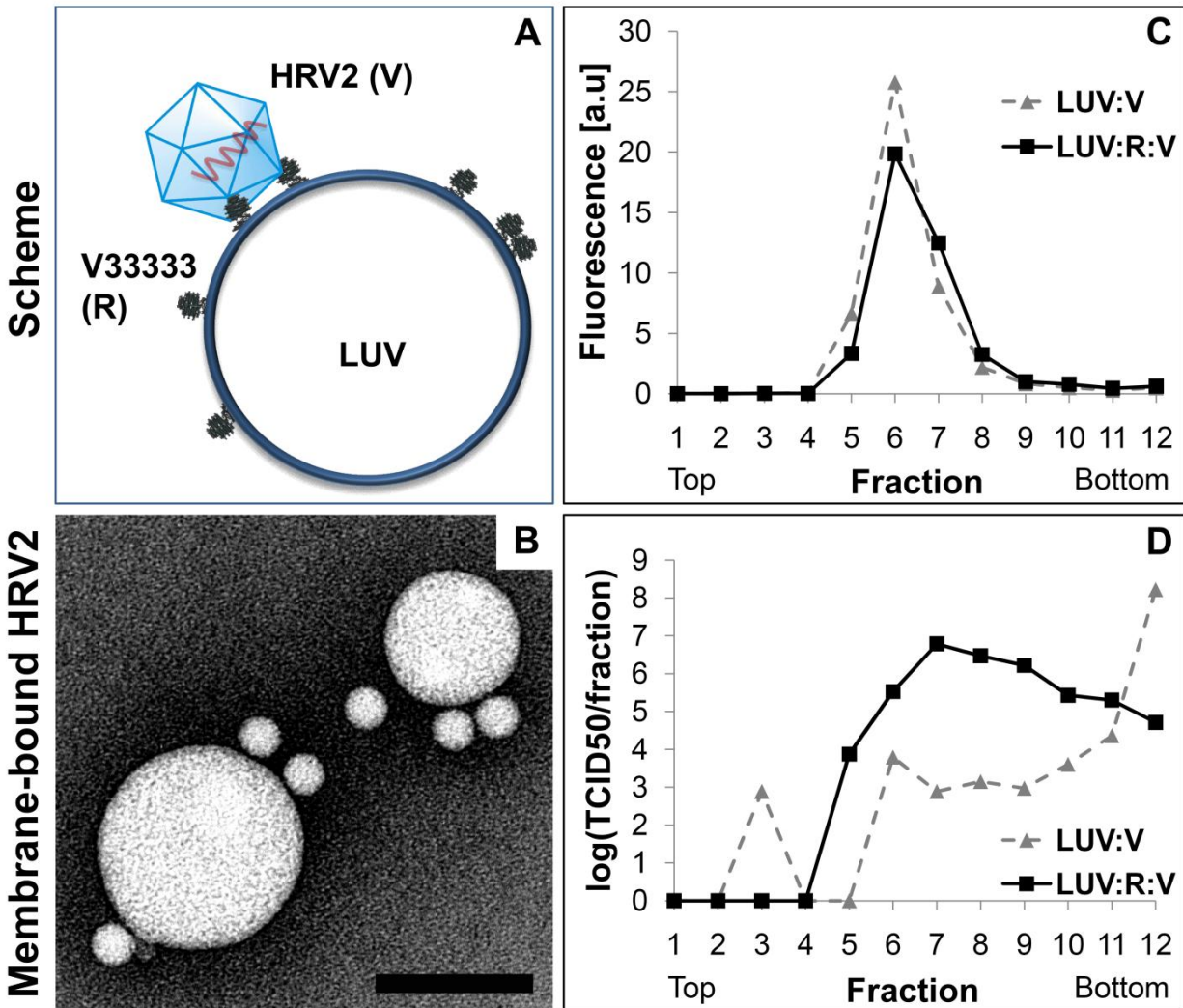
Figure 35 HRV2 specifically binds to liposomes decorated with the VLDLR minireceptor V33333. Large unilamellar vesicles (LUV), containing NTA- and fluorescent tracer lipids, were decorated with the His6-tagged recombinant receptor V33333 (R). HRV2 (V) specifically attached to these model membranes (A). LUV:R:V complexes as well as a control lacking receptor (LUV:V) were overlaid with a 50%/25%/0% sucrose step gradient and subjected to ultracentrifugation. Liposomes and virus were detected by fluorescence measurements (C) and TCID50 infectivity assays (D), respectively. HRV2 co-flotated only with V33333-decorated liposomes; in the absence of receptor, virtually all virions remained at the bottom of the gradient. The peak fraction of the complex was applied to glow-discharged carbon-coated copper grids and negatively stained with 2% phosphotungstate pH 7.2. Images were taken in an 80 kV Morgagni TEM using an 11 Mpixel CCD camera. Attachment of virions to lipid vesicles can be clearly seen. Size bar = 100 nm (B). TEM images and flotation data are representatives of three independent experiments. Flotations and TCID50 assays by Nena Matscheko and Irene Gösler, respectively.

Aiming at single particle reconstruction of cryo-EM data, conditions for complex formation were optimized in negative stain TEM to maximize virus binding without causing significant aggregation. As each virus has 12 receptor binding sites, receptors attached to different vesicles can simultaneously bind to the same virion, thereby forming aggregates, useless for single particle reconstruction. Molar ratios of 8.4*104 mol lipid : 79 mol receptor : 1 mol virus gave the best results. Considering the different sizes of the individual lipids as well as the diameter of the extruded liposomes, this corresponds to an average of about 5 virions per liposome. It has to be noted that not all virions attached to liposomes and that even after separating complexes from free virus via flotation, virions fell off the vesicles again. This reduced the theoretical number to effectively 2 to 3 bound virions per vesicle (Figure 35B). Increasing the receptor concentration did improve virus attachment but lead to considerable aggregation of complexes.

6.2.2 Cryo-EM of membrane-attached HRV2

Using conditions for complex formation as determined by negative stain TEM, membrane-attached HRV2 was frozen for cryo-electron microscopy. Surprisingly, cryo-images showed considerable portions of free virus and undecorated liposomes.

It may be that grid adsorption in negative stain TEM promoted co-localization of virus with liposomes. However, efficient complex formation was demonstrated via flotation, making this unlikely (Figure 35).

According to Kelly DF *et al.* (2008), plunge freezing during cryo-preparation could affect the NTA:His6 interaction. Their data on binding of His6-tagged transferrin receptor to NTA-containing lipid monolayers showed that for comparable binding,

vitrified samples required higher concentrations of NTA-lipids than negative stain preparations. Liposomes were thus prepared containing their recommended 20 % of NTA-lipids. Alternatively, vesicles with 5 % tris-NTA lipid were made that bind hexa-histidines with significantly higher affinity than conventional mono-NTA (Huang Z *et al.*, 2009). Different virus:receptor:liposome ratios were screened as well as pre-charging NTA groups with excess of Ni2+ ions. However, conditions yielding more membrane-attached particles also led to aggregation. These preparations could not be used for cryo-EM imaging.

HRV2, bound to liposomes with 10 % NiNTA lipids, was thus frozen and cryo-imaged in a Philips CM200 TEM. Per micrograph an average of 13 membrane-attached virions were imaged, yielding a total of 653 particles for an initial reconstruction (Figure 36). Binding levels of HRV2 to receptor-decorated liposomes were thus comparable to that of poliovirus (Bubeck D *et al.*, 2008).

Cryo-data were analyzed with the auto3dem package (Yan X *et al.*, 2007). Particles were manually picked and CTF-corrected. Images were aligned by icosahedral projection matching, using the X-ray structure of native HRV2, filtered to 25 Å, as starting map.

Considering a Fourier Shell Correlation of 0.5, the EM-map of membrane-attached HRV2 was solved to 23.8 Å resolution. It showed characteristic rhino-viral features such as the tri-angular plateau at the 3- and the depression at the 2-fold axis. At 1 σ contour level, additional density was seen at the 5-fold axis, when compared to the structure of native HRV2. This density formed a ring-like structure around the star-shaped dome of the virus, corresponding well to bound receptor, as it was resolved in

the X-ray structure of receptor-decorated HRV2 (Verdaguer N *et al.*, 2004; Querol-Audi J *et al.*, 2009). In the EM-map, the density of the receptor was less pronounced, indicating partial occupancy. This was expected, as the samples contained a 106-fold molar excess of NTA-lipids to His6-tagged V33333. The majority of the receptor should thus be membrane-bound and not free in solution, so that it could not saturate the viral pentamers.

Due to icosahedral averaging the attachment site of the virus on liposomal membrane was not resolved (Figure 36).

Membrane-bound HRV2　　Verdaguer N *et al.* (2004)
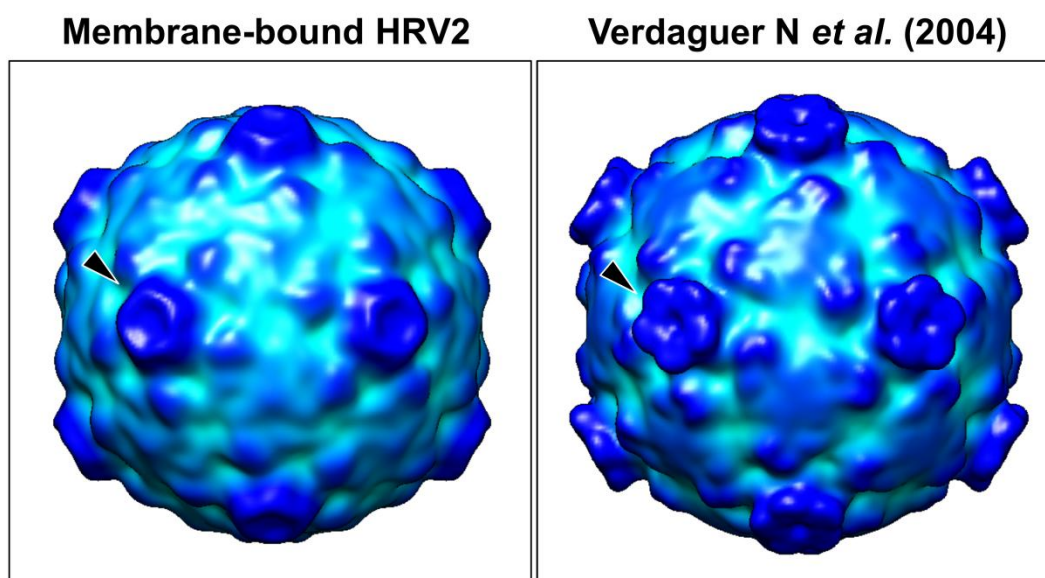
Figure 36 The icosahedral reconstruction of membrane-bound HRV2 shows partial receptor occupancy. HRV2 was attached to liposomes with NTA-lipids via the His6-tagged receptor V33333. It was reconstructed from cryo-images by icosahedral projection matching, using the software package auto3dem (Yan X *et al.*, 2007). In the EM map weaker density is visible for the receptor, when compared to the X-ray structure of receptor-decorated HRV2, filtered to 25 Å (Verdaguer N *et al.*, 2004). This indicates partial receptor occupancy. Figures were made in chimera. EM and X-ray maps were contoured to 1 σ and radially colored.

The low resolution EM map confirms that the established model system of membrane-bound HRV2 can be successfully used in cryo-EM studies.

6.2.3 Membrane-attached uncoating intermediates

The used receptor V33333 was shown to have anti-viral activity by stabilizing the capsid and thereby inhibiting uncoating of minor group rhinoviruses (Moser R *et al.*, 2005; Nicodemou A *et al.*, 2005). To reduce the inhibitory influence of the receptor during the study of membrane-attached uncoating intermediates, liposomes were decorated with V33333 and complexes were separated from unbound receptor via flotation. HRV2 was attached at a virus to lipid ratio of $1.85*10\text{-}6$.

In analogy to *in vivo*, uncoating of membrane-attached HRV2 was triggered by exposure to pH 5.4, a pH value also found in late endosomes (Schmid S *et al.*, 1989). Complexes were acidified for different time intervals for up to 30 min and uncoating was halted by negative stain sample preparation. In that way a time course of RNA release could be visualized in TEM.

Without trigger, most particles were native virus with homogenous electron density. Within 2 min of exposure to pH 5.4, intermediates formed, identifiable by partial stain penetration. Surprisingly, these virions looked considerably different from A-particles; part of their RNA density was already released. For most intermediates, the residual internal density was rod-shaped and spanned the viral capsid, suggesting a common stage in the uncoating process (Figure 37B). Prolonged acidification, for over 15 min, lead to complete loss of internal density. The particles visually resembled empty capsids but remained membrane-associated (Figure 37C).
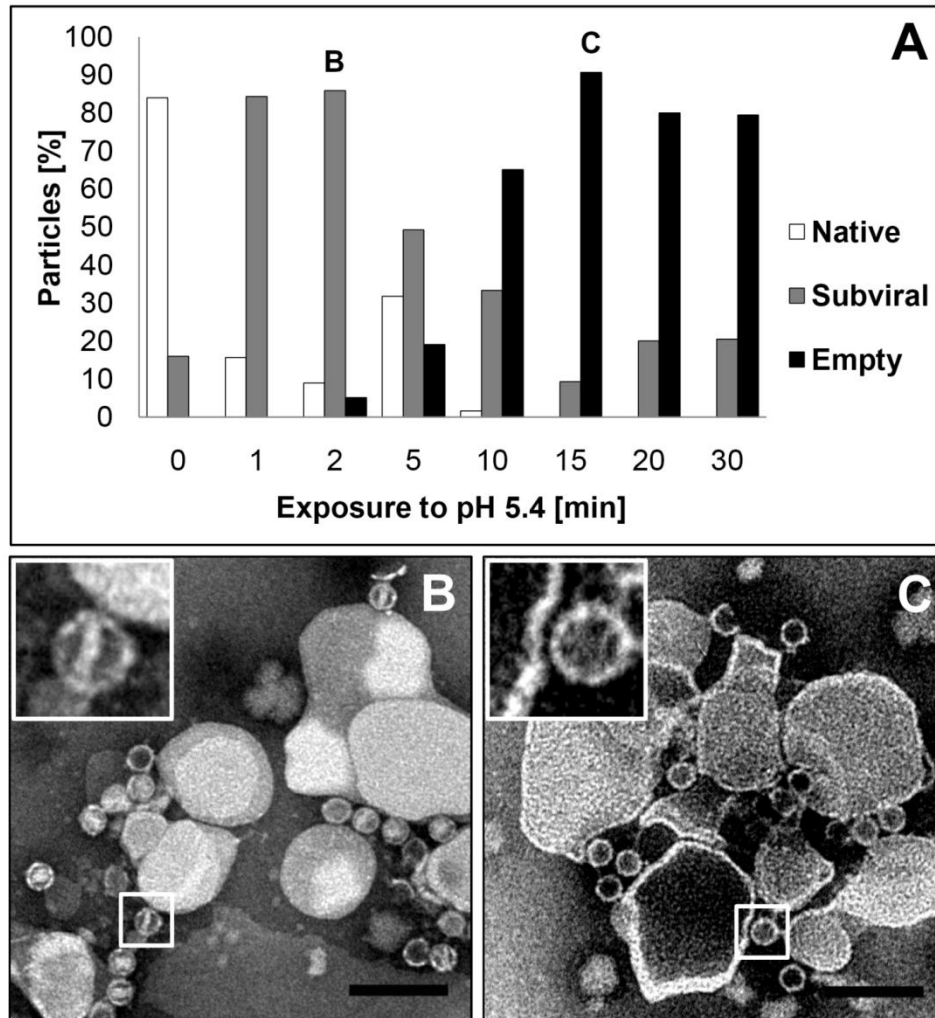
Figure 37 Uncoating of membrane-attached HRV2 involves a new uncoating intermediate with partially released RNA. Liposomes with NTA-lipids were decorated with His6-tagged V33333. Free receptor was removed via flotation in a sucrose gradient. HRV2 was bound and acidified to pH 5.4 for the times indicated. Uncoating was halted by sample adsorption to carbon-coated copper grids and negative staining with 2 % phospho-tungstate pH 7.2. Samples were imaged in an 80 kV TEM. Particles were classified according to different degrees of stain penetration (A). Without acidification, most membrane-attached virions are native HRV2. After 2 min exposure to pH 5.4, intermediate particles form with partially released RNA (B). Uncoating is completed after 15 min acidification, when most particles are membrane-attached empty capsids (C). Per time point about 200 particles were examined.

It has to be mentioned that different virus preparations differed slightly in their pH stability. The peak of their individual particle species was thus obtained after slightly different exposure times to pH 5.4, but the sequence of particle species was consistent for all preparations tested.

Using the experimental conditions described here, Bilek G *et al.* (submitted) demonstrated that membrane-attached HRV2 transferred its genome into the liposomal lumen. They detected the trans-located RNA within the vesicle via an encapsidated reverse transcription mix and via subsequent amplification of the generated cDNA by PCR. Their results prove the validity of using receptor-decorated liposomes for studying rhino-viral uncoating in the context of membranes.

6.2.4 Rhino-viral uncoating on membranes proceeds faster than in solution and terminates in a lipophilic empty capsid

Comparing rhino-viral uncoating in solution and on membranes, two main differences became apparent.

The time course of RNA release was much faster for membrane-bound virus. Already within 2 min incubation at pH 5.4, the majority of virions partially released their genome. In solution, however, acidification of HRV2 at pH 5.0 for 15 min resulted in A-particles, still harboring the full viral genome. The lower pH of exposure for generating A-particles would rather be expected to accelerate the uncoating process. It seems thus that there is an additional factor accelerating RNA release in the context of membranes. The used receptor was shown to inhibit uncoating, the trigger for RNA release may thus be the lipid bi-layer itself or the pH gradient across it.

After RNA translocation, empty capsid remained attached to the membrane. This was in contrast to B-particles, generated in solution, that failed to attach to lipid bi-layers (Lonberg-Holm K *et al.*, 1976).

Solving the structure of membrane-attached intermediates in the future will elucidate the differences between subviral particles in solution and attached to

membranes. In addition, it may help to show how rhinoviruses transfer their genome

through lipid bi-layers.

7 Discussion

In the current thesis the EM-maps of HRV2 A- and B-particles were solved to resolutions better than 10 Å. The structural changes of the capsid during uncoating were revealed by their comparison with the X-ray structure of native HRV2. Using a liposome-based model system, viral conversion was also investigated in the context of membranes. Thereby new intermediate particles with partially released RNA were discovered.

7.1 Uncoating of minor group rhinoviruses: Proposed model

Considering these results in the context of already published data on HRV2, we propose the following model for uncoating of minor group rhinoviruses.

Upon binding to receptors of the LDLR family, minor group rhinoviruses are internalized via clathrin-mediated endocytosis (*Snyers L et al.*, 2003). They are transported to endosomal carrier vesicles and late endosomes. At the low pH within these vesicles, the receptor forms an intra-molecular bond, releasing the bound virus (Brabec M *et al.*, 2003; Konecsni T *et al.*, 2009). The acidic pH also triggers conformational changes of the viral capsid, generating the hydrophobic A-particle (Lonberg-Holm K and Noble-Harvey J, 1973). The amphipathic N-terminus of VP1 is externalized via the pseudo-3-fold axis and VP4 is expelled at a yet unknown site. As externalization of the VP1 N-terminus occurs at a specific location on the viral capsid, it is expected that A-particles attach to the membrane in a defined orientation, even in the absence of receptor binding.

The orientation of subviral particles on membranes is yet unknown. At the 2-fold axis the largest pore opens in the capsid and the genome localizes directly beneath this opening. We thus propose that the virus approaches the membrane with its 2-fold axis. In that case, two VP1 N-termini, externalized in proximity to the hole at the 2-fold axis, would anchor the A-particle in the endosomal membrane. In negative stain images of membrane-attached uncoating intermediates, viral particles are often engulfed by the liposomal membrane, indicating that also distant VP1 N-termini contribute to the attachment.

Structurally, A- and B-particles are very similar. However, the pores in the capsid are larger in A-particles and also the rotation of the star-shaped dome at the 5-fold axis is more pronounced than in empty capsids. It seems thus that A-particles represent an expanded or strained state of the final capsid structure, probably to facilitate RNA release. Such expanded intermediate particles have already been suggested for poliovirus (Levy HC *et al.*, 2010).

Within minutes of exposure to acidic pH, virions start to release their genome. This probably occurs in discrete steps, because intermediates with partially released RNA have a consistent appearance in negative stain TEM. Their residual RNA is visible as rod-shaped density within an otherwise empty capsid. Brandenburg B *et al.* (2007) presented evidence for poliovirus RNA exiting the capsid in a single-stranded form. As also suggested for PV, it may be that the release of rhino-viral RNA is halted at certain points of RNA unwinding, corresponding to the observed intermediate particles.

Bilek *et al.* (submitted) demonstrated that HRV2 transferred its genome into liposomes without disrupting vesicle integrity, indicating the formation of a pore for

trans-membrane release of RNA into the cytoplasm. The externalized N-terminus of VP1 and the expelled VP4 have been implicated in that, as both permeabilize membranes at acidic pH (Zauner W *et al.*, 1995; Weiss VU *et al.*, 2010). As mentioned above, the exit site of VP4 on the capsid is unknown. Based on low resolution structures, the 5-fold axis has been suggested as site of externalization (Hewat EA *et al.*, 2002; Hewat EA and Blaas D, 2004). However, in the current structures of A- and B-particles at sub-nanometer resolution, the N-terminus of VP3 narrows the channel at the 5-fold axis, making it an unlikely site for VP4 externalization. Alternatively, Xing L *et al.* (2003) proposed that in uncoating intermediates of receptor-decorated HRV3, VP4 was released from the capsid via the pseudo-3-fold axis. At the same site, a hole is visible in the structure of HRV2 B-particles (Verdaguer N *et al.*, in preparation). The trans-membrane pore may consequently form close to the viral 2-fold axis, from where the viral genome is released. It is likely that this occurs at an asymmetric site on the capsid, induced by the presence of the membrane, as already proposed for PV (Levy HC *et al.*, 2010).

Upon RNA release, the empty capsid remains attached to the endosomal membrane. After fusion of late endosomes with lysosomes, it is degraded.

7.2 Uncoating of minor group rhinoviruses: Similarities and differences to major group rhinoviruses and poliovirus

Structural changes during uncoating of one receptor group of rhinoviruses are often generalized to the other. In addition, many results on uncoating of the closely related poliovirus (PV) are extrapolated to rhinoviruses.

For the main conformational changes of the capsid this turns out to be valid and uncoating of minor and major group HRVs but also of PV shows similarities. Uncoating of both virus species occurs in endosomes and via a stable intermediate, the A-particle. It is enlarged by roughly 4 %, when compared to native virions, and the RNA genome forms a density shell in close proximity to the capsid (Xing L *et al.*, 2003; Bubeck D *et al.*, 2005b). The VP1 N-terminus of A-particles is externalized and VP4 is expelled. Both interact with membranes (Tosteson MT and Chow M, 1997; Danthi P *et al.*, 2003; Weiss VU *et al.*, 2010) and are believed to aid in transferring the viral genome from endosomes into the cytoplasm.

However, essential differences between the virus species were also demonstrated, underlining that extrapolations have to be considered with caution.

7.2.1 Receptor

Poliovirus and major group rhinoviruses share a similar receptor binding site, the canyon, a depression in the capsid surface surrounding the viral 5-fold axis. Their receptors, Poliovirus Receptor (PVR) and ICAM-1, respectively, have immunoglobulin-like ectodomains that bind to the floor of the canyon and thereby induce structural changes of the capsid. In PV this leads directly to the formation of A-particles. In accordance to that, ICAM-1 directly induces uncoating of some major group serotypes such as HRV3 (Greve JM *et al.*, 1991; Xing L *et al.*, 2003). For other serotypes, including HRV14, a combination of ICAM-1 binding and low pH is required for uncoating (Nurani G *et al.*, 2003). The receptors of minor group rhinoviruses, the members of the LDLR family, already differ structurally from PVR and ICAM-1. They consist of complement repeats that attach in a ring-shaped conformation around the viral star-

shaped dome at the 5-fold axis. LDLRs have no catalytic activity and serve merely as vehicle for endocytosis. At the acidic pH found in endosomes, they form an intra-molecular bond and thereby release the bound virus. Solely the low pH within endosomes is thus responsible for the formation of A-particles of minor group rhinoviruses (Prchla E *et al.*, 1994).

7.2.2 A- and B-particles

For rhinoviruses, A- and B-particle have similar capsid structures at sub-nanometer resolution and differ only in the location of the VP1 N-terminus and the presence or release of the genome. Already in A-particles pores form at the 2- and 5-fold axes. They remain open also during the transition to B-particles, although they become slightly reduced in size. The EM map of B-particles was reconstructed from about 3000 images to sub-nanometer resolution and the X-ray structure was recently solved with essentially the same result at 10 Å resolution (Verdaguer N *et al.*, in preparation). It is thus unlikely that structurally different classes of B-particles exist.

In contrast, Bubeck D *et al.* (2005b) described an intact protein shell for PV A-particles. Its further conversion to empty capsids occurs in discrete steps, involving an early and a late B-particle that differ significantly at sub-nanometer resolution. Early B-particles have intact capsids with thinned density at the 2-fold axis. They transform into late B-particles with visible holes in their protein shell (Levy HC *et al.*, 2010).

The positions of these openings in the capsid also differ between rhino- and poliovirus. As previously described, direct channels open in the capsid of HRV2 at the 2- and 5-fold axes. An additional pore is seen in B-particles at the pseudo-3-fold axis. For the major group HRV14, the channel at the 5-fold axis was also described. At the 2-

fold axis, only a thinning of the capsid was observed but not a direct opening. This is probably due to the limited resolution of the map (Hewat EA and Blaas D, 2004). In the structure of receptor-decorated B-particles of HRV3, another major group rhinovirus, the dome at the 5-fold axis remains intact during uncoating, but a channel opens at the pseudo3-fold axis (Xing L *et al.*, 2003).

In PV, however, the 2-fold axis of late B-particles has a completely different appearance. A density bridge spans the 2-fold axis and two holes open adjacent to it, between the 2- and pseudo-3-fold axes. Consistent with data from HRV2, the star-shaped dome at the 5-fold axis rotates during uncoating of PV but it remains intact. For PV B-particles, the channel at the pseudo-3-fold axis was also described (Levy HC *et al.*, 2010).

7.2.3 Externalization of the VP1 N-terminus and VP4

A further difference between the viruses is the exit site of the VP1 N-terminus. In HRV2 A-particles, the protein residues are externalized at the pseudo-3-fold axis via a spherical area, filled with solvent in native virus. Externalization of the VP1 N-terminus at this point would be blocked by bound ICAM-1 or PVR in major gourp HRVs and PV, respectively. Accordingly, in HRV14, the solvent-filled bubble at the pseudo-3-fold axis remains unchanged during uncoating. Hewat EA and Blaas D (2004) proposed the base of the canyon, between two neighboring VP1s, as alternative exit site of the VP1 N-terminus. Consistent with major group rhinoviruses, the VP1 N-terminus of poliovirus is externalized at the same location (Bubeck D *et al.*, 2005b).

Considering the release of VP4, HRV2 and PV behave similarly during uncoating. Both viruses release most of their inner capsid protein that is believed to

form a trans-membrane pore for RNA transfer into the cytoplasm (Weiss VU, 2009; Bilek G *et al.*, submitted). In contrast, the major group HRV3 and HRV14 were shown to only partially expel VP4 (Casasnovas JM and Springer TA, 1994; Hewat EA and Blaas D, 2004). This is consistent with data by Schober D *et al.* (1998) who showed that major group HRVs disrupt the endsome during uncoating, rather than forming a pore for RNA release.

7.2.4 RNA release

For poliovirus the structure of an additional subviral particle was solved to 45 Å, an intermediate between A- and B-particle, caught in the act of RNA release. It constitutes about 5 % of particles in heat-triggered preparations of empty capsids and is structurally assigned to the class of early B-particles (Bostina M *et al.*, 2011). In TEM, caught-in-the-act particles of PV resemble membrane-attached rhino-viral intermediates, generated by acidification at pH 5.4 for 2 min. Both types of particles appear as empty capsids with rod-shaped internal RNA density.

In PV, averaging of sub-tomograms of caught-in-the-act particles reveals externalization of the viral genome via one of the holes between the 2- and pseudo-3-fold axes. Bostina M *et al.* (2011) suggested that viral protein residues may catalyze unwinding of the RNA for its single-stranded release from the capsid. In the structure of PV A-particles, protein-RNA interactions are localized to the pseudo-3- and 5-fold axes (Bubeck D *et al.*, 2005b). In contrast, in HRV2 A-particles, the genome contacts the protein capsid at the 2- and pseudo-3-fold axes. Density of ordered RNA extends also beneath the capsid hole at the 2-fold axis, making this the probable site for RNA

release. Solving the structure of intermediates with rod-shaped RNA density may elucidate rhino-viral RNA externalization in the future.

Literature

1.   Aebi U, Pollard TD. A glow discharge unit to render electron microscope grids and other surfaces hydrophilic. J Electron Microsc Tech 1987; 7: 29-33.

2.   Andersen OM, Christensen LL, Christensen PA, Sørensen ES, Jacobsen C, Moestrup SK, Etzerodt M, Thogersen HC. Identification of the minimal functional unit in the low density lipoprotein receptor-related protein for binding the receptor-associated protein (RAP). A conserved acidic residue in the complement-type repeats is important for recognition of RAP. J Biol Chem 2000; 275: 21017-24.

3.   Andries K, Dewindt B, Snoeks J, Wouters L, Moereels H, Lewi PJ, Janssen PA. Two groups of rhinoviruses revealed by a panel of antiviral compounds present sequence divergence and differential pathogenicity. J Virol 1990; 64: 1117-23.

4.   Arnold E and Rossmann MG. Analysis of the structure of a common cold virus, human rhinovirus14, refined at a resolution of 3.0 Å. J Mol Biol 1990; 211: 763–801.

5.   Bayer N, Schober D, Hüttinger M, Blaas D, Fuchs R. Inhibition of clathrin-dependent endocytosis has multiple effects on human rhinovirus serotype 2 cell entry. J Biol Chem 2001; 276: 3952-62.

6.   Beaumelle BD, Hopkins CR. High-yield isolation of functionally competent endosomes from mouse lymphocytes. Biochem J 1989; 264: 137-49.

7.   Bilek G, Kremser L, Wruss J, Blaas D, Kenndler E. Mimicking early events of virus infection: capillary electrophoretic analysis of virus attachment to receptor-decorated liposomes. Anal Chem 2007; 79: 1620-5.

8.   Bilek G, Matscheko NM, Pickl-Herk A, WeissVU , Subirats X, Kenndler E, Blaas D. Liposomal Nanocontainers as Models for Viral Infection: Monitoring Viral Genomic RNA Transfer through Lipid Membranes. J Virol. Submitted.

9.   Blacklow SC. Versatility in ligand recognition by LDL receptor family proteins: advances and frontiers. Curr Opin Struct Biol 2007; 17: 419-26.

10. Blake K, O'Connell S. Virus Culture, *In* D. R. Harper (ed.), Virology Labfax. Blackwell Scientific Publications, West Smithfield, London EC1A 7BE, UK. 1993. p. 81-122.

11. Bochkov YA, Palmenberg AC, Lee WM, Rathe JA, Amineva SP, Sun X, Pasic TR, Jarjour NN, Liggett SB, Gern JE. Molecular modeling, organ culture and reverse genetics for a newly identified human rhinovirus C. Nat Med 2011.

12. Bostina M, Levy H, Filman DJ, Hogle JM. Poliovirus RNA is released from the capsid near a twofold symmetry axis. J Virol 2011; 85: 776-83.

13. Brabec M, Baravalle G, Blaas D, Fuchs R. Conformational changes, plasma membrane penetration, and infection by human rhinovirus type 2: role of receptors and low pH. J Virol 2003; 77: 5370-7.

14. Brabec M, Schober D, Wagner E, Bayer N, Murphy RF, Blaas D, Fuchs R. Opening of size-selective pores in endosomes during human rhinovirus serotype 2 in vivo uncoating monitored by single-organelle flow analysis. J Virol 2005; 79: 1008-16.

15. Brandenburg B, Lee LY, Lakadamyali M, Rust MJ, Zhuang X, Hogle JM. Imaging poliovirus entry in live cells. PLoS Biol 2007; 5: e183.

16. Brown MS, Herz J, Goldstein JL. LDL-receptor structure. Calcium cages, acid baths and recycling receptors. Nature 1997; 388: 629-30.

17. Bubeck D, Filman DJ, Hogle JM. Cryo-electron microscopy reconstruction of a poliovirus-receptor-membrane complex. Nat Struct Mol Biol 2005a; 12: 615-8.

18. Bubeck D, Filman DJ, Cheng N, Steven AC, Hogle JM, Belnap DM. The structure of the poliovirus 135S cell entry intermediate at 10-angstrom resolution reveals the location of an externalized polypeptide that binds to membranes. J Virol 2005b; 79: 7745-55.

19. Bubeck D, Filman DJ, Kuzmin M, Fuller SD, Hogle JM. Post-imaging fiducial markers aid in the orientation determination of complexes with mixed or unknown symmetry. J Struct Biol 2008; 162: 480-90.

20. Carragher B, Kisseberth N, Kriegman D, Milligan RA, Potter CS, Pulokas J, Reilein A. Leginon: an automated system for acquisition of images from vitreous ice specimens. J Struct Biol 2000; 132: 33-45.

21. Casasnovas JM, Springer TA. Pathway of rhinovirus disruption by soluble intercellular adhesion molecule 1 (ICAM-1): an intermediate in which ICAM-1 is bound and RNA is released. J Virol 1994; 68: 5882-9.

22. Chapman MS, Rossmann MG. Comparison of surface properties of picornaviruses: strategies for hiding the receptor site from immune surveillance. Virology 1993; 195: 745-56.

23. Danthi P, Tosteson M, Li QH, Chow M. Genome delivery and ion channel properties are altered in VP4 mutants of poliovirus. J Virol 2003; 77: 5266-74.

24. Fernández JJ, Luque D, Castón JR, Carrascosa JL. Sharpening high resolution information in single particle electron cryomicroscopy. J Struct Biol 2008; 164: 170-5.

25. Filman DJ, Syed R, Chow M, Macadam AJ, Minor PD, Hogle JM. Structural factors that control conformational transitions and serotype specificity in type 3 poliovirus. EMBO J 1989; 8: 1567-79.

26. Fricks CE, Hogle JM. Cell-induced conformational change in poliovirus: externalization of the amino terminus of VP1 is responsible for liposome binding. J Virol 1990; 64: 1934-45.

27. Fuchs R, Blaas D. Uncoating of human rhinoviruses. Rev Med Virol 2010; 20: 281-97.

28. Greve JM, Davis G, Meyer AM, Forte CP, Yost SC, Marlor CW, Kamarck ME, McClelland A. The major human rhinovirus receptor is ICAM-1. Cell 1989; 56: 839-47.

29. Greve JM, Forte CP, Marlor CW, Meyer AM, Hoover-Litty H, Wunderlich D, McClelland A. Mechanisms of receptor-mediated rhinovirus neutralization defined by two soluble forms of ICAM-1. J Virol 1991; 65: 6015-23.

30. Gruenberger M, Pevear D, Diana GD, Kuechler E, Blaas D. Stabilization of human rhinovirus serotype 2 against pH-induced conformational change by antiviral compounds. J Gen Virol 1991; 72: 431-3.

31. Hadfield AT, Lee W, Zhao R, Oliveira MA, Minor I, Rueckert RR, Rossmann MG. The refined structure of human rhinovirus 16 at 2.15 A resolution: implications for the viral life cycle. Structure 1997; 5: 427-41.

32. Haghighat A, Svitkin Y, Novoa I, Kuechler E, Skern T, Sonenberg N. The eIF4G-eIF4E complex is the target for direct cleavage by the rhinovirus 2A proteinase. J Virol 1996; 70: 8444-50.

33. Harris JM 2nd, Gwaltney JM Jr. Incubation periods of experimental rhinovirus infection and illness. Clin Infect Dis 1996; 23: 1287-90.

34. Heikkinen T, Järvinen A. The common cold. Lancet 2003; 361: 51-9.

35. Herz J, Strickland DK. LRP: a multifunctional scavenger and signaling receptor. J Clin Invest 2001; 108: 779-84.

36. Hewat EA, Neumann E, Blaas D. The concerted conformational changes during human rhinovirus 2 uncoating. Mol Cell 2002; 10: 317-26.

37. Hewat EA, Blaas D. Cryoelectron microscopy analysis of the structural changes associated with human rhinovirus type 14 uncoating. J Virol 2004; 78: 2935-42.

38. Heymann JB, Belnap DM. Bsoft: image processing and molecular modeling for electron microscopy. J Struct Biol 2007; 157: 3-18.

39. Hofer F, Gruenberger M, Kowalski H, Machat H, Huettinger M, Kuechler E, Blaas D. Members of the low density lipoprotein receptor family mediate cell entry of a minor-group common cold virus. Proc Natl Acad Sci USA 1994; 91: 1839-42.

40. Hogle JM, Chow M, Filman DJ. Three-dimensional structure of poliovirus at 2.9 A resolution. Science 1985; 229: 1358-65.

41. Huber M, Brabec M, Bayer N, Blaas D, Fuchs R. Elevated endosomal pH in HeLa cells overexpressing mutant dynamin can affect infection by pH-sensitive viruses. Traffic 2001; 2: 727-36.

42. Jackson RJ, Kaminski A. Internal initiation of translation in eukaryotes: the picornavirus paradigm and beyond. RNA 1995; 1: 985-1000.

43. Jennings LC, Anderson TP, Beynon KA, Chua A, Laing RT, Werno AM, Young SA, Chambers ST, Murdoch DR. Incidence and characteristics of viral community-acquired pneumonia in adults. Thorax 2008; 63: 42-8.

44. Johnston SL. Overview of virus-induced airway disease. Proc Am Thorac Soc 2005; 2: 150-6.

45. Juvén T, Mertsola J, Waris M, Leinonen M, Meurman O, Roivainen M, Eskola J, Saikku P, Ruuskanen O. Etiology of community-acquired pneumonia in 254 hospitalized children. Pediatr Infect Dis J 2000; 19: 293-8.

46. Kaminski A, Pöyry TA, Skene PJ, Jackson RJ. Mechanism of initiation site selection promoted by the human rhinovirus 2 internal ribosome entry site. J Virol 2010; 84: 6578-89.

47. Katpally U, Fu TM, Freed DC, Casimiro DR, Smith TJ. Antibodies to the buried N terminus of rhinovirus VP4 exhibit cross-serotypic neutralization. J Virol 2009; 83: 7040-8.

48. Kelly DF, Dukovski D, Walz T. Monolayer purification: a rapid method for isolating protein complexes for single-particle electron microscopy. Proc Natl Acad Sci USA 2008; 105: 4703-8.

49. Kobayashi T, Beuchat MH, Chevallier J, Makino A, Mayran N, Escola JM, Lebrand C, Cosson P, Kobayashi T, Gruenberg J. Separation and characterization of late endosomal membrane domains. J Biol Chem 2002; 277: 32157-64.

50. Konecsni T, Kremser L, Snyers L, Rankl C, Kilár F, Kenndler E, Blaas D. Twelve receptor molecules attach per viral particle of human rhinovirus serotype 2 via multiple modules. FEBS Lett 2004; 568: 99-104.

51. Konecsni T, Berka U, Pickl-Herk A, Bilek G, Khan AG, Gajdzig L, Fuchs R, Blaas D. Low pH-triggered beta-propeller switch of the low-density lipoprotein receptor assists rhinovirus infection. J Virol 2009; 83: 10922-30.

52. Korant BD, Lonberg-Holm K, Noble J, Stasny JT. Naturally occurring and artificially produced components of three rhinoviruses. Virology 1972; 48: 71-86.

53. Kremser L, Petsch M, Blaas D, Kenndler E. Influence of detergent additives on mobility of native and subviral rhinovirus particles in capillary electrophoresis. Electrophoresis 2006; 27: 1112-21.

54. Kremser L, Blaas D, Kenndler E. Virus analysis using electromigration techniques. Electrophoresis 2009; 30: 133-40.

55. Laine P, Savolainen C, Blomqvist S, Hovi T. Phylogenetic analysis of human rhinovirus capsid protein VP1 and 2A protease coding sequences confirms shared genus-like relationships with human enteroviruses. J Gen Virol 2005; 86: 697-706.

56. Lau SK, Yip CC, Tsoi HW, Lee RA, So LY, Lau YL, Chan KH, Woo PC, Yuen KY. Clinical features and complete genome characterization of a distinct human rhinovirus (HRV) genetic cluster, probably representing a previously undetected HRV species, HRV-C, associated with acute respiratory illness in children. J Clin Microbiol 2007; 45: 3655-64.

57. Ledford RM, Patel NR, Demenczuk TM, Watanyar A, Herbertz T, Collett MS, Pevear DC. VP1 sequencing of all human rhinovirus serotypes: insights into genus phylogeny and susceptibility to antiviral capsid-binding compounds. J Virol 2004; 78: 3663-74.

58. Levy HC, Bostina M, Filman DJ, Hogle JM. Catching a virus in the act of RNA release: a novel poliovirus uncoating intermediate characterized by cryo-electron microscopy. J Virol 2010; 84: 4426-41.

59. Li Q, Yafal AG, Lee YM, Hogle J, Chow M. Poliovirus neutralization by antibodies to internal epitopes of VP4 and VP1 results from reversible exposure of these sequences at physiological temperature. J Virol 1994; 68: 3965-70.

60. Lomax NB, Yin FH. Evidence for the role of the P2 protein of human rhinovirus in its host range change. J Virol 1989; 63: 2396-9.

61. Lonberg-Holm K, Korant BD. Early interaction of rhinoviruses with host cells. J Virol 1972; 9: 29-40.

62. Lonberg-Holm K, Noble-Harvey J. Comparison of in vitro and cell-mediated alteration of a human Rhinovirus and its inhibition by sodium dodecyl sulfate. J Virol 1973; 12: 819-26.

63. Lonberg-Holm K, Yin FH. Antigenic determinants of infective and inactivated human rhinovirus type 2. J Virol 1973; 12: 114-23.

64. Lonberg-Holm K, Gosser LB, Shimshick EJ. Interaction of liposomes with subviral particles of poliovirus type 2 and rhinovirus type 2. J Virol 1976; 19: 746-9.

65. Mallia P, Message SD, Kebadze T, Parker HL, Kon OM, Johnston SL. An experimental model of rhinovirus induced chronic obstructive pulmonary disease exacerbations: a pilot study. Respir Res 2006; 7: 116.

66. Marlovits TC, Abrahamsberg C, Blaas D. Very-low-density lipoprotein receptor fragment shed from HeLa cells inhibits human rhinovirus infection. J Virol 1998; 72: 10246-50.

67. Matsuo H, Chevallier J, Mayran N, Le Blanc I, Ferguson C, Fauré J, Blanc NS, Matile S, Dubochet J, Sadoul R, Parton RG, Vilbois F, Gruenberg J. Role of LBPA and Alix in multivesicular liposome formation and endosome organization. Science 2004; 303: 531-4.

68. McKinlay MA, Pevear DC, Rossmann MG. Treatment of the picornavirus common cold by inhibitors of viral uncoating and attachment. Annu Rev Microbiol 1992; 46: 635-54.

69. Mellman I, Fuchs R, Helenius A. Acidification of the endocytic and exocytic pathways. Annu Rev Biochem 1986; 55: 663-700.

70. Message SD, Laza-Stanca V, Mallia P, Parker HL, Zhu J, Kebadze T, Contoli M, Sanderson G, Kon OM, Papi A, Jeffery PK, Stanciu LA, Johnston SL. Rhinovirus-induced lower respiratory illness is increased in asthma and related to virus load and Th1/2 cytokine and IL-10 production. Proc Natl Acad Sci USA 2008; 105: 13562-7.

71. Mindell JA, Grigorieff N. Accurate determination of local defocus and specimen tilt in electron microscopy. J Struct Biol 2003; 142: 334-47.

72. Moser R, Snyers L, Wruss J, Angulo J, Peters H, Peters T, Blaas D. Neutralization of a common cold virus by concatemers of the third ligand binding module of the VLDL-receptor strongly depends on the number of modules. Virology 2005; 338: 259-69.

73. Mosser AG, Vrtis R, Burchell L, Lee WM, Dick CR, Weisshaar E, Bock D, Swenson CA, Cornwell RD, Meyer KC, Jarjour NN, Busse WW, Gern JE. Quantitative and qualitative analysis of rhinovirus infection in bronchial tissues. Am J Respir Crit Care Med 2005; 171: 645-51.

74. Mukherjee S, Ghosh RN, Maxfield FR. Endocytosis. Physiol Rev 1997; 77: 759-803.

75. Neubauer C, Frasel L, Kuechler E, Blaas D. Mechanism of entry of human rhinovirus 2 into HeLa cells. Virology 1987; 158: 255-8.

76. Neumann E, Moser R, Snyers L, Blaas D, Hewat EA. A cellular receptor of human rhinovirus type 2, the very-low-density lipoprotein receptor, binds to two neighboring proteins of the viral capsid. J Virol 2003; 77: 8504-11.

77. Nicodemou A, Petsch M, Konecsni T, Kremser L, Kenndler E, Casasnovas JM, Blaas D. Rhinovirus-stabilizing activity of artificial VLDL-receptor variants defines a new mechanism for virus neutralization by soluble receptors. FEBS Lett 2005; 579: 5507-11.

78. Noble J, Lonberg-Holm K. Interactions of components of human rhinovirus type 2 with Hela cells. Virology 1973; 51: 270-8.

79. Nurani G, Lindqvist B, Casasnovas JM. Receptor priming of major group human rhinoviruses for uncoating and entry at mild low-pH environments. J Virol 2003; 77: 11985-91.

80. Okun VM, Blaas D, Kenndler E. Separation and biospecific identification of subviral particles of human rhinovirus serotype 2 by capillary zone electrophoresis. Anal Chem 1999; 71: 4480-5.

81. Okun VM, Nizet S, Blaas D, Kenndler E. Kinetics of thermal denaturation of human rhinoviruses in the presence of anti-viral capsid binders analyzed by capillary electrophoresis. Electrophoresis 2002; 23: 896-902.

82. Palmenberg AC, Pallansch MA, Rueckert RR. Protease required for processing picornaviral coat protein resides in the viral replicase gene. J Virol 1979; 32: 770-8.

83. Palmenberg AC, Spiro D, Kuzmickas R, Wang S, Djikeng A, Rathe JA, Fraser-Liggett CM, Liggett SB. Sequencing and analyses of all known human rhinovirus genomes reveal structure and evolution. Science 2009; 324: 55-9.

84. Papadopoulos NG, Bates PJ, Bardin PG, Papi A, Leir SH, Fraenkel DJ, Meyer J, Lackie PM, Sanderson G, Holgate ST, Johnston SL. Rhinoviruses infect the lower airways. J Infect Dis 2000; 181: 1875-84.

85. Pettersen EF, Goddard TD, Huang CC, Couch GS, Greenblatt DM, Meng EC, Ferrin TE. UCSF Chimera--a visualization system for exploratory research and analysis. J Comput Chem 2004; 25: 1605-12.

86. Phelps DK, Rossky PJ, Post CB. Influence of an antiviral compound on the temperature dependence of viral protein flexibility and packing: a molecular dynamics study. J Mol Biol 1998; 276: 331-7.

87. Prchla E, Kuechler E, Blaas D, Fuchs R. Uncoating of human rhinovirus serotype 2 from late endosomes. J Virol 1994; 68: 3713-23.

88. Querol-Audí J, Konecsni T, Pous J, Carugo O, Fita I, Verdaguer N, Blaas D. Minor group human rhinovirus-receptor interactions: geometry of multimodular attachment and basis of recognition. FEBS Lett 2009; 583: 235-40.

89. Resch GP, Brandstetter M, Koenigsmaier L, Urban E, Pickl-Herk A. Immersion Freezing of Suspended Particles and Cells for Cryo Electron Microscopy. Cold Spring Harb Protoc. Submitted.

90. Roivainen M, Piirainen L, Rysä T, Närvänen A, Hovi T. An immunodominant N-terminal region of VP1 protein of poliovirion that is buried in crystal structure can be exposed in solution. Virology 1993; 195: 762-5.

91. Rollinger JM, Schmidtke M. The human rhinovirus: human-pathological impact, mechanisms of antirhinoviral agents, and strategies for their discovery. Med Res Rev 2011; 31: 42-92.

92. Ronacher B, Marlovits TC, Moser R, Blaas D. Expression and folding of human very-low-density lipoprotein receptor fragments: neutralization capacity toward human rhinovirus HRV2. Virology 2000; 278: 541-50.

93. Rossmann MG, Arnold E, Erickson JW, Frankenberger EA, Griffith JP, Hecht HJ, Johnson JE, Kamer G, Luo M, Mosser AG, et al. Structure of a human common cold virus and functional relationship to other picornaviruses. Nature 1985; 317: 145-53.

94. Rossmann MG. The canyon hypothesis. Hiding the host cell receptor attachment site on a viral surface from immune surveillance. J Biol Chem 1989; 264: 14587-90.

95. Rossmann, M. G. Picornavirus structure overview. *In* Molecular Biology of Picornaviruses. Semler, B. L. & E. Wimmer, eds. ASM Press, Washington, D.C. 2002; pp. 27-38.

96. Rudenko G, Henry L, Henderson K, Ichtchenko K, Brown MS, Goldstein JL, Deisenhofer J. Structure of the LDL receptor extracellular domain at endosomal pH. Science 2002; 298: 2353-8.

97. Savolainen-Kopra C, Blomqvist S, Kilpi T, Roivainen M, Hovi T. Novel species of human rhinoviruses in acute otitis media. Pediatr Infect Dis J 2009; 28: 59-61.

98. <u>Scheres SH</u>, Valle M, Nuñez R, Sorzano CO, Marabini R, Herman GT, Carazo JM. Maximum-likelihood multi-reference refinement for electron microscopy images. J Mol Biol 2005; 348: 139-49.

99. <u>Schmid S</u>, Fuchs R, Kielian M, Helenius A, Mellman I. Acidification of endosome subpopulations in wild-type Chinese hamster ovary cells and temperature-sensitive acidification-defective mutants. J Cell Biol 1989; 108: 1291-300.

100. <u>Schober D</u>, Kronenberger P, Prchla E, Blaas D, Fuchs R. Major and minor receptor group human rhinoviruses penetrate from endosomes by different mechanisms. J Virol 1998; 72: 1354-64.

101. <u>Shaikh TR</u>, Gao H, Baxter WT, Asturias FJ, Boisset N, Leith A, Frank J. SPIDER image processing for single-particle reconstruction of biological macromolecules from electron micrographs. Nat Protoc 2008; 3: 1941-74.

102. <u>Siebert X, Navaza J</u>. UROX 2.0: an interactive tool for fitting atomic models into electron-microscopy reconstructions. Acta Crystallogr D Biol Crystallogr 2009; 65: 651-8.

103. <u>Skern T</u>, Sommergruber W, Blaas D, Gruendler P, Fraundorfer F, Pieler C, Fogy I, Kuechler E. Human rhinovirus 2: complete nucleotide sequence and proteolytic processing signals in the capsid protein region. Nucleic Acids Res 1985; 13: 2111-26.

104. <u>Skern T</u>, Neubauer C, Frasel L, Gründler P, Sommergruber W, Zorn M, Kuechler E, Blaas D. A neutralizing epitope on human rhinovirus type 2 includes amino acid residues between 153 and 164 of virus capsid protein VP2. J Gen Virol 1987; 68: 315-23.

105. <u>Snyers L</u>, Zwickl H, Blaas D. Human rhinovirus type 2 is internalized by clathrin-mediated endocytosis. J Virol 2003; 77: 5360-9.

106. <u>Sorzano CO</u>, Marabini R, Velázquez-Muriel J, Bilbao-Castro JR, Scheres SH, Carazo JM, Pascual-Montano A. XMIPP: a new generation of an open-source image processing package for electron microscopy. J Struct Biol 2004; 148: 194-204.

107. <u>Stanway G</u>, Hughes PJ, Mountford RC, Minor PD, Almond JW. The complete nucleotide sequence of a common cold virus: human rhinovirus 14. Nucleic Acids Res 1984; 12: 7859-75.

108. Svitkin YV, Gradi A, Imataka H, Morino S, Sonenberg N. Eukaryotic initiation factor 4GII (eIF4GII), but not eIF4GI, cleavage correlates with inhibition of host cell protein synthesis after human rhinovirus infection. J Virol 1999; 73: 3467-72.

109. Tosteson MT, Chow M. Characterization of the ion channels formed by poliovirus in planar lipid membranes. J Virol 1997; 71: 507-11.

110. Toyoda H, Nicklin MJ, Murray MG, Anderson CW, Dunn JJ, Studier FW, Wimmer E. A second virus-encoded proteinase involved in proteolytic processing of poliovirus polyprotein. Cell 1986; 45: 761-70.

111. Turner RB, Weingand KW, Yeh CH, Leedy DW. Association between interleukin-8 concentration in nasal secretions and severity of symptoms of experimental rhinovirus colds. Clin Infect Dis 1998; 26: 840-6.

112. Van Meer G, Voelker DR, Feigenson GW. Membrane lipids: where they are and how they behave. Nat Rev Mol Cell Biol 2008; 9: 112-24.

113. Verdaguer N, Blaas D, Fita I. Structure of human rhinovirus serotype 2 (HRV2). J Mol Biol 2000; 300: 1179-94.

114. Verdaguer N, Fita I, Reithmayer M, Moser R, Blaas D. X-ray structure of a minor group human rhinovirus bound to a fragment of its cellular receptor protein. Nat Struct Mol Biol 2004; 11: 429-34.

115. Vlasak M, Roivainen M, Reithmayer M, Goesler I, Laine P, Snyers L, Hovi T, Blaas D. The minor receptor group of human rhinovirus (HRV) includes HRV23 and HRV25, but the presence of a lysine in the VP1 HI loop is not sufficient for receptor binding. J Virol 2005; 79: 7389-95.

116. Weiss VU. Chip Electrophoresis of Human Rhinovirus and Receptor Decorated Liposomes as Model Membranes for the Analysis of Key Steps in the Viral Infection Pathway. University of Vienna, PhD Thesis 2009.

117. Weiss VU, Bilek G, Pickl-Herk A, Subirats X, Niespodziana K, Valenta R, Blaas D, Kenndler E. Liposomal leakage induced by virus-derived peptides, viral proteins, and entire virions: rapid analysis by chip electrophoresis. Anal Chem 2010; 82: 8146-52.

118. White J, Helenius A. pH-dependent fusion between the Semliki Forest virus membrane and liposomes. Proc Natl Acad Sci USA 1980; 77: 3273-7.

119. Wimmer E. Genome-linked proteins of viruses. Cell 1982; 28: 199-201.

120. Winther B, Farr B, Turner RB, Hendley JO, Gwaltney JM Jr, Mygind N. Histopathologic examination and enumeration of polymorphonuclear leukocytes in the nasal mucosa during experimental rhinovirus colds. Acta Otolaryngol Suppl 1984; 413: 19-24.

121. Winther B, Gwaltney JM Jr, Mygind N, Turner RB, Hendley JO. Sites of rhinovirus recovery after point inoculation of the upper airway. JAMA 1986; 256: 1763-7.

122. Winther B, McCue K, Ashe K, Rubino JR, Hendley JO. Environmental contamination with rhinovirus and transfer to fingers of healthy individuals by daily life activity. J Med Virol 2007; 79: 1606-10.

123. Wruss J, Rünzler D, Steiger C, Chiba P, Köhler G, Blaas D. Attachment of VLDL receptors to an icosahedral virus along the 5-fold symmetry axis: multiple binding modes evidenced by fluorescence correlation spectroscopy. Biochemistry 2007; 46: 6331-9.

124. Xing L, Casasnovas JM, Cheng RH. Structural analysis of human rhinovirus complexed with ICAM-1 reveals the dynamics of receptor-mediated virus uncoating. J Virol 2003; 77: 6101-7.

125. Yan X, Sinkovits RS, Baker TS. AUTO3DEM--an automated and high throughput program for image reconstruction of icosahedral particles. J Struct Biol 2007; 157: 73-82.

126. Yin FH, Lomax NB. Host range mutants of human rhinovirus in which nonstructural proteins are altered. J Virol 1983; 48: 410-8.

127. Zauner W, Blaas D, Kuechler E, Wagner E. Rhinovirus-mediated endosomal release of transfection complexes. J Virol 1995; 69: 1085-92.

128. Zhang Y, Simpson AA, Ledford RM, Bator CM, Chakravarty S, Skochko GA, Demenczuk TM, Watanyar A, Pevear DC, Rossmann MG. Structural and virological studies of the stages of virus replication that are affected by antirhinovirus compounds. J Virol 2004; 78: 11061-9.

129. Zhou ZH. Towards atomic resolution structural determination by single-particle cryo-electron microscopy. Curr Opin Struct Biol 2008; 18: 218-28.

Curriculum Vitae

DI (FH) Angela Maria Pickl-Herk

Unterer Paigerweg 56

A-8754 Thalheim

angela.pickl-herk@univie.ac.at

Date of birth   02.02.1984

Nationality   Austria

ACADEMIC EDUCATION

03/2007 – 04/2011   University of Vienna, Austria

PhD Studies Molecular Biology

PhD thesis: "Structural changes of minor group human

rhinoviruses during uncoating"

01/2009 – 04/2009   Purdue University, Indiana, USA

EMBO Short Term Fellowship

07/2005 – 02/2006   University of Texas, Southwestern Medical Center, USA

Diploma thesis: "Production of antibodies against *Bacillus*

anthracis' antigens with different affinities for FcRn"

09/2002 – 06/2006   University of Applied Sciences Krems, Austria

Diploma studies Medical/Pharmaceutical Biotechnology

PUBLICATIONS

1.   Bilek G, Matscheko NM, <u>Pickl-Herk A</u>, Weiss VU, Subirats X, Kenndler E, Blaas D. Liposomal Nanocontainers as Models for Viral Infection: Monitoring Viral Genomic RNA Transfer through Lipid Membranes. J. Virol. (submitted).

2.   Khan AG, <u>Pickl-Herk A</u>, Gajdzig L, Marlovits TC, Fuchs R, Blaas D. Entry of a Heparan Sulphate-Binding HRV8 Variant Strictly Depends on Dynamin but not on Clathrin, Caveolin, and Flotillin. Virol 2011; 412: 55-67.

3.   Gavryushina ES, Bryantseva SA, Nadezhdina ES, Zatsepin TS, Toropygin IY, <u>Pickl-Herk A</u>, Blaas D, Drygin YF. Immunolocalization of Picornavirus RNA in infected cells with antibodies to Tyr-pUp, the covalent linkage unit between VPg and RNA. J Virol Methods (2011; 171: 206-11.

4.   Weiss VU, Bilek G, <u>Pickl-Herk A</u>, Subirats X, Niespodziana K, Valenta R, Blaas D, Kenndler E. Liposomal leakage induced by virus-derived peptides, viral proteins, and entire virions: rapid analysis by chip electrophoresis. Anal Chem 2010; 82: 8146-52.

5.   Khan AG, Pickl-Herk A, Gajdzig L, Marlovits TC, Fuchs R, Blaas D. Human Rhinovirus 14 Enters Rhabdomyosarcoma Cells Expressing ICAM-1 by a Clathrin, Caveolin, and Flotillin-independent Pathway. J Virol (2010); 84: 3984-92.

6.   Bilek G, Weiss VU, <u>Pickl-Herk A</u>, Blaas D, Kenndler E. Chip electrophoretic characterization of liposomes with biological lipid composition: Coming closer to a model for viral infection. Electrophoresis 2009; 30: 4292-9.

7.   Konecsni T, Berka U, <u>Pickl-Herk A</u>, Bilek G, Khan AG, Gajdzig L, Fuchs R, Blaas D. Low pH-triggered beta-propeller switch of the low-density lipoprotein receptor assists rhinovirus infection. J Virol 2009; 83: 10922-30.

8.   Weber C, <u>Pickl-Herk A</u>, Khan AG, Strauss S, Carugo O, Blaas D. Predictive bioinformatic identification of minor receptor group human rhinoviruses. FEBS Lett 2009; 583: 2547-51.

9.   Weiss VU, Bilek G, <u>Pickl-Herk A</u>, Blaas D, Kenndler E. Mimicking virus attachment to host cells employing liposomes: Analysis by chip electrophoresis. Electrophoresis 2009; 30: 2123-8.

10.   Katsarou K, Serti E, Tsitoura P, Lavdas AA, Varaklioti A, <u>Pickl-Herk AM</u>, Blaas D, Oz-Arslan D, Zhu R, Hinterdorfer P, Mavromara P, Georgopoulou U. Green fluorescent protein - Tagged HCV non-enveloped capsid like particles: development of a new tool for tracking HCV core uptake. Biochimie 2009; 91: 903-15.

CONGRESS PRESENTATION

1.   <u>Pickl-Herk A</u>, Bilek G, Hafenstein S, Kenndler E, Marlovits T, Blaas D. Uncoating of minor group human rhinoviruses. Sixth International Virus Assembly Symposium, Greece 2009.

POSTER PRESENTATIONS

1.   <u>Pickl-Herk A</u>, Bilek G, Weiss VU, Subirats X, Hafenstein S, Marlovits T, Blaas D. Structural studies of rhinoviral uncoating. Keystone Symposium on Virus Entry, Replication and Pathogenesis, New Mexico, USA 2010.

2.   <u>Pickl-Herk A</u>, Bilek G, Kenndler E, Blaas D. Structural changes during human rhinovirus uncoating. EUROPIC, Spain 2008.

Thalheim, 20.04.2011